Experimental Investigation of Bent and Flattened Heat Pipes for Thermal Management of Defense and Aerospace Electronics

by

Christopher Anthony Lewis Gomes

A thesis submitted to the Graduate Faculty of
Auburn University
in partial fulfillment of the
requirements for the Degree of
Master of Science

Auburn, Alabama
May 2, 2020

Keywords: heat pipes, electronics cooling, bent, flattened, sintered felt wick, copper/water

Approved by

Dr. Daniel K. Harris, Chair, Associate Professor of Mechanical Engineering
Dr. Roy W. Knight, Associate Professor of Mechanical Engineering
Dr. Nicholas Tsolas, Assistant Professor of Mechanical Engineering
Dr. W. Joel D. Johnson, Advanced Technology Manager, L3Harris Technologies

ABSTRACT

Heat pipes are passive heat transport devices composed of a sturdy outer shell, a porous wick material, and a hermetically sealed inner chamber filled with a working fluid. These devices transfer heat energy from a heat source to a heat sink through a passive, cyclic phase change of the internal working fluid and can exhibit effective thermal conductivities orders of magnitude greater than some of the best known thermally conductive materials on Earth. Typically, heat pipes are designed, tested, and produced in a standard straight-round geometry, but in the application of electronics thermal management, complicated geometrical constraints can interfere with the compatibility of straight-round heat pipes. Thermal management solutions requiring geometrically modified heat pipes are very common, and the alterations of these heat pipes can drastically affect their overall behavior and performance. For this reason, an experimental investigation was performed to observe the effects that post-fabrication geometric modifications, such as bending and flattening, have on the operational limits and thermal behavior of sintered felt wick heat pipes. This study provides an experimental database and observed performance trends which were used to characterize geometrically modified heat pipes in terms of their limits and capabilities. With these results, companies in the defense and aerospace industry will be better equipped to provide efficient thermal management solutions for terrestrial, aerial, and space-based high-powered electronic systems.

ACKNOWLEDGEMENTS

I would like to express my appreciation and gratitude to my thesis advisor, Dr. Daniel K. Harris for his unrelenting support and advice throughout this project. I would also like to thank Don George and Joel Johnson of L3Harris Technologies for facilitating this collaborative project and helping to guide this research towards its application. I would like to thank Jason Smith and Matt Montgomery for assisting in the fabrication of the test system and heat pipe test articles. I want to thank all of my colleagues and mentors from Mississippi State University, Auburn University, and NASA MSFC for encouraging me and helping me to continuously pursue academic, professional, and personal excellence. I would especially like to thank my parents, grandparents, and sister for their continued love and support throughout my journey in engineering. Lastly, I would like to thank my wonderful girlfriend, Jourden, for her constant love, care, and patience throughout the rigor and challenges I faced in graduate school.

VITA

Christopher Anthony Lewis Gomes, son of Anthony F. Gomes and Heidi Y. Gomes, was born on June 11, 1995 in Fairfax, Virginia. He grew up in Madison, Alabama where he graduated from Bob Jones High School. In August 2013 he entered the Bagely College of Engineering at Mississippi State University and earned the degree of Bachelor of Science in Mechanical Engineering, graduating cum laude. He interned for NASA Marshall Space Flight Center throughout his undergraduate education working in structural and mechanical design and propulsion systems applied to both deep space missions and private sector launch vehicle development. He was also a member of the summer 2016 NASA Propulsion Academy. After graduating from Mississippi State University in May 2018, Christopher worked at Dynetics, Inc. as an intern in the Space Propulsion Division prior to his enrollment in the Samuel Ginn College of Engineering Graduate Program at Auburn University. Christopher was awarded the American Society for Engineering Education (ASEE) Cooperative and Experiential Education Division (CEED) National Co-op Student of the Year Award 2017-2018. During his time at Auburn University, Christopher participated in an internship at L3Harris Technologies. Christopher has a passion for human space exploration and will pursue a career dedicated to developing critical technology for exploring the vast horizons of deep space. Upon completion of his master's degree in May 2020, Christopher began his professional career as a Human Spaceflight Integration and Operations Systems Engineer at United Launch Alliance (ULA) in Denver, Colorado working on the development of the Space Launch System (SLS) launch vehicle for the NASA Artemis program.

This thesis paper is dedicated to Anthony and Heidi Gomes. Thank you mom and dad for raising Kyra and I with an innate desire to achieve greatness, happiness, and a strong relationship with the Lord. I attribute my success and the establishment of my education and career to the love, kindness, and teaching that I have received from you both my entire life. Thank you for raising me to believe in the Lord Jesus Christ and to put all of my faith in Him. Dad, thank you for teaching me how to be a leader and how to recognize the truth in the world. Mom, thank you for your unconditional love and kindness and the continuous example you set for me and Kyra. I am so grateful to have such wonderful parents and I pray that I can continue in your footsteps throughout my journey in life.

TABLE OF CONTENTS

Abstract 2
Acknowledgements 3
Vita 4
Table of Contents 6
List of Tables 9
List of Figures 10
List of Symbols 13
1 Heat Pipes 16
1.1 Introduction 16
1.2 Heat Pipe Operation 17
1.2.1 Heat Path and Thermal Resistance Network 18
1.2.2 Vapor and Liquid Pressure Drop 20
1.3 Operating Limits 23
1.3.1 Capillary Limit 25
1.4 Heat Pipe Design Considerations 26
1.4.1 Operating Temperatures 26
1.4.2 Wick Structures 27
1.4.3 Compatibility of Materials 29
1.5 Heat Transfer Performance 30
1.6 Application and Benefits 31
1.6.1 The Unique Role of Heat Pipes in Electronics Thermal Management 32
1.6.2 The Advantages of Passive Multiphase Heat Transfer Devices Compared to COTS Heat Spreaders 32
2 Background 35
2.1 Scope of Geometrically Modified Heat Pipes 35
2.1.1 Application to Electronics in Defense and Aerospace 36
2.1.2 Electronics Chassis Example 36
2.2 Literature Review 40
2.2.1 Bending and Flattening 41

2.2.2 Gravitational Orientation 46
3 Factors Affecting Performance and Limits 48
3.1 External Factors, Interfaces, and Applications 48
3.2 Design Parameters Investigated 49
3.2.1 Flattening the Evaporator and Condenser Regions 50
3.2.2 Bending the Adiabatic Region 52
3.2.3 Gravitational Orientation 53
3.2.4 Parameters Held Constant 54
3.3 Effects of Bending the Adiabatic Region 55
3.3.1 Vapor Core Theoretical Analysis 55
3.3.2 Theoretical Analysis of Liquid Flow in the Wick Structure 59
3.4 Effects of Flattening the Evaporator/Condenser 64
4 Testing 67
4.1 Test Matrix 67
4.2 Test Set-up 69
4.2.1 Test Rig Description 69
4.2.2 DAQ Description 72
4.3 Preparation and Fill Procedure 73
4.4 Test Procedure 74
4.5 Test Duration and Uniformity 74
5 Data Reduction 76
5.1 Performance Evaluation 76
5.1.1 Copper Equivalence 77
5.1.2 Evaporator Temperature 78
5.1.3 Total Thermal Resistance 78
5.2 Raw Data Analysis 79
5.2.1 Heat Pipe Data Analyzer (HP-DAN) 79
5.2.2 Thermocouple Calibration 80
5.2.3 Parasitic Loss Model 81
5.2.4 Effective Thermal Conductivity 83
5.3 Data Uncertainty Analysis 84
6 Results and Discussion 86
6.1 Heat Pipe Operating Parameters 86

6.2 Determining the Capillary Limit 87
6.3 Comprehensive Testing Results 90
6.3.1 Effects of Gravitational Orientation on SRHP Performance 95
6.3.2 Effects of Bending on Performance 101
6.3.3 Comparing the Effects of Bending to Similar Research 111
6.3.4 Comparing the Experimental Results to the Vapor Core Theoretical Analysis ... 114
6.3.5 Effects of Flattening on Performance 115
6.3.7 Performance at Capillary Limit for All Heat Pipes 120
6.4 Explanation of Unknown Parameters 123
6.5 Usefulness and Application of Data 124
7 Conclusion 127
7.1 Data Application 127
7.2 Limits on Results 129
7.3 Future Work 129
References 131
Appendix A. Heat Pipe Preparation and Fill Procedure 133
Appendix B. Parasitic Loss Model 135
Appendix C. Uncertainty Analysis 138

LIST OF TABLES

Table 1-1: Material Compatibility with Working Fluid [4] 30
Table 2-1: CCA Component Maximum Temperatures 39
Table 2-2: List of References Dedicated to the Effects of Bending and Flattening 45
Table 3-1: Working Fluid Properties for Liquid Capillary Limit Analysis 61
Table 3-2: Heat Pipe Container and Wick Properties for Liquid Capillary Limit Analysis 61
Table 5-1: Heat Pipe and Insulation Dimensions 83
Table 6-1: Heat Pipe Dimensions and Properties 87
Table 6-2: Results Data at Capillary Limits 90
Table 6-3: D.D. Odhekar's Heat Pipe Specifications [16] 111
Table 6-4: Parameters of Heat Pipes Compared to Former Research 112
Table 6-5: Reported Values Evaporator Temperature and Corresponding Capillary Limit for Bent Heat Pipe Tests in Current and Former Research 112
Table B-1: Parasitic Loss Model Reference Dimensions 135

LIST OF FIGURES

Figure 1-1: Heat Pipe Schematic under Normal Operating Conditions 18
Figure 1-2: Steady Path of Heat Transfer through a Heat Pipe 19
Figure 1-3: Heat Pipe Thermal Resistance Network 19
Figure 1-4: Liquid Vapor Interface at Low Vapor Flow Rates [4] 21
Figure 1-5: Liquid and Vapor Pressure Distributions [4] 22
Figure 1-6: Heat Pipe Operating Limits 24
Figure 1-7: Heat Pipe Wick Structures [6] 29
Figure 1-8: Effective thermal conductivity of Phase III TGPs in DARPA TMT Program [1] 33
Figure 2-1: Electronics Chassis and CCA 37
Figure 2-2: Chassis Front View: CCA Heat Path to Lateral Heat Sinks 37
Figure 2-3: CCA Thermal Profile 38
Figure 2-4: Heat Pipe Integrated Into Electronics Chassis 40
Figure 3-1: Heat Pipe Integrated onto Dell Inspiron 5423 CPU 48
Figure 3-2: Flattened End Conditions 51
Figure 3-3: HP1 Bending Process (Top View) 53
Figure 3-4: HP2 Bending Process (Top View) 53
Figure 3-5: Gravitational Orientations 54
Figure 3-6: Affected Length of Bending 58
Figure 3-7: Liquid Capillary Limit: T_l = 20°C 62
Figure 3-8: Liquid Capillary Limit: T_l = 40°C 62
Figure 3-9: Liquid Capillary Limit: T_l = 60°C 63
Figure 3-10: Liquid Capillary Limit: T_l = 80°C 63
Figure 3-11: Flattening Ratio 65
Figure 4-1: Test Matrix 68
Figure 4-2: Test Set-up 70
Figure 4-3: DAQ Unit and Data Interface 71
Figure 4-4: Test Article Instrumentation Schematic 72
Figure 5-1: HP-DAN Process 79
Figure 5-2: Data File Naming Convention 80
Figure 5-3: Parasitic Loss Model 82
Figure 6-1: Steady-state Temperature Profiles of HP1 SRHP – GAN (Capillary Limit Criteria Example) 88
Figure 6-2: Effective Thermal Conductivity of HP1 SRHP – GAN (Capillary Limit Criteria Example) 89
Figure 6-3: HP1 SRHP Image 91
Figure 6-4: HP1 [1-15°] Image 91
Figure 6-5: HP1 [1-30°] Image 91
Figure 6-6: HP1 [1-45°] Image 91
Figure 6-7: HP1 [1-90°] Image 92
Figure 6-8: HP1 [2-90°, 45°] Image 92
Figure 6-9: HP1 [2-90°, 90°] Image 92
Figure 6-10: HP2 SRHP Image 93
Figure 6-11: HP2 [1-45°] Image 93

Figure 6-12: HP2 [1-90°] Image **93**
Figure 6-13: HP2 [2-90°, 45°] Image **93**
Figure 6-14: HP2 [2-90°, 90°] Image **94**
Figure 6-15: HP4 –Flattened Evaporator Image **94**
Figure 6-16: HP4 –Flattened Condenser Image **94**
Figure 6-17: HP4 –Both Ends Flat Image **94**
Figure 6-18: HP1-GAN Cu Equivalence **98**
Figure 6-19: HP1-GAN Evaporator Temperature **98**
Figure 6-20: HP1-GAN Total Resistance **98**
Figure 6-21: HP2 GAN Cu Equivalence **98**
Figure 6-22: HP2-GAN Evaporator Temperature **98**
Figure 6-23: HP2-GAN Total Resistance **98**
Figure 6-24: HP1-GAS Cu Equivalence **99**
Figure 6-25: HP1-GAS Evaporator Temperature **99**
Figure 6-26: HP1-GAS Total Resistance **99**
Figure 6-27: HP2-GAS Cu Equivalence **99**
Figure 6-28: HP2-GAS Evaporator Temperature **99**
Figure 6-29: HP2-GAS Total Resistance **99**
Figure 6-30: HP1-GAD Cu Equivalence **100**
Figure 6-31: HP1-GAD Evaporator Temperature **100**
Figure 6-32: HP1-GAD Total Resistance **100**
Figure 6-33: HP2-GAD Cu Equivalence **100**
Figure 6-34: HP2-GAD Evaporator Temperature **100**
Figure 6-35: HP2-GAD Total Resistance **100**
Figure 6-36: HP1 [1-15°] Cu Equivalence **105**
Figure 6-37: HP1 [1-15°] Evaporator Temperature **105**
Figure 6-38: HP1 [1-15°] Total Resistance **105**
Figure 6-39: HP1 [1-30°] Cu Equivalence **105**
Figure 6-40: HP1 [1-30°] Evaporator Temperature **105**
Figure 6-41: HP1 [1-30°] Total Resistance **105**
Figure 6-42: HP1 [1-45°] Cu Equivalence **106**
Figure 6-43: HP1 [1-45°] Evaporator Temperature **106**
Figure 6-44: HP1 [1-45°] Total Resistance **106**
Figure 6-45: HP1 [1-90°] Cu Equivalence **106**
Figure 6-46: HP1 [1-90°] Evaporator Temperature **106**
Figure 6-47: HP1 [1-90°] Total Resistance **106**
Figure 6-48: HP1 [2-90°, 45°] Cu Equivalence **107**
Figure 6-49: HP1 [2-90°, 45°] Evaporator Temperature **107**
Figure 6-50: HP1 [2-90°, 45°] Total Resistance **107**
Figure 6-51: HP1 [2-90°, 90°] Cu Equivalence **107**
Figure 6-52: HP1 [2-90°, 90°] Evaporator Temperature **107**
Figure 6-53: HP1 [2-90°, 90°] Total Resistance **107**
Figure 6-54: HP2 [1-45°] Cu Equivalence **108**
Figure 6-55: HP2 [1-45°] Evaporator Temperature **108**
Figure 6-56: HP2 [1-45°] Total Resistance **108**
Figure 6-57: HP2 [1-90°] Cu Equivalence **108**
Figure 6-58: HP2 [1-90°] Evaporator Temperature **108**
Figure 6-59: HP2 [1-90°] Total Resistance **108**
Figure 6-60: HP2 [2-90°, 45°] Cu Equivalence **109**
Figure 6-61: HP2 [2-90°, 45°] Evaporator Temperature **109**
Figure 6-62: HP2 [2-90°, 45°] Total Resistance **109**
Figure 6-63: HP2 [2-90°, 90°] Cu Equivalence **109**

Figure 6-64: HP2 [2-90°, 90°] Evaporator Temperature 109
Figure 6-65: HP2 [2-90°, 90°] Total Resistance 109
Figure 6-66: Cu Equivalence HP1 (All Bending Angles) 110
Figure 6-67: Cu Equivalence HP2 (All Bending Angles) 110
Figure 6-68: Capillary Limit Comparison 113
Figure 6-69: Evaporator Temperature Comparison 113
Figure 6-70: HP4 – Flattened Evaporator Cu Equivalence 118
Figure 6-71: HP4 – Flattened Evaporator Evaporator Temperature 118
Figure 6-72: HP4 – Flattened Evaporator Total Resistance 118
Figure 6-73: HP4 – Flattened Condenser Cu Equivalence 118
Figure 6-74: HP4 – Flattened Condenser Evaporator Temperature 118
Figure 6-75: HP4 – Flattened Condenser Total Resistance 118
Figure 6-76: HP4 – Double-Flat Cu Equivalence 119**
Figure 6-77: HP4 – Double-Flat Evaporator Temperature 119**
Figure 6-78: HP4 – Double-Flat Total Resistance 119**
Figure 6-79: Cu Equivalence HP4 (All Flattened End Conditions) 120
Figure 6-80: Capillary Limits and Corresponding Cu Equivalence 122
Figure 6-81: Evaporator Temperature and Corresponding Heat Input for Operational Range of All Heat Pipes 126
Figure A-1: Heat Pipe Fill System 133
Figure A-2: 3-way Valve Positions 134
Figure B-1: Parasitic Loss Model Schematic 135

LIST OF SYMBOLS

Acronyms

CCA	Circuit card assembly
CL	Capillary limit
COTS	Commercial off-the-shelf
CPU	Central processing unit
DARPA	Defense Advanced Research Projects Agency
FEC	Flattened end condition
GAD	Gravity adverse
GAN	Gravity neutral
GAS	Gravity assist
HP	Heat pipe
HP1	0.25 in. diameter heat pipe
HP2	0.375 in. diameter heat pipe
HP4	0.5 in. diameter heat pipe
HP-DAN	Heat Pipe Data Analyzer
SRHP	Straight-round heat pipe
SWaP	Size, weight, and power
TC	Thermocouple
TGP	Thermal Ground Plane [1]
TMT	Thermal Management Technologies [2]

English Letter Symbols

A	Surface area
A_c	Cross-sectional area
A_v	Cross-sectional area of vapor core
A_w	Cross-sectional area of wick
C	Condenser
Cu	Copper 110

D	Diameter
De	Dean number
dx	Thermocouple spacing
E	Evaporator
F	Frictional coefficient
f	Darcy friction factor
f_s	Fanning friction factor
f_b	Bending friction factor
g	Gravitational constant
h_{fg}	Latent heat of vaporization
I	Intuitive observation (designation for results and observations in Ch. 6)
K_b	Bending loss coefficient
k	Thermal conductivity
k_{eff}	Effective thermal conductivity
L	Length
NI	Non-intuitive observation (designation for results and observations in Ch. 6)
NO	Neutral observation (designation for results and observations in Ch. 6)
Q_{actual}	Heat input corrected by parasitic loss model (W)
Q_{in}	Heat input from linear power supply (W)
$(QL)_{cap,max}$	Liquid capillary limit (W)
R	Thermal resistance
Re	Reynold's number
$Re_{z,v}$	Axial vapor Reynold's number
R_v	Radius of vapor core
r_b	Bending radius
r_{eff}	Effective pore radius
T	Temperature
V_{avg}	Mean velocity

Greek Symbols

ε	Emissivity
ρ	Density
μ	Dynamic viscosity
ϕ	Inclination angle
φ	Wick porosity (void volume)
σ	Surface tension / Stefan-Boltzmann constant
K	Permeability

Subscripts

ad	Adiabatic region
amb	Ambient lab environment
c	Condenser region
cer	Ceramic crucible
conv	Convection
e	Evaporator region
eff	Effective
f	Sintered wick fiber
foam	Foam insulation
HP	Heat pipe
i	Inner
l	Liquid
o	Outer
rad	Radiation
ref,HP	Heat pipe used for experimental wick characterization (fill procedure)
tot	Total
v	Vapor
w	Wick

1 HEAT PIPES

This chapter serves as a general synopsis of the fundamentals of construction, operation, physical phenomena, and direct benefits of heat pipes. This includes heat pipe material compatibility, operating limits, design considerations, performance evaluation, and applications. Additionally, a short overview of the history of heat pipes and their niche role in electronics thermal management is discussed

1.1 Introduction

Heat pipes have been a major focal point in thermal management research since the early 1960s. They were first introduced by George M. Grover of Los Alamos National Laboratory as a method removing waste heat energy from a nuclear space reactor core and routing it to a radiator [3]. From there, heat pipe technology was further developed by NASA for the application of thermal management of satellite transponders. Heat pipes are passive, cyclic heat exchangers capable of routing large amounts of heat energy from a heat source to a heat sink at very low temperature gradients. Since their inception, heat pipes have become ubiquitous in many industries involving high-performance electronics such as commercial PCs, handheld devices, and defense and aerospace electronics. Their popularity in these industries has grown rapidly due to their unique ability to significantly decrease the overall size, weight, and volume of electronics packaging. Albeit heat pipes are typically small relative to the components and devices they interface with, there is a need for increasing the utility of heat pipes to cater to complex electronics packages, specifically in the application of defense systems electronics. The ability to integrate heat pipes into confined spaces requires them to be able to undergo geometric modifications while still

operating correctly. This research effort investigates the effects that post-fabrication bending and flattening has on the thermal performance and operational limits of copper/water sintered felt wick heat pipes.

1.2 Heat Pipe Operation

Heat pipes are composed of a rigid, metallic shell, a porous wick, and a working fluid. They are divided up into three primary segments in the axial direction: the evaporator, the condenser, and the adiabatic region, as seen in Figure 1-1. The evaporator is classified as the area of the heat pipe where the working fluid is evaporated due to the incoming heat flux. The condenser region is the area of the heat pipe, opposite from the evaporator, where the heat sink is located. In this region, hot vapor that has traveled from the evaporator is condensed back into a liquid phase where it re-enters the circumferential wick and begins traveling back to the evaporator region through capillary pumping force in the wick structure. During normal operations, this cyclic process is what transfers the heat energy from the heat source through the heat pipe and out to the heat sink. The middle segment of the heat pipe is commonly referred to as the adiabatic region. In this section, vapor and liquid flow axially in opposite directions within the wick and the vapor core. During normal operations, the adiabatic region surface temperature of the heat pipe is relatively constant along the axis.

Heat pipes initiate passive operation the moment a heat flux is applied. Although heat pipes are simple systems with only a few components, the transport processes that occur within a heat pipe can be complicated. By exploiting a cyclic phase change process, heat pipes are capable of transferring heat energy through the latent heat of vaporization of the working fluid. This process is passive meaning that it requires no external energy source other than the applied heat flux from

the heat source. During normal operations, the heat pipe wick is full of condensed liquid and the hollow core is full of heated vapor. Figure 1-1 shows a schematic of a heat pipe under normal operating conditions.

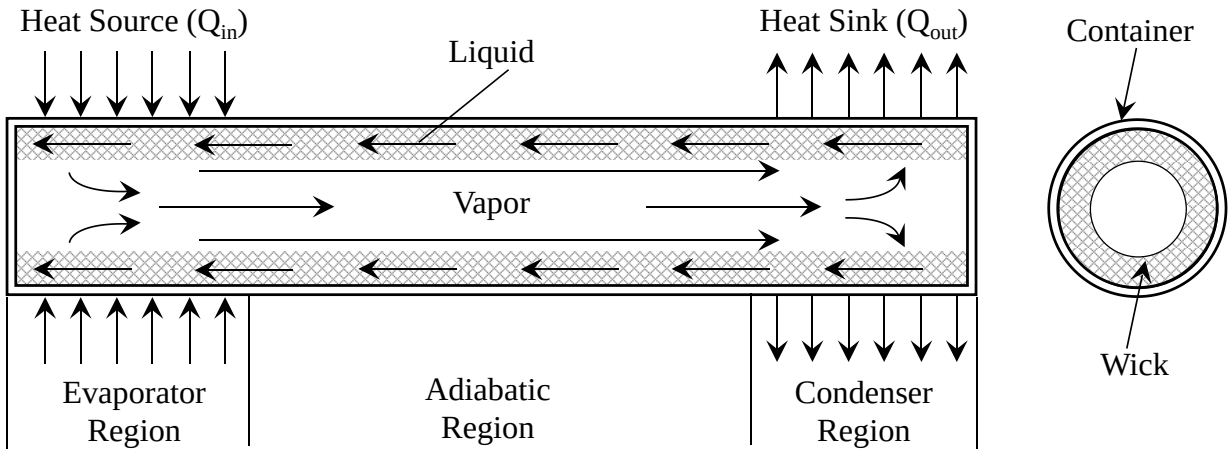

Figure 1-1: Heat Pipe Schematic under Normal Operating Conditions

1.2.1 Heat Path and Thermal Resistance Network

The steady heat transfer path into and out of a heat pipe can be broken down by examining the different components of a heat pipe individually. When heat enters the heat pipe on the external surface of the evaporator region, it spreads through the case radially and axially. The amount of heat conducted axially through the metal case is determined by the thermal conductivity of the case material. The heat that is transmitted through the heat pipe radially travels through the metallic case, through the liquid populated wick, and into the vapor core of the heat pipe. Once the liquid in the wick is heated, it vaporizes and enters the vapor core region. The heat transfer path into and out of the heat pipe can be seen in Figure 1-2.

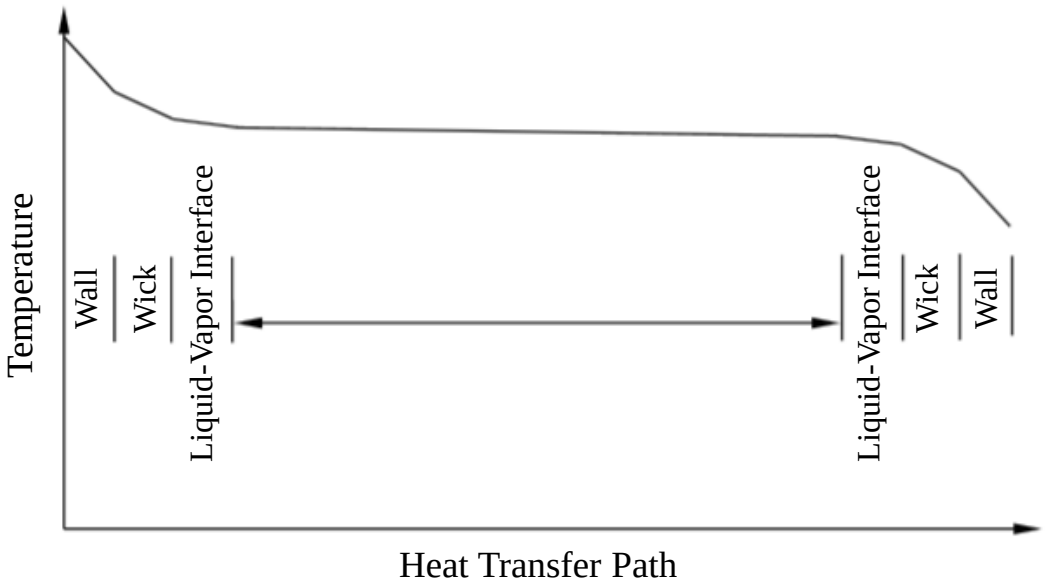

Figure 1-2: Steady Path of Heat Transfer through a Heat Pipe

Based on this heat path, steady transfer of heat throughout the entire heat pipe can be analyzed by breaking down the individual components of the heat pipe into a two-dimensional thermal resistance network, which is displayed in Figure 1-3.

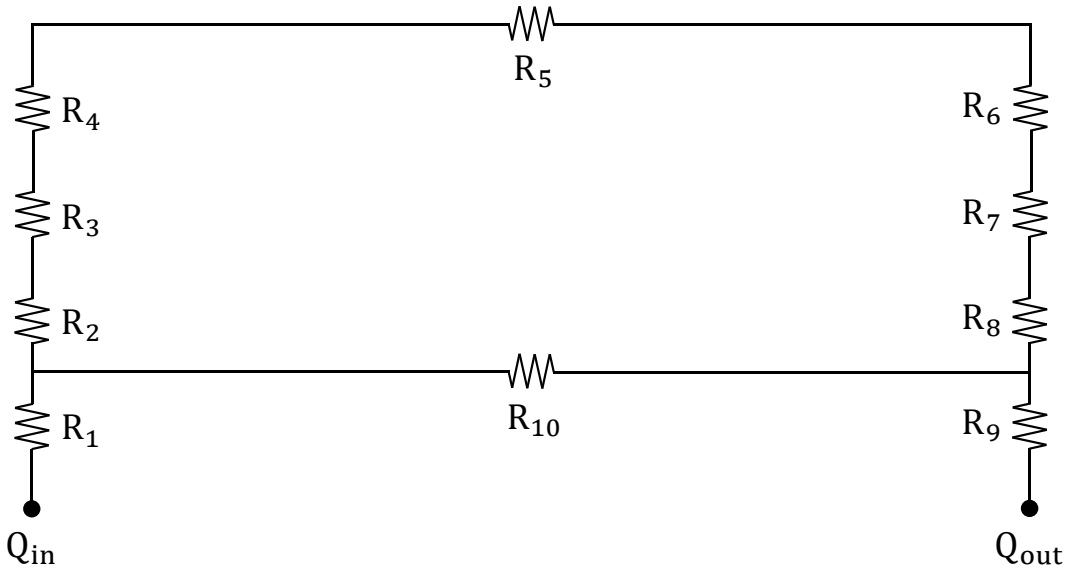

Figure 1-3: Heat Pipe Thermal Resistance Network

- R_1: Thermal resistance of the interface between the heat source and the evaporator region
- R_2: Radial thermal resistance of the metallic shell as heat enters through the evaporator region
- R_3: Radial thermal resistance of the liquid populated wick as heat enters through the evaporator region. Typically limited by the low thermal conductivity of the working fluid.
- R_4: Thermal resistance of the liquid-vapor interface in the evaporator region
- R_5: Axial thermal resistance of the vapor between the evaporator and condenser regions
- R_6: Thermal resistance of the liquid-vapor interface in the condenser region
- R_7: Radial thermal resistance of the liquid populated wick as heat exits through the condenser region
- R_8: Radial thermal resistance of the metallic shell as heat exits through the condenser region
- R_9: Thermal resistance of the interface between the condenser region and the heat sink
- R_{10}: Axial thermal resistance of the metallic shell over the effective length of the heat pipe between the evaporator and condenser regions

1.2.2 Vapor and Liquid Pressure Drop

During normal operations, the velocity of the vapor in the heat pipe is relatively low and represents laminar flow. In the evaporator section, as the working fluid is vaporized, the remaining liquid recedes into the wick resulting in highly curved menisci [4]. Alternatively, on the condenser side, the menisci flatten out, as seen in Figure 1-4.

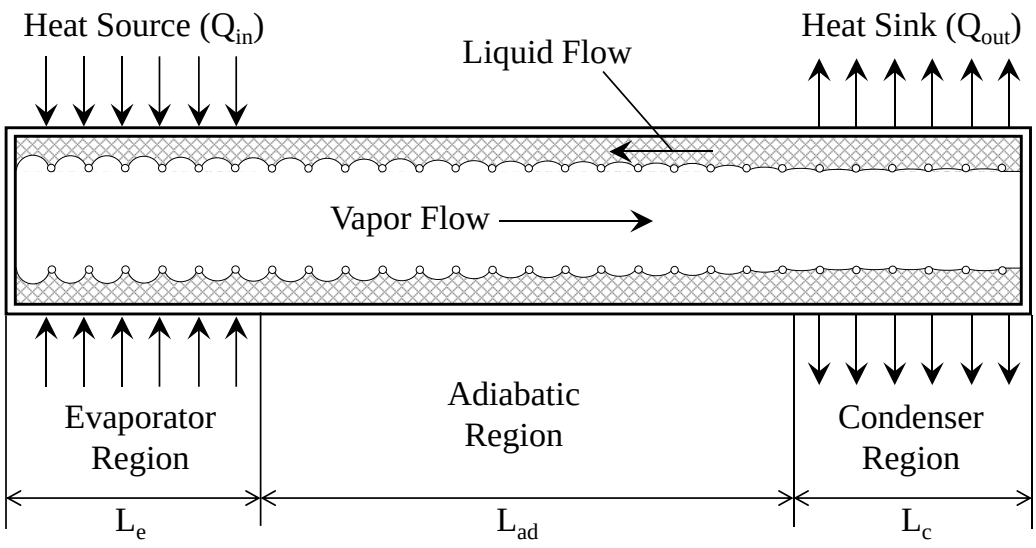

Figure 1-4: Liquid Vapor Interface at Low Vapor Flow Rates [4]

This difference in the menisci radii combined with the surface tension properties of the working fluid results in a capillary pressure drop in the axial direction of the heat pipe. This pressure gradient serves to circulate the fluid in the wick against the liquid and vapor pressure losses and against gravitational force, depending on the inclination angle of the heat pipe. It is for this reason that heat pipes can operate in any orientation relative to gravitational forces.

The liquid and vapor pressure drop trends for normal operations of a low-temperature heat pipe, such as the Cu/water heat pipes used in this study, can be seen in Figure 1-5. The vapor pressure drop is attributed to a combination of frictional and inertial losses in the adiabatic region in addition to sucking and blowing through the porous wick as a result of the cyclic multiphase process in the evaporator and condenser regions. The liquid pressure drop, however, is primarily due to frictional losses [4]. It can be seen that the liquid pressure drop in the wick is much greater in gravity adverse compared to a gravity neutral orientation. In the presence of an adverse gravitational field, the capillary pumping force must overcome an additional opposing axial force. Therefore, it must work harder to transport the fluid through the wick. As a result, heat pipes have lower capillary

limits in gravitational adverse compared to any other gravitational orientation. The relationship between the liquid and vapor pressure drops is important when determining the behavior of a heat pipe. The location in the heat pipe where the pressures in the vapor and liquid are equal to one another is known as the wet point [4]. For the highest achievable heat pipe conductance, the wet point will exist at the beginning of the cooling zone, or condenser region. In this case, only the total pressure drop in the evaporator and adiabatic regions govern the heat pipe's operational limit. If the wet point occurs at the end of the condenser region near the heat pipe condenser end cap, then the pressure drop between the liquid and vapor in the condenser region is increased. This results in a lower heat pipe conductance compared to when the wet point is located at the entrance of the condenser.

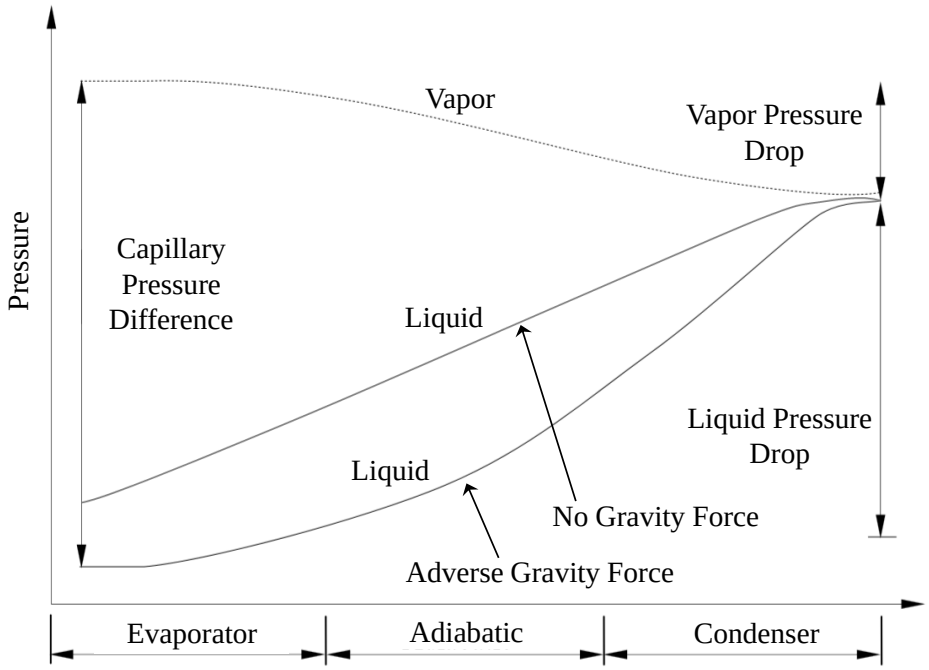

Figure 1-5: Liquid and Vapor Pressure Distributions [4]

1.3 Operating Limits

In contrast to pure, solid metallic rods, heat pipes have limits to the amount of heat energy that can be transferred. These limits are known as operating limits. Heat pipes can be designed for optimal performance under a specific heat load and condenser condition. Any load above or below this design point will either result in below average performance or even a failed operation due to wick dry-out. As a heat pipe approaches an operating limit, it slowly begins to lose its heat transport capabilities. At ultimate failure, the wick is dried out and is no longer pumping liquid to the evaporator region. This results in a very low thermal conductance of the heat pipe. Heat pipe dry-out can occur for many different reasons. Depending on the type of heat pipe and the operating conditions, the limits that govern the operable heat load range for a heat pipe are known as the viscous limit, sonic limit, entrainment limit, boiling limit, and capillary limit. These limits are all dependent on the design of the heat pipe, the operating conditions, and the heat flux applied, as seen in Figure 1-6. Each of these limits bound the maximum allowable heat flux that can be applied to a heat pipe prior to wick dry-out.

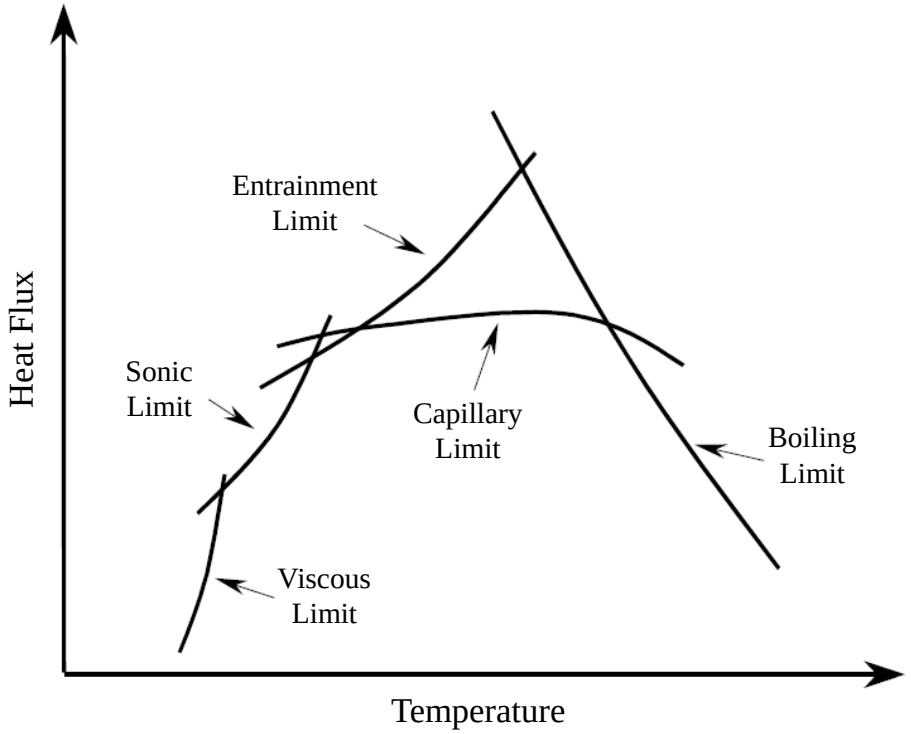

Figure 1-6: Heat Pipe Operating Limits

The viscous limit is important at very low operating temperatures and is typically not very significant in the application of electronics cooling. This limit occurs when the vapor pressure difference between the evaporator and condenser regions is very small. In this scenario, the vapor may stagnate resulting in a decrease in effective thermal conductivity. The viscous limit is typically a necessary consideration when dealing with cryogenic heat pipes. The sonic limit, or start-up limit, occurs when the local velocity at the evaporator exit reaches local sonic velocity. As the heat load is increased, the vapor mass flow rate is increased, with a corresponding reduction in condenser pressure. Eventually, the vapor velocity reaches sonic condition and represents choked flow. The entrainment limit occurs at very high vapor velocities. In the right conditions, liquid droplets from the wicked region may be entrained in the vapor flow. This results in excess liquid accumulation in the condenser region and a dry-out at the evaporator. The boiling limit occurs at

very high heat loads. At a high enough heat load, nucleate boiling can occur in the wick structure. The vapor bubbles impede liquid flow returning from the condenser and cause the evaporator to dry-out. The capillary limit is defined by the ability of a particular capillary structure to provide circulation for a given working fluid [4]. In this research, the capillary limit is the only limit that is acutely observed. Each of these limits result in a starvation of liquid in the evaporator region of a heat pipe which results in a high evaporator temperature and a low effective thermal conductivity. During normal operations, heat pipes are capable of achieving thermal conductivities orders of magnitude greater than copper. For instance, a 30-mm-diameter 1-m-long copper rod may transfer 1 kW of heat at a temperature difference of 900°C, whereas a similar size heat pipe may transfer the same amount of heat with an axial temperature difference of only 10°C. In this example, the heat pipe has a thermal conductivity 90 times higher than that of a copper rod.

1.3.1 Capillary Limit

The capillary limit is the most common limit encountered by low-temperature heat pipes. This limit is reached when the combined liquid and vapor pressure drops overcome the maximum capillary pumping force within the wick [4]. The pumping force is a function of the physical properties and parameters of the wick. In other words, $\Delta P_{capillary} \geq \left|\Delta P_{vapor} + \Delta P_{liquid}\right|$ must hold true at all times or else the wick at the evaporator end dries out, causing an operational failure. As the heat load is increased, the capillary pumping force is exceeded by the pressure drop of the working fluid which results in an eventual dry-out of the wick and a substantial increase in temperature on the surface of the evaporator region. For this research, the capillary limit was experimentally determined for each heat pipe configuration. Test data showed that regardless of the heat pipe dimensions or modifications, the capillary limit of a SRHP was always highest when

the heat pipe was in a gravity assist (GAS) orientation. The GAS orientation is when the condenser region is directly above the evaporator region and the axis of the heat pipe is normal to the gravitational field. The experimentally determined capillary limits in the opposing gravity adverse (GAD) orientation were lower for each heat pipe compared to the gravity neutral and gravity assist orientations. The capillary limit controls the maximum allowable heat load that a heat pipe is capable of transferring through the condenser prior to wick dry-out. This limit is necessary to consider when designing or analyzing a low-temperature heat pipe as it will result in a complete system failure if achieved.

1.4 Heat Pipe Design Considerations

Although heat pipes have incredible performance potential, there are several design parameters and interrelated phenomena that must be taken into consideration in order to safely maximize the performance and sustainability of a heat pipe for its particular application. As previously mentioned, a traditional heat pipe consists of three major components: the shell, the wick, and the working fluid. The materials and design traits of each of these components depends on the application of the heat pipe. Some of the major parameters to consider when designing a heat pipe are operating temperature, wick structure, and material compatibility. Each of these parameters bounds and influences the design of the components of the heat pipe, and therefore the heat pipe itself.

1.4.1 Operating Temperatures

Traditionally, heat pipes are categorized into four groups based on operating temperature: cryogenic, low, medium, and high temperature. Cryogenic heat pipes operate in a temperature

range between 4 and 200 K. These heat pipes utilize cryogenic liquid as the working fluid, such as argon, oxygen, helium, or krypton, and are used in applications with very low heat fluxes in extreme cold environments. Low-temperature heat pipes are fairly common in the application of electronics thermal management and operate within a range of 200 to 500 K. These heat pipes have the benefit of operating in a range of temperatures that is less hazardous to humans. Low-temperature heat pipes typically employ ammonia, acetone, Freon, or water as a working fluid. Medium temperature heat pipes operate in the range of 550 to 750 K. It is at this temperature range that some liquid metals, such as mercury, are employed as a working fluid. Another common working fluid for medium temperature heat pipes is sulfur. High-temperature heat pipes operate at temperatures exceeding 750 K and use sodium, lithium, silver, or sodium-potassium as a working fluid [4].

1.4.2 Wick Structures

When designing the wick structure of a heat pipe, the parameters of interest are pore size, radial thickness, and thermal conductivity in addition to material compatibility. The wick material must be compatible with the container material and working fluid. Pore size determines the capillary head and permeability of the wick. An increase in pore size increases the permeability of the wick. However, the maximum capillary head generated by a wick increases with decreasing pore size. Pore size must be optimized with consideration to both of these properties. An increase in the thickness of a wick raises the heat transport capability of a heat pipe. The effective thermal conductivity of a wick is a weighted average of the liquid (working fluid) and solid (wick material) thermal conductivities. The weighting of the conductivities depends upon the wick geometry [5]. The choice of wick structure depends on the desired performance characteristics. The two main types of wicks are homogenous and composite. A homogenous wick is constructed with one type

of material or machining method. Homogenous wicks have the advantages of being easy to design, manufacture, and install. Composite wicks have multiple materials or machining methods. They have the benefits of increasing the capillary pressure. The disadvantage of the homogenous wick is that it typically cannot produce the capillary pressure that the composite wick can. However, composite wicks typically have the disadvantage of being expensive and difficult to manufacture. One example of a homogenous wick is a screen mesh. An example of a composite wick is multiple screen meshes with different pore sizes [4].

Depending on the performance requirements, available materials and manufacturing methods, and environmental influence, a heat pipe wick can take on one of several unique structural designs, as seen in Figure 1-7. Each wick design has its own list of benefits and drawbacks. In this research, a sintered metal wick was required to allow for post-fabrication bending and flattening. However, sintered metal felt wicks typically provide a lower permeability than the axial groove design which can result in reduced capillary limits.

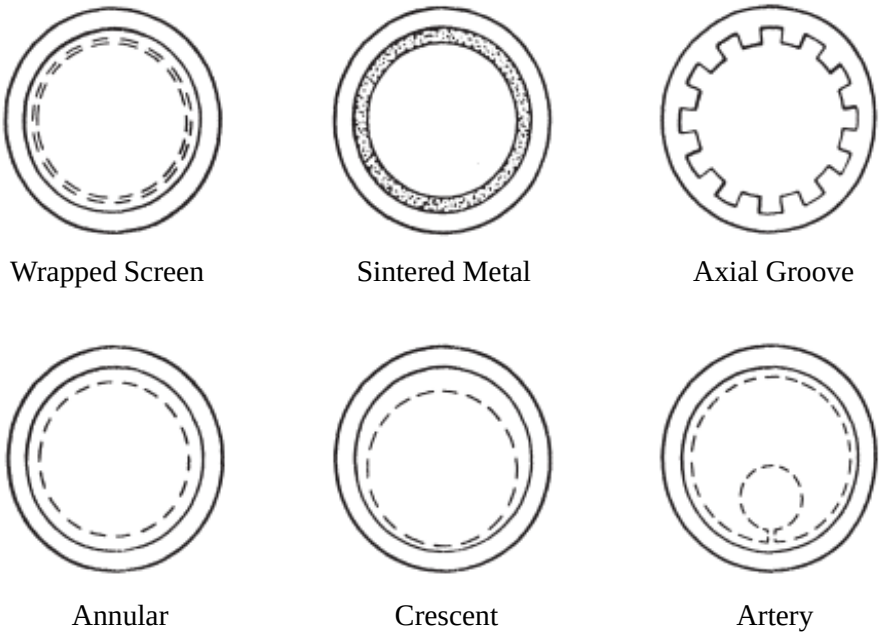

Figure 1-7: Heat Pipe Wick Structures [6]

1.4.3 Compatibility of Materials

The working fluid, the container, the wick, and welding materials must all be compatible with one another in order to prevent structural degradation. Improper matches can lead to galvanic cells or decomposition of the working fluid. Table 1-1 shows a list of compatible materials.

Table 1-1: Material Compatibility with Working Fluid [4]

Operating Temperature	Working Fluid	Compatible Material	Incompatible Material
250 - 400 K	Ammonia	Aluminum, Stainless steel, Iron, Nickel	Copper
	Methanol	Stainless steel, Iron, Copper, Brass Silica, Nickel	Aluminum
	Acetone	Aluminum, Stainless steel, Iron, Copper, Brass, Silica	
300 - 425 K	Water	Stainless steel, Copper, Nickel, Titanium	Aluminum, Inconel
625 - 850 K	Cesium	Titanium, Niobium	
	Mercury	Austentic, Stainless steel	Molybdenum, Nickel, Tantalum, Inconel, Titanium, Niobium
> 750 K	Sodium	Stainless steel, Nickel, Inconel, Niobium	Titanium
	Silver	Tungsten, Tantalum	Rhenium

1.5 Heat Transfer Performance

Heat pipe performance is often measured by a quantity known as effective thermal conductivity (k_{eff}). This parameter characterizes how much heat can be transported through a medium at a particular temperature difference. By harnessing the benefits of phase-change heat transfer, heat pipes are capable of exhibiting effective thermal conductivities orders of magnitude greater than highly conductive metals. However, unlike metals, heat pipe conductance is a very strong function of the applied heat load. Most heat pipes will exhibit lower effective thermal conductivity values for lower powers and increase gradually with power until peak performance is reached. This peak occurs when the maximum amount of heat that the heat pipe is capable of transferring under normal

operating conditions is applied. Any additional heat applied past this point will push the heat pipe further and further towards complete dry-out as the heat pipes effective thermal conductivity continues to degrade rapidly. This behavior is inherent to almost all heat pipes and must be considered during heat pipe design, particularly when post-fabrication modifications are made. Traditionally in application, a heat pipe would be used to enhance a heat path from a high-powered device to an efficient condenser heat sink. If the component's thermal design power (TDP) and failure temperature were known, a heat pipe/heat sink solution could be designed by taking into account the conditions of the component it is cooling and the expected thermal behavior of the candidate heat pipe.

1.6 Application and Benefits

Heat pipes provide a niche role of aiding in the implementation of traditional thermal management technology when obstacles such as geometric constraints or weight limitations present a need for expanding the integrability of these traditional thermal management systems. Heat pipes alone cannot provide the complete thermal management solution for an electronics system, but when paired with traditional thermal management technology such as fan/heat sink assemblies or radiative surfaces, they can increase the feasibility of designing and optimizing a thermal management system towards minimal size, weight, and power consumption (SWaP). A heat pipe's ability of helping to provide a thermal management solution that minimizes cost, weight, volume footprint, and power consumption is the reason why so many companies dealing with high-powered electronics use heat pipes. Aside from the commercial electronics industry, where heat pipes are the most prevalent, the defense and aerospace industry relies on heat pipes as thermal management enhancers in communications systems, controls, power devices, and other electronic systems as technology becomes more advanced. Heat pipes are often employed in both ground-

based and aerial electronics packages. Additionally, since heat pipes do not depend on gravitational forces to operate, they are commonly employed as thermal management enhancers on satellites and other space-based systems.

1.6.1 The Unique Role of Heat Pipes in Electronics Thermal Management

Heat pipes, for all intents and purposes, can be considered efficient heat conduits. In other words, in order for heat pipes to benefit a thermal management system, they must operate in conjunction with a traditional method of heat removal such as an actively cooled heat sink. The heat sink provides the necessary thermal conditions on the external surface of the heat pipe's condenser region for the heat pipe to serve as an efficient heat path from the heat source to the heat sink. Based on this understanding, heat pipes should not be compared to traditional methods of direct cooling, but rather to other solutions of heat moving and heat spreading such as metallic spreaders, vapor chambers, and other advanced technological devices that aid in the thermal management of high-powered electronics.

1.6.2 The Advantages of Passive Multiphase Heat Transfer Devices Compared to COTS Heat Spreaders

The Defense Advanced Research Project Agency (DARPA) has lead research dedicated to improving state-of-the-art passive multiphase heat transfer devices, such as heat pipes and vapor chambers by capitalizing on their fundamental benefits of high thermal conductivity and ease of integration. The DARPA Thermal Management Technologies (TMT) research portfolio has investigated methods of developing hybrid cooling systems that expand the design and integration domain of enhanced electronics thermal management systems even further. One of the goals of this research was to investigate the means of improving advanced electronics cooling technology

by developing Thermal Ground Planes (TGP) that would leverage the benefits of hermetically sealed multiphase heat exchangers while also matching variable thermal expansion coefficients (CTE) of silicon and ceramic microelectronic components [1]. This research effort included contributions from several industrial entities and academic institutions such as Raytheon, Northrop Grumman, The University of Colorado - Boulder, UCLA, UC Santa Barbara, Teledyne, UC Berkley, and GE [2]. Each of these technological leaders has pursued the development of TGP technology that harnesses the benefits of high effective thermal conductivity combined with a flexible form-factor [2]. Figure 1-8 compares the TGPs developed by each of the participating entities to COTS heat spreaders, such as highly conductive materials and vapor chambers. It can be seen in Figure 1-8 that the vapor chamber and TGP technology exhibits much higher effective thermal conductivities than graphite and diamond, which are known to be good heat spreaders.

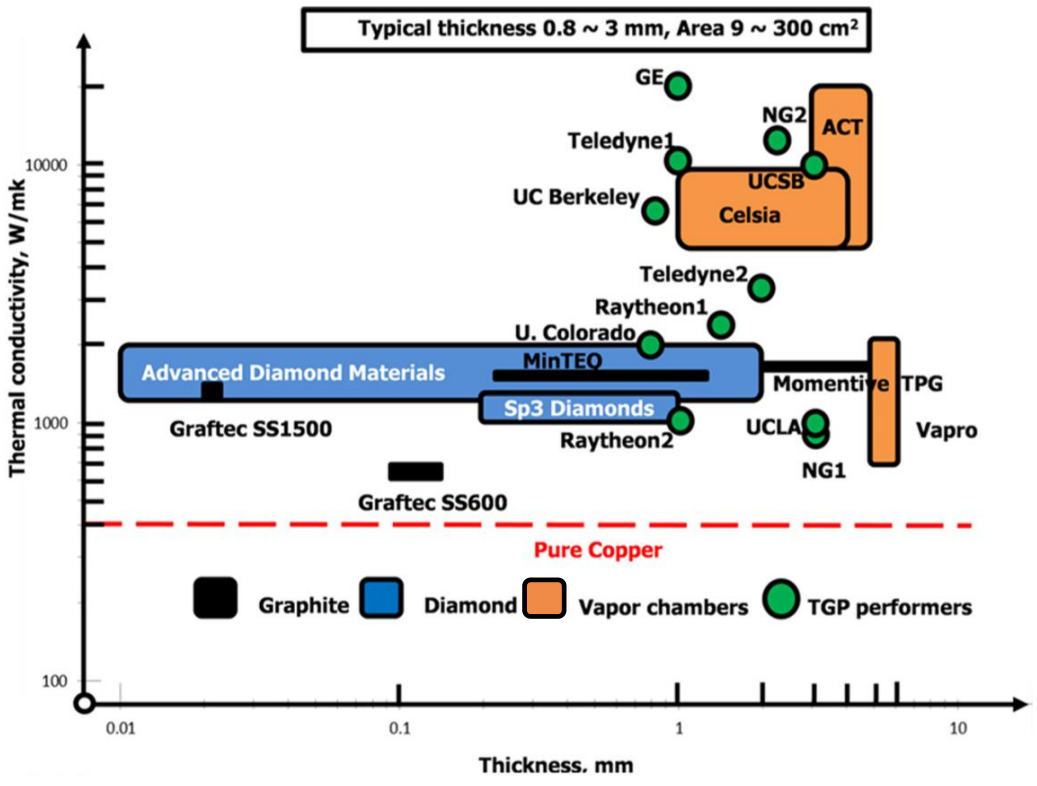

Figure 1-8: Effective thermal conductivity of Phase III TGPs in DARPA TMT Program [1]

The sintered felt wick heat pipes investigated in this study are capable of exhibiting effective thermal conductivities on the order of 80,000 W/m-K. Although they are not optimized for CTE matching and minimal thickness, like the technology in the DARPA TGP research, these sintered wick Cu/water heat pipes are capable of performing at the same effective thermal conductivity levels as the state-of-the-art TGPs and the COTS vapor chambers. This research, provided by the DARPA TMT portfolio, serves as a classical representation of the major benefits provided by employing passive multiphase heat spreading devices, such as heat pipes, in the application of defense system electronics.

2 BACKGROUND

This chapter serves to contextualize the scope of the novelty of this research, which is to investigate the effects of post-fabrication bending and flattening on the performance and operational limits of Cu/water sintered felt wick heat pipes. A generalized description of application of this information is discussed as well as a summary of similar research dedicated to understanding geometric modifications of other various types of heat pipes.

2.1 Scope of Geometrically Modified Heat Pipes

Heat pipes are often selected as thermal management solutions for systems that have strict weight, volume footprint, power, and special requirements. In many applications, namely space-based systems, the major driving design parameters are size, weight, and power (SWaP). Typically, system requirements limit the available volume or spatial configuration of a component, meaning that a heat pipe may have to conform to odd shapes or orientations within in a system. Since heat pipes are traditionally manufactured as straight-round rods, in order to be integrated into these systems and meet geometric requirements and performance goals, the heat pipe may need to be geometrically modified through bending and/or flattening. For the purposes of this research, the range of geometric modifications was predetermined based on the style and size-scale heat pipe applicable to electronics thermal management. A test matrix was created based on the applicable and feasible geometric modifications to 0.25 in., 0.375 in., and 0.5 in. diameter heat pipes. Several design parameters of the heat pipes were not investigated in order to maintain a reasonable sized test matrix. The neglected parameters are discussed in Chapter 7 and may be explored in a future continuation of this research.

2.1.1 Application to Electronics in Defense and Aerospace

Heat pipes are ubiquitous in the world of electronics thermal management. Many modern electronics systems, such as laptops or smartphones, employ heat pipes as a part of their thermal management solutions. In almost all instances, these electronic components have a cubic or rectangular profile with flat surfaces. A heat pipe can be integrated onto a flat electronic component quite easily, especially when being able to conform to the spatial requirements of the system. Heat pipes inherently minimize SWaP due to their small volumetric footprint and lack of operational power consumption. With all of these benefits, heat pipes are highly employable as thermal management solution aids for electronic systems in many applications such as defense systems communications and controls. Another unique benefit of heat pipes is their ability to function in microgravity environments. With the only necessary driving forces within a heat pipe being the vapor pressure drop and capillary driven forces, a heat pipe can operate at a very high level of performance in outer space. They provide a range of solutions for thermal management of space-based electronics such as small-satellites, nanolaunch vehicles, and a variety of other systems.

2.1.2 Electronics Chassis Example

A thermal analysis was performed, using FloTHERM, on a sample high-powered electronics chassis product from L3Harris Technologies. This chassis contained several electronics modules arranged in parallel, as seen in Figure 2-1. It was outfitted with two lateral, straight-fin heat sinks that were actively cooled by COTS fans. These heat sinks provided edge cooling for the electronics modules. Each module was comprised of a circuit-card assembly (CCA) and its own central heat sink which served as the heat path for edge-cooling of the CCA. The CCA heat sinks were outfitted with mounting rails to accommodate wedge-locks which enhanced the edge-cooling of the CCAs.

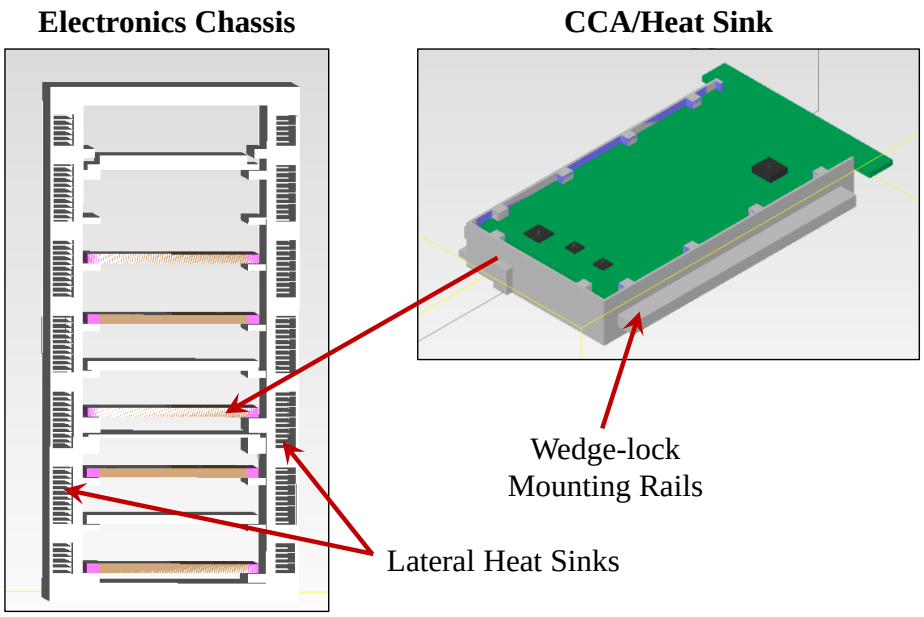

Figure 2-1: Electronics Chassis and CCA

A single CCA contained multiple electronic components, each of which dissipated heat ranging from less than 1 W to more than 100 W. The heat path from the individual components on the CCA to the actively cooled heat sinks can be seen in Figure 2-2. The heat transfer from the chips through the circuit card was enhanced by thermal vias.

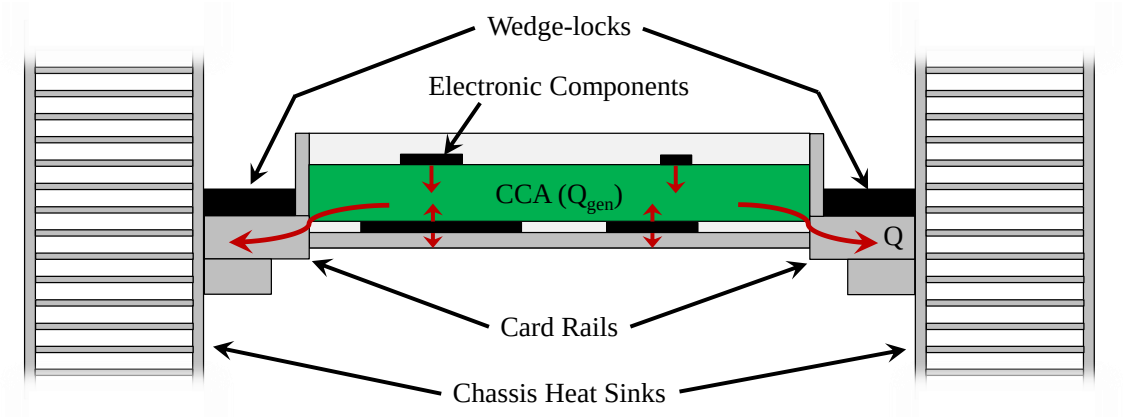

Figure 2-2: Chassis Front View: CCA Heat Path to Lateral Heat Sinks

The CCA selected for thermal analysis contained 10 electronic components of various sizes and operating powers. These components populated both sides of the CCA. The side with the majority

of the components was oriented to interface directly with the CCA heat sink, while the side with the least amount of components faced away from the heat sink and was exposed to ambient quiescent air. The heat dissipated by these components was conducted through the CCA and out through the card rails as a function of the temperature difference between the CCA and the lateral heat sink walls. A thermal profile representing the maximum steady-state temperatures of each electronic component on the CCA was developed through this thermal analysis, and can be seen in Figure 2-3. The tabulated values for maximum temperature of each electronic component are displayed in Table 2-1.

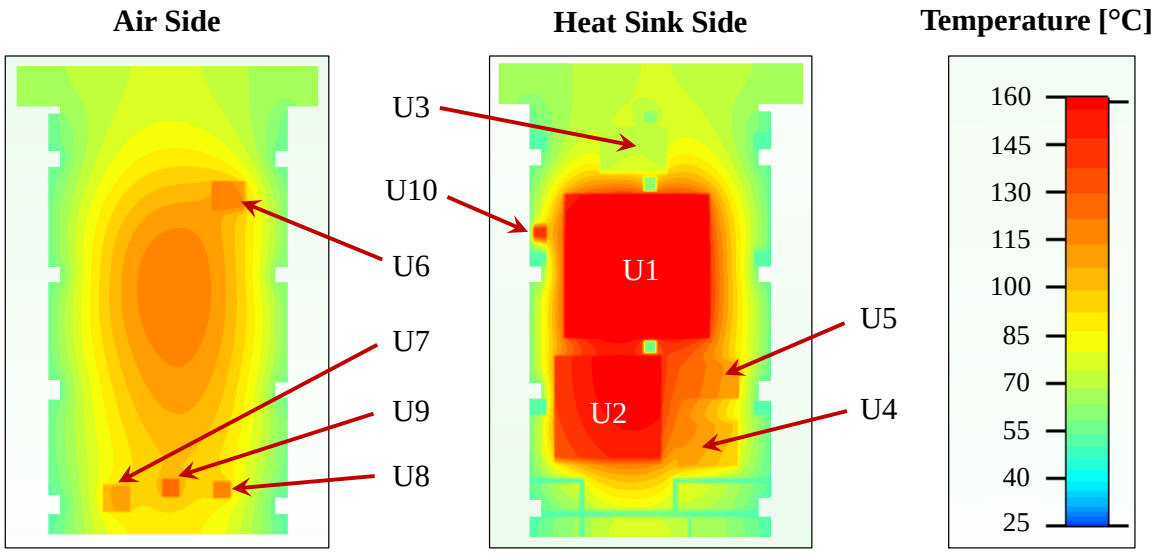

Figure 2-3: CCA Thermal Profile

Table 2-1: CCA Component Maximum Temperatures

Component		Max. Temperature [°C]
Heat Sink Side	U1	158.8
	U2	156.9
	U3	61.3
	U4	118.5
	U5	130
	U10	145.5
Ambient Side	U6	117.5
	U7	108.9
	U8	116.3
	U9	123.8

The maximum temperatures approximated in this thermal analysis represent worst case scenario assumptions and serve as a conservative estimate of what the operating temperatures would be in reality. Several assumptions were applied to this model in favor of this conservative estimate, such as insulating all heat paths other than the path through the CCA heat sink, neglecting radiation, and assuming minimum dimensions according to tolerance of the electronic components. Albeit the maximum temperatures yielded from this thermal analysis may be overestimated by 25-30%, this exercise proves that the high-powered components in this system could be capable of reaching temperatures that are hazardous to electrical operations. A traditional solution for this problem could involve a complete re-design of the chassis and a much more robust active cooling system to enhance the edge cooling of the CCAs. However, with the ability to integrate heat pipes into the chassis design, the thermal management of the electronic components can be improved without increasing the volume footprint, power consumption, or weight of the system. As seen in Figure 2-4, a heat pipe could be integrated into this chassis to provide a direct heat path from the high-powered component to the actively cooled heat sink.

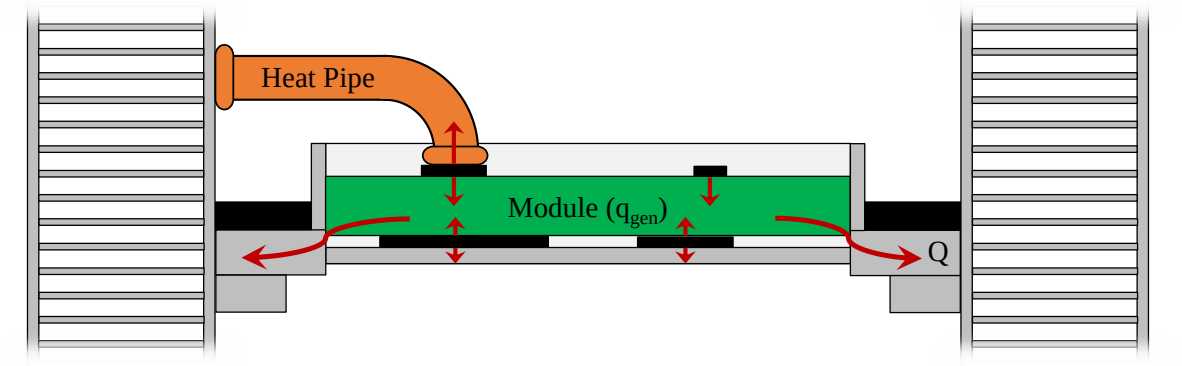

Figure 2-4: Heat Pipe Integrated Into Electronics Chassis

In this example, rather than relying purely on the conduction through the CCA thermal vias and out through the module rails, the chip is outfitted with a geometrically modified heat pipe that regulates its temperature to prevent thermal failure. The hypothetical heat pipe in this design is oriented such that the evaporator region is located on the surface of the electronic component and the condenser region is located on the lateral heat sink wall. The actively cooled heat sink would provide the necessary condenser boundary condition required to transfer the heat dissipated by the electronic chip at a low temperature difference, which would result in a lower operating temperature of the chip. If the heat pipe performance could be characterized under bending and flattening, it could be designed with the required effective thermal conductivity to regulate the chip temperature, which would prevent having to re-design the chassis structure and the active cooling system. This electronics chassis is a good example of a candidate system for the application of bent and flattened heat pipes.

2.2 Literature Review

Heat pipes and their applications have become a highly researched topic in the field of defense and aerospace electronics. With a wide range of available designs and configurations of heat pipes comes a myriad of diverse applications. Heat pipe literature is comprehensive in the research of

straight-round heat pipes of various sizes, materials, and working fluids. However, there is not as much research dedicated to understanding the effects that bending and flattening have on the thermal performance of heat pipes. This fine scope of research and the respective results found in the small amount of available literature has been summarized to establish an idea of the current progress in understanding these effects. Additionally, since a secondary effort of this research was to investigating the performance of SRHPs in gravity assist and gravity adverse configurations, some available literature dedicated to exploring these gravitational effects has been included in this synopsis.

2.2.1 Bending and Flattening

The performance characteristics of cryogenic sintered-wick miniature bent and flattened heat pipes were experimentally investigated by N. Sangpab [7]. The heat pipes used in this research were fabricated from oxygen free copper and employed nitrogen as the working fluid. The wick structure was composed of sintered copper powder laid over axial grooves. The heat pipe test articles had original dimensions of 6 mm in the outer diameter and a length of 200 mm. The heat pipes were bent at angles of 0°, 30°, 60° and 90° and flattened to thicknesses of 2.5, 3.0, 4.0 mm. The operating point for these heat pipes was in the cryogenic range at approximately 78 K. From this researched it was determined that both bending and flattening increased the overall thermal resistance. The bending increased the thermal resistance from 0.88 to 1.07 K/W (6mm, 0° to 6mm, 90°) and the flattening increased the thermal resistance from 0.88 to 2.24 K/W (6mm, 0° to 2.5mm, 0°). The thermal resistance under combined bending and flattening increased from 0.88 to 1.56K/W (6mm, 0° to 3mm, 90°). Sangpab suggested that bending affected the heat pipe performance by deforming the wick which resulted in an obstruction to the liquid flowing from the condenser to the evaporator [7]. Sangpab also concluded that flattening affected the thermal

resistance by collapsing the wick structure which also resulted in an impedance of liquid returning from the condenser to the evaporator by liquid becoming trapped in the condenser region [7].

The performance effects of flattening sintered copper powder wick heat pipes was also investigated by K.T. Lin [8]. Cu/water heat pipes with an original diameter of 6 mm and length of 30 cm were flattened and tested to observe the effects that flattening had on maximum heat load and overall thermal resistance. The heat pipes were tested in straight-round configurations, flattened evaporator, and completely flat at a thicknesses of 2.5 mm and 3 mm. It was observed that the capillary limit was not affected significantly when the evaporator was flattened to 3 mm. The limit was approximately 28 W for the straight-round and flattened evaporator configurations. However, when the entire heat pipe was flattened to 3 mm, the capillary limit decreased to approximately 20 W, and when it was flattened further to a thickness of 2.5 mm, the capillary limit decreased to approximately 7.5 W. The overall resistance was not affected significantly when the heat pipe was flattened to 3 mm, maintaining a value of approximately 0.3 K/W. However, when the entire heat pipe was flattened to 2.5 mm, the overall thermal resistance increased to approximately 0.6 K/W. Lin suggested that the main degradation mechanism of the flattened sintered powder heat pipes was liquid clogging the condenser region [8].

The effects of bending grooved wick flat-plate heat pipes (FPHP) with respect to capillary limit, effective thermal conductivity, and total resistance were experimentally investigated by J. Chen [9]. This research also explored the effects of total heat pipe length and working fluid charge ratio on the performance of FPHPs. Since those parameters were not investigated in the current research, the focus of this discussion will lie with Chen's bending results. The FPHPs used in this experimental analysis had a width of 50 mm and a thickness of 2.5 mm. The heat pipes were bent at 0°, 30°, 60°, and 90° from the original straight heat pipe plane. The varying bend angle tests

were performed at unique heat input ranges and it was observed that bending angle had a noticeable effect on capillary limit, effective thermal conductivity, and total resistance of the heat pipes. The straight heat pipe (bending angle of 0°) reached its capillary limit at approximately 45 W where it exhibited a k_{eff} of approximately 1800 W/m-K and a total resistance of 0.7 K/W. When the heat pipe was bent to 30°, its capillary limit increased to 70 W where it exhibited a k_{eff} of 3000 W/m-K and a total resistance of 0.5 K/W. As the heat pipe was bent further to 60°, neither the capillary limit nor the total resistance increased, but the k_{eff} increased slightly to a value of 3200 W/m-K. The 90° bending angle test exhibited a significant increase in performance reaching a capillary limit of 75 W, a k_{eff} of 6400 W/m-K, and a total resistance of 0.2 W/m-K. It was observed that as the bending angle increased, both the capillary limit and the maximum effective thermal conductivity increased as well.

An investigation into the effects that flattening mini-axial grooved heat pipes (AGHP) has on capillary limit and total resistance was performed by H. Tao [10]. The heat pipes used in this experimental investigation were straight-round with an outer diameter of 6 mm and a length of 210 mm. The SRHPs were pressed into AGHPs with varying flattened thicknesses. Each AGHP was evaluated for capillary limit and total thermal resistance at an operating temperature of 50°C. The original SRHP reached its capillary limit at approximately 55 W where it exhibited a total thermal resistance of 0.04 K/W. The SRHP was then pressed to thicknesses of 3.5, 3.0, 2.5, and 2.0 mm where it exhibited capillary limits of 46, 38, 25, and 17 W and total thermal resistances of 0.07, 0.1, 0.1, and 0.76 K/W, respectively. It was observed that decreased flattening thickness resulted in a decrease in capillary limit and an increase in total thermal resistance. This indicated that although there was not much of an effect on thermal resistance for the larger flattened

thicknesses, when the heat pipe was pressed to a flattened thickness of 2.0 mm the overall thermal performance was significantly degraded.

An experimental investigation of the combined effects of bending and assistive gravitational forces was performed by D.D. Odhekar [11]. The heat pipe used in this research was a 6.35 mm diameter Cu/water heat pipe with a sintered copper felt wick. The heat pipe was tested in gravity assist orientation at various bending angles and incrementing heat input levels. The capillary limit and effective thermal conductivity relative to copper was recorded. The unit of measurement used to compare the effective thermal conductivity of the heat pipes to that of solid copper is known as Cu equivalence, and is further discussed in Chapter 6. The SRHP was tested in GAS where it exhibited a capillary limit of 36 W and a corresponding effective thermal conductivity 194 times greater than the thermal conductivity of copper. As the heat pipe was bent 15°, the capillary limit increased to 44 W and the Cu equivalence increased to 254. Increasing the bend angle to 30° did not change the capillary limit from 44 W, but the Cu equivalence decreased to 164. When the bend angle was increased to 45°, the capillary limit decreased to 40 W, but the Cu equivalence increased significantly to approximately 355. The bend angle of 60° yielded a decrease in capillary limit and Cu equivalence to 36 W and 108, respectively. However, when the pipe was bent to its final tested bend angle of 90°, the capillary limit decreased to 32 W, but the Cu equivalence increased sharply to 495. The 90° bend angle configuration reached a higher Cu equivalence than any other configuration, including the SRHP, but also exhibited the lowest capillary limit. Odhekar recognized the high Cu equivalence values seen in the experimental data of the 45° and 90° bending angles, but was unable to relate this behavior to a definitive source.

Table 2-2: List of References Dedicated to the Effects of Bending and Flattening

Reference	Shell Material and Wick Type	Outer Diameter	Working Fluid	Bending	Flattening	Grav. Orientation	Major Results
N. Sangpab [7]	Cu heat pipe with composite sintered copper powder and grooved wick	6 mm (0.236 in.)	Nitrogen (Cryogenic)	0°, 30°, 60° and 90° (Bend radius 21 mm)	Flattened thickness: 2.5, 3.0, 4.0 mm	GAN	Total Thermal Resistance (heat input < 1W) - SRHP (0°): -- 0.88 K/W - Bent 90°: -- 1.07 K/W - Flattened to 2.5 mm: -- 2.24 K/W
K.T. Lin [8]	Cu heat pipe with sintered copper powder wick	6 mm (0.236 in.)	Water	--	Flattened evap. and total heat pipe flattened. Thicknesses of 2.5 and 3.0 mm	GAN	Capillary limit, Total Thermal Resistance - SRHP: -- 28 W -- 0.3 K/W - Flat evap. (3 mm): -- 28 W -- 0.2 K/W - Totally flat (3 mm): -- 20 W -- 0.3 K/W - Totally flat (2.5 mm): -- 7.5 W -- 0.6 K/W
J. Chen [9]	Aluminum flat-plate heat pipe (FPHP) with grooved wick	50 mm [W] x 2.5 mm [Th.]	Acetone	0°, 30°, 60°, and 90°	FPHP but effects of flattening not exploited	GAN	Capillary Limit, k_{eff}, Total Thermal Resistance - Bent 0°: -- 45 W -- 1800 W/m-K -- 0.7 K/W - Bent 30°: -- 70 W -- 3000 W/m-K -- 0.5 K/W - Bent 60°: -- 70 W -- 3200 W/m-K -- 0.5 K/W - Bent 90°: -- 75 W -- 6400 W/m-K -- 0.2 K/W
H. Tao [10]	Cu heat pipe with axial grooved wick	6 mm (0.236 in.)	Water	--	Flattened thickness: 2.0, 2.5, 3.0, 3.5 mm	GAN	Capillary Limit, Total Thermal Resistance - SRHP: -- 55 W -- 0.04 K/W - Flat, 3.5 mm: -- 46 W -- 0.07 K/W - Flat, 3 mm: -- 38 W -- 0.1 K/W - Flat, 2.5 mm: -- 25 W -- 0.1 K/W - Flat, 2 mm: -- 17 W -- 0.76 K/W
D.D. Odhekar [11]	Cu heat pipe with sintered copper felt wick	6.35 mm (0.25 in.)	Water	0°, 15°, 30°, 45°, 60°, and 90°	--	GAS	Capillary Limit, Cu Equivalence - SRHP (0°): -- 36 W -- 194 - Bent 15°: -- 44 W -- 245 - Bent 30°: -- 44 W -- 164 - Bent 45°: -- 40 W -- 355 - Bent 60°: -- 36 W -- 108 - Bent 90°: -- 32 W -- 495

2.2.2 Gravitational Orientation

Although only a small portion of this research was dedicated to examining the effects of gravitational forces on the performance and limits of sintered felt wick heat pipes, a general synopsis of some relative literature has been included to provide context to the other types of research dedicated to understanding how gravity influences heat pipe behavior.

Gravitational orientation is a very important parameter to consider when exploring the behavior and capabilities of heat pipes. Depending on the wick structure, gravity can be a major contributing factor to the performance and operating range of a heat pipe. C.K. Loh and Enertron, Inc. explored the effects that gravitational orientation has on the performance of metal powder wick heat pipes [12]. In this investigation, a metal powder wick heat pipe with a diameter 6 mm was tested at incrementing heat input level and various inclination angles. The inclination angles ranged from -90° (GAD) to 90° (GAS) in rotational increments of 30° for a total of seven different gravitational configurations. Each heat pipe was tested at 5, 10, 15, 20, 25, and 30 W of heat input at each inclination angle. The performance of these heat pipes was characterized by evaluating the total temperature difference from the evaporator region to the condenser region. It was discovered that at low powers (5 W and 10 W) the inclination angle had almost no effect on the total temperature difference, which was maintained at approximately 4°C. However, for the 15 W tests, it was observed that at the inclination angles of -90° and -60°, the temperature difference increased to 12°C and 10°C, respectively, while the rest of the inclination angles yielded a temperature difference of 5°C. As the heat input was increased to 25 W, the differential temperature increase was observed at all negative value inclination angles as well as gravity neutral configuration (0° inclination angle). The heat pipe failed to operate at 25 W in the GAD configuration and exhibited a temperature difference of approximately 38°C at an inclination angle of 60°. The positive

inclination angles each exhibited a temperature difference of approximately 7°C at a heat input of 25 W. When the heat was increased to 30 W, the heat pipe failed to operate at any negative inclination angle. The temperature difference in GAN was approximately 37°C and in the positive inclination angles it was approximately 10°C. These results suggested that the metal powder wick heat pipes operated without penalty due to gravitational forces at powers < 10 W. As heat input was increased, the temperature difference penalty was seen in the negative inclination angle tests. Additionally, the heat pipes had a much lower operational range with regards to heat input for negative inclination angles.

3 FACTORS AFFECTING PERFORMANCE AND LIMITS

This chapter elaborates on the specific heat pipe design and operational parameters that were investigated. An overview of the external factors that influence heat pipe design is discussed, with an emphasis on the specific geometric modifications and configurations chosen for this study. The calculated effects of these design and operational parameters on the performance and limits of the heat pipes are discussed using theory found in literature.

3.1 External Factors, Interfaces, and Applications

In application, heat pipes almost always interface with other heat transfer devices to provide a useful thermal management design. For example, the heat pipe seen in Figure 3-1 is integrated into a personal laptop device to aid in the thermal management of the CPU.

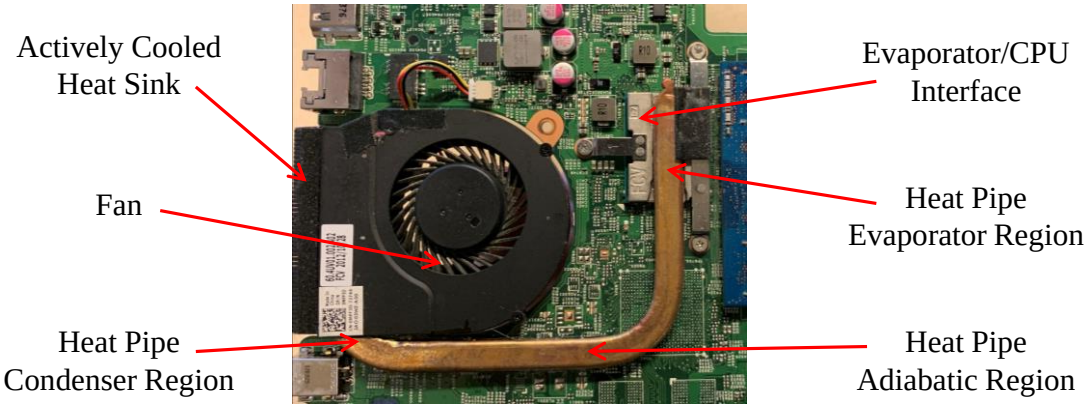

Figure 3-1: Heat Pipe Integrated onto Dell Inspiron 5423 CPU

In this thermal management system, the heat pipe operates as an efficient heat path between the high powered CPU and the actively cooled heat sink. The external factors influencing the design of the heat pipe are the CPU and the fan/heat sink assembly. The CPU influences the design

through a pre-determined operating temperature/power, geometry, and location within the electronics package. The fan/heat sink assembly influences the heat pipe design by providing a limited amount of cooling capability. In reality, the fan/heat sink assembly may be designed or selected in conjunction with the heat pipe, but the condenser region heat sink typically limits the heat pipe's capability to transfer heat at a particular temperature difference. The thermal management system shown in Figure 3-1 is very compact and requires a heat pipe to rout the waste heat from the small CPU to a location where the heat can be rejected from the system through forced convection. There are many more applications for low-temperature heat pipes besides personal electronics. Each of these applications present their own unique limitations, obstacles, and nuances dealing with the external factors and the way they interface with the heat pipe. For this reason, it is important to investigate and characterize heat pipe performance under various post-fabrication geometric modifications in order to expand the design domain of the heat pipe and the thermal management solutions as a whole.

3.2 Design Parameters Investigated

A handful of specific heat pipe design and operational parameters were selected for this study. These parameters were prioritized based on the desired operational performance information, availability of materials, application of the heat pipes, and testing feasibility. There were six relevant parameters selected for this research: diameter, flattened end condition, number of bends, bend angle, gravitational angle, and heat input. Each of these parameters was varied in order to observe the effects that they had on effective thermal conductivity, steady-state temperatures of the measured locations, and the capillary limits of the heat pipes. The diameter was varied based on COTS available Copper 110 tubes. The size scale of the electronic systems for the application

of these heat pipes influenced the decision to investigate the performance of 0.25 in., 0.375 in., and 0.5 in diameter heat pipes. The heat pipes used in this experiment were fabricated from commercially available Cu 110 tubes and were outfitted with a metal felt sintered fiber wick which was made from fibrous strands of copper. The wick was constructed by sintering the copper fibers to the inner surface of the copper tube which created a continuous, porous, inner circumferential mesh structure along the entire length of the tube. The actual porosity and fiber diameter of the wick were unknown, but the radial thickness of the wick was measured as approximately 0.0125 in. (0.3175 mm) for each heat pipe. The porosity was measured by imbibing the wicks with SF96-50 oil. The copper fiber diameters were likely somewhere between 10 and 200 μm, but were not measured directly. The wick thickness did not vary significantly between the different diameter heat pipes, but the vapor core geometry was a function of the heat pipe's length and diameter. The dimensions of each heat pipe used in this experimental investigation can be seen in Table 6-1. The heat pipes were tested horizontally in bent, flattened, and straight-round configurations, but they were not tested under combined bending and flattening.

3.2.1 Flattening the Evaporator and Condenser Regions

The flattened end condition (FEC) is a novelty of this particular research effort. The FEC is a parameter describing whether or not the evaporator and condenser regions of a heat pipe are round or flattened. As seen in Figure 3-2, there were four varied FECs in this investigation: straight-round (A), flattened evaporator (B), flattened condenser (C), and both ends flattened (D). A 0.5 in. diameter heat pipe (HP4) was flattened and tested in this study. The purpose of these tests was to observe the effective thermal conductivity, operating temperatures, and capillary limits of heat pipes with flattened evaporator and condenser regions. The 0.25 in. diameter heat pipe was not selected for flattening because it was too small a diameter to withstand flattening and still leave

ample volume in the vapor core to facilitate normal operations. The 0.375 in. diameter heat pipe was capable of withstanding flattening, but it was not included in the flattened portion of the test matrix due to lack of available materials. The evaporator and condenser regions of the 0.5 in. diameter heat pipe (HP4) were flattened to a nominal thickness of 0.25 in. using machined aluminum blocks.

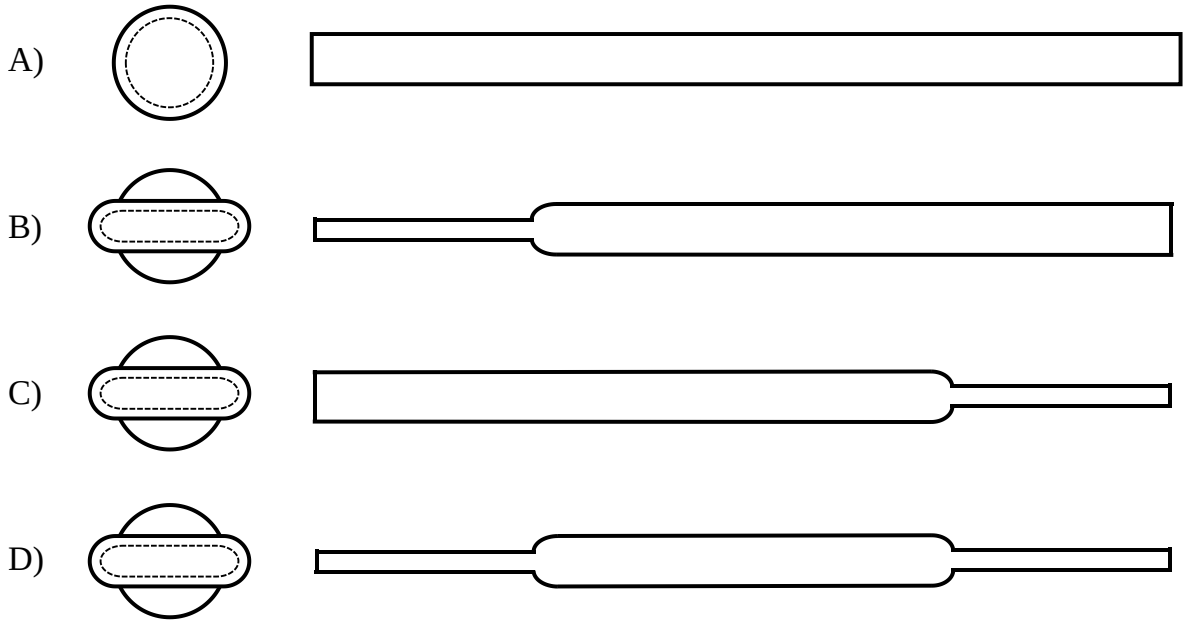

Figure 3-2: Flattened End Conditions

Exploring the effects of flattening on the performance and limits of heat pipes was an important part of this investigation because in the application of low-temperature heat pipes, a flattened surface at the interface between the heat pipe and the interfacing components will decrease the interfacial thermal resistance by increasing the surface area in contact with the heat sink or heat source. If the performance and limits of a flattened heat pipe can be understood, the acceptable design domain for many applications of these low-temperature heat pipes can be increased tremendously.

3.2.2 Bending the Adiabatic Region

Another novelty of this research effort is the investigation of how bending the adiabatic region affects the thermal performance of the Cu/water sintered wick heat pipes. Unlike most heat pipes, sintered felt wick heat pipes are capable of undergoing post-fabrication bending without compromising the structural integrity of the wick. The structure and composition of the sintered felt wick provides flexibility under strain due to bending. A heat pipe capable of undergoing bending and flattening can be designed towards a variety of applications and cater to strict weight and geometry constraints while still serving its purpose as an efficient heat path. In order to better understand the effects that bending has on the thermal performance of these heat pipes, two heat pipes of diameters 0.25 in. (HP1) and 0.375 in. (HP2) were tested under bent configurations. The purpose of these tests was to compare the effective thermal conductivity, operating temperatures, and limits of bent heat pipes to that of the same respective heat pipe in the straight-round configuration. HP1 was tested in configurations 1 through 7, as seen in Figure 3-3, and HP2 was tested in configurations 1 through 5, as seen in Figure 3-4, with configuration 1 being the straight-round configuration. The goal of these tests was to gather information about how multiple bending angles, and the magnitude of those angles, affected heat pipe performance. The heat pipes were bent using a tube bending device. The device used to bend HP1 applied a constant bend radius of 9/16 in. and the one used for HP2 applied a constant bend radius of 15/16 in.

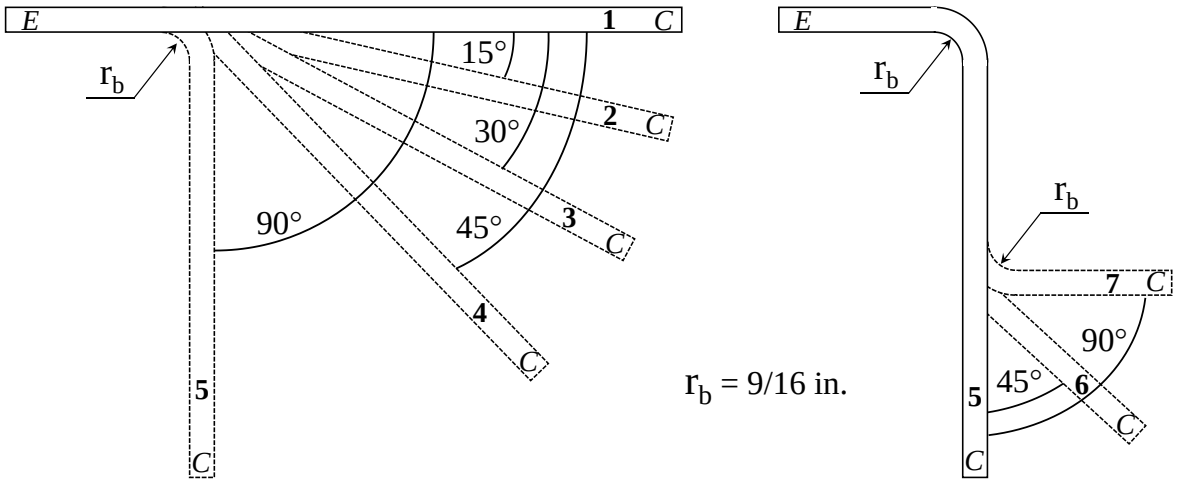

Figure 3-3: HP1 Bending Process (Top View)

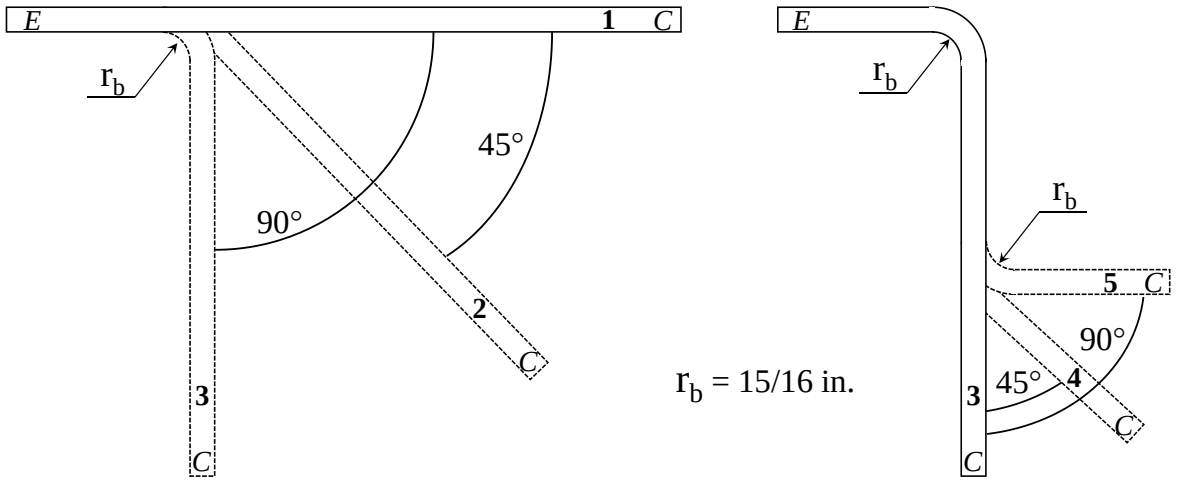

Figure 3-4: HP2 Bending Process (Top View)

3.2.3 Gravitational Orientation

Gravity plays a big role in heat pipe performance. As the liquid travels back to the evaporator region in the condenser, it must overcome all body forces acting against the capillary pumping force which results in either an enhancement or a degradation of heat pipe performance depending on the gravitational orientation. A heat pipe in gravity assist (GAS), allows the liquid in the wick

to return to the evaporator region in the direction of the body force. The assist of the gravitational force enhances the fluid flow through the wick and therefore improves the heat pipe performance. In contrast, a heat pipe in gravity adverse (GAD) must pump liquid in opposition to the gravitational force which results a reduced flow in the wick and therefore degraded heat pipe performance. A heat pipe in gravity neutral (GAN) operates with the liquid and vapor flow paths normal to the gravitational force. Therefore, the body force has a negligible influence on the heat pipe's performance. Each gravitational orientation is illustrated in Figure 3-5.

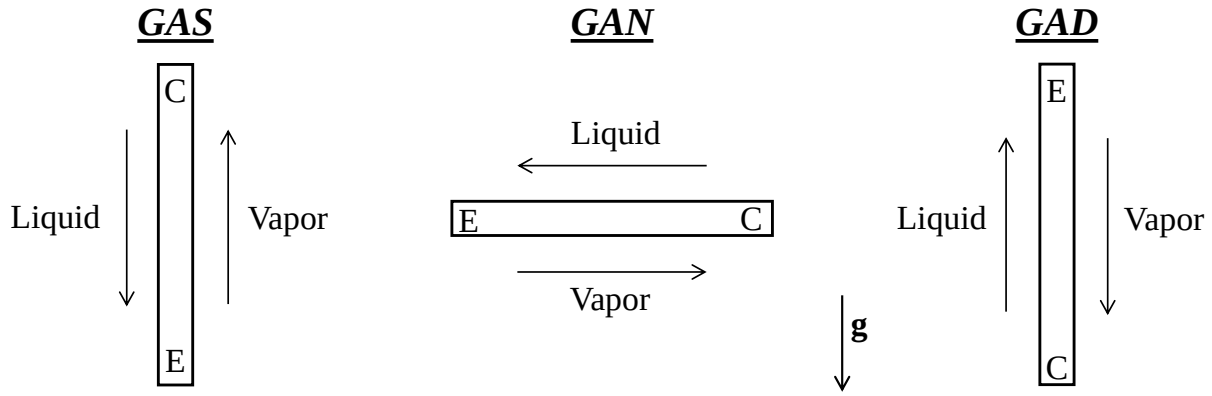

Figure 3-5: Gravitational Orientations

In this research, the SRHPs were tested in GAN, GAS, and GAD until their capillary limits were reached. The observed capillary limit and the effective thermal conductivity behavior was much different in each gravitational orientation. The geometrically modified heat pipes were tested in the GAN configuration only.

3.2.4 Parameters Held Constant

Although heat pipes are relatively simple systems with only three major components, there is a wide variety of variable parameters to explore. For the purposes of this study, the only independent parameters were diameter, FEC, number of bends, bend angle, gravitational orientation, and heat

load. Other heat pipe research may involve changing materials of the shell, wick, and/or working fluid, or varying other dimensional quantities. Some examples of heat pipe parameters that were not varied in this research are wick parameters (porosity, thickness, and material), heat pipe shell material, working fluid parameters (charge ratio and choice of fluid), evaporator, condenser, and adiabatic lengths, severity of flattening, and several others. As heat pipe research becomes increasingly more popular, these parameters among others may be exploited to enhance the technology and its application.

3.3 Effects of Bending the Adiabatic Region

A preliminary investigation of the effects of bending the adiabatic region of the heat pipe was performed by analyzing the liquid and vapor flow within the wick and vapor core, respectively. The dimensions of the heat pipe used for this analysis were the same as HP1. Since the internal wick geometry of HP1 was unknown, estimations of the dimensions were made and results were developed for a range of wick fiber diameters and porosities.

3.3.1 Vapor Core Theoretical Analysis

The vapor core radial boundary is defined by the internal diameter of the wick. For a standard 0.25 in. heat pipe with a sintered felt wick, a good estimation of this value is approximately 0.145 in. (R_v = 0.0725 in.). Within this cylindrical core, vapor flows from the evaporator region to the condenser region due to the pressure drop created by the heat flux applied to the evaporator. The steady-state pressure and temperature drop within the vapor core was analyzed using correlations developed by Fagrhi [13]. The purpose of this analysis was to observe the temperature difference of the vapor in a straight-round heat pipe to determine if bending could affect this difference by increasing the pressure drop within the vapor core. One of the major assumptions supporting this

analysis was that for laminar, incompressible, internal flow through a cylindrical duct, the working fluid could be treated as a saturated vapor in the vapor core region. This assumption, while not representative of reality, was validated by examining that the compressibility factor of the working fluid at various temperatures was always close to unity. This analysis provides theoretical trends for heat pipe temperature difference penalties due to bending. To determine the vapor pressure drop in terms of the heat input to the heat pipe, a relation between the radial Reynolds number and the heat input, as well as the adiabatic mean velocity was derived by an energy balance in each section of the heat pipe at steady-state [13]. This analysis was performed for a range of heat input levels and vapor temperatures. The influence of temperature on the thermophysical properties of the water vapor was taken into account. First, the radial Reynolds numbers in the evaporator and condenser regions were calculated using equations (3-1) and (3-2).

$$\mathrm{Re_e} = \frac{\mathrm{Q_{in}}}{2\pi \mathrm{L_e} h_{fg} \mu_v} \tag{3-1}$$

$$\mathrm{Re_c} = \frac{\mathrm{Q_{in}}}{2\pi \mathrm{L_c} h_{fg} \mu_v} \tag{3-2}$$

The average vapor velocity was then calculated, using equation (3-3), which allowed for the axial Reynolds number within the adiabatic region to be calculated, using equation (3-4) [13].

$$\mathrm{V_{avg}} = \frac{\mathrm{Q_{in}}}{\rho_v \pi {\mathrm{R_v}}^2 h_{fg}} \tag{3-3}$$

$$\mathrm{Re_{ad}} = \frac{\rho_v \mathrm{V_{avg}} \mathrm{D_{h,v}}}{\mu_v} \tag{3-4}$$

It was discovered that the Reynolds numbers represented laminar flow in all regions of the heat pipe. The pressure drop in the evaporator, condenser, and adiabatic regions was then calculated using equations (3-5), (3-6), and (3-7), respectively [13].

$$\Delta P_e = \left(-8|Re_e| - \frac{16}{3}{Re_e}^2\right)\left(\frac{{\mu_v}^2}{\rho_v {R_v}^2}\right){L_e}^2 \tag{3-5}$$

$$\Delta P_c = \left(-8|Re_c| - \frac{16}{3}{Re_c}^2\right)\left(\frac{{\mu_v}^2}{\rho_v {R_v}^2}\right){L_c}^2 + \left(\frac{16}{3}|Re_c| - 8\right)\left(\frac{\mu_v V_{avg}}{{R_v}^2}\right) \tag{3-6}$$

$$\Delta P_{ad} = \left(\frac{-8\mu_v V_{avg}}{{R_v}^2}\right)L_{ad} \tag{3-7}$$

The total pressure drop was calculated as the sum of the pressure drops in each region of the heat pipe, as seen in equation (3-8). Once the total pressure drop was known, the total temperature difference within the vapor core for a SRHP was calculated using equation (3-9) where the change in temperature relative to the change in pressure was determined by the Clausius–Clapeyron equation.

$$\Delta P_{tot} = \Delta P_e + \Delta P_{ad} + \Delta P_c \tag{3-8}$$

$$\Delta T_{tot} = \Delta P_{tot}\left(\frac{dT}{dP}\right)_{sat} \tag{3-9}$$

The correlations above were used to calculate the theoretical temperature difference in a straight-round heat pipe. In order to calculate this temperature difference in a bent heat pipe, equation (3-7) was rearranged in terms of the friction factor as seen in equation (3-10).

$$\Delta P_{ad} = f{V_{avg}}^2 \rho \frac{L_a}{R_v} \tag{3-10}$$

This form of the adiabatic pressure drop allows for the substitution of different friction factors. When the Fanning friction factor is employed, this equation yields the pressure drop for a SRHP. However, the additional pressure drop in the adiabatic region due to bending can be accounted for by substituting in the bending friction factor, which can be calculated using equation (3-11) [14].

$$\frac{f_b}{f} = \left\{1 - \left[1 - \left(\frac{11.6}{De}\right)^{0.45}\right]^{2.222}\right\}^{-1} \tag{3-11}$$

This equation is a function of the Dean number and calculates friction factor of internal flow through a bent circular duct for De < 1000. The Dean number characterizes the effects of an adverse pressure gradient generated from the curvature of the duct. This non-dimensional parameter is a function of the Reynold's number, the radius of curvature of the bend, and the hydraulic diameter of the duct, as seen in equation (3-12).

$$De = Re\sqrt{\frac{R_v}{r_b}} \tag{3-12}$$

It can be seen that the correlation for bending friction factor is independent of the bending angle. This correlation was developed for flow through a continuous helical coil. Since the heat pipe adiabatic length is not long enough to allow for flow recovery after a bend, this formulation can be applied to characterize the general pressure drop due to bending based on the hydraulic diameter of the heat pipe vapor core and the bending radius. The bending friction factor was implemented into equation (3-10) to calculate the adiabatic region pressure drop in a bent heat pipe. This correlation accounts for the additional pressure drop due to bending by assuming that the vapor flow field is affected from the beginning of the bend until the end of the remaining adiabatic region. Since the heat pipes in this research were bent just outside of the evaporator region, the effective length used in this calculation was the entire adiabatic length of the heat pipe, as seen in Figure 3-6.

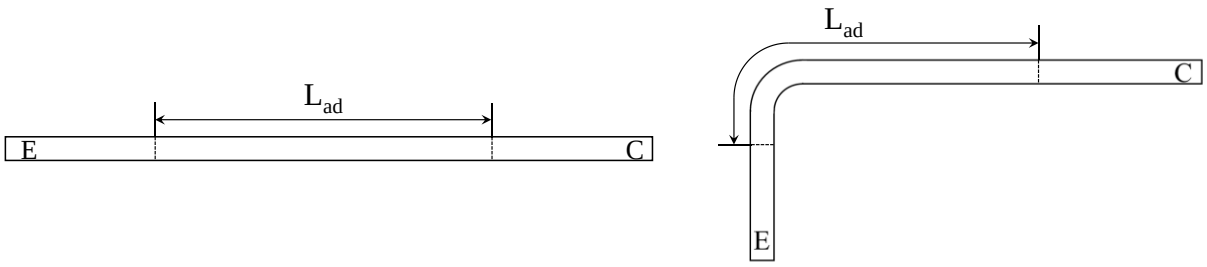

Figure 3-6: Affected Length of Bending

The temperature drop along the heat pipe is proportional to the total thermal resistance. A comparison of the total resistance penalty due to bending between this theoretical exercise and the experimental data can be found in Chapter 6.

3.3.2 Theoretical Analysis of Liquid Flow in the Wick Structure

In addition to the vapor core, the wick structure was analyzed to develop a baseline understanding of the effects of liquid flow on the thermal behavior of sintered felt wick heat pipes. A closed-form solution for the liquid capillary limit within a round heat pipe was suggested by Faghri. This solution holds true under the following assumptions [13]:

- Laminar incompressible vapor flow in the core
- Pressure drops due to evaporation and condensation at liquid-vapor interface are neglected
- Uniform heating distribution along the evaporator ad condenser sections
- A_w and K remain constant along the length of the heat pipe

The equations used to derive the formulation for the liquid capillary limit can be seen in equations (3-13) through (3-18). The wick permeability was calculated using equations (3-13) and (3-14).

$$K = \frac{A(X^2-1)}{X^2+1} \tag{3-13}$$

$$X = 1 + \frac{BD_f{}^2\varphi^3}{(1-\varphi)^2} \tag{3-14}$$

The effective pore radius was calculated using equation (3-15).

$$r_{eff} = \frac{D_f}{2(1-\varphi)} \tag{3-15}$$

Once the permeability and effective pore radius were known, the liquid capillary limit was calculated using equations (3-16), (3-17), and (3-18).

$$F_l = \frac{\mu_l}{\rho_l A_w K h_{fg}} \tag{3-16}$$

$$F_v = \frac{(f_s Re_{z,v})\mu_v}{2{R_v}^2 A_v \rho_v h_{fg}} \tag{3-17}$$

$$(QL)_{cap,max} = \frac{\frac{2\sigma}{r_{eff}} - \rho_l g L_{tot} \sin(\phi)}{F_l + F_v} \tag{3-18}$$

The limit was calculated by varying the wick fiber diameter, porosity, and working fluid temperature for a 0.25 in. diameter Cu/water sintered wick heat pipe. Table 3-1 shows the working fluid properties and Table 3-2 shows the container and wick properties used in this analysis. Figure 3-7 through Figure 3-10 display the trends of the maximum liquid capillary limit as a function of the wick porosity, wick fiber diameters, and working fluid temperature. The values from this analysis depend on the specific heat pipe design and wick properties. The results shown in Figure 3-7 through Figure 3-10 are based upon the properties and values given in Table 3-2.

Table 3-1: Working Fluid Properties for Liquid Capillary Limit Analysis

T_o °C	h_{fg} kJ/kg	ρ_l kg/m^3	ρ_v kg/m^3	k_l W/m°C	μ_l (Pa-s) * 10^{-3}	μ_v (Pa-s) * 10^{-3}	P_v Bar	σ_l N/m
20	2448	998	0.02	0.603	1.00	0.0096	0.02	0.0728
40	2402	992	0.05	0.630	0.65	0.0104	0.07	0.0696
60	2359	983	0.13	0.649	0.47	0.0112	0.20	0.0662
80	2309	972	0.29	0.668	0.36	0.0119	0.47	0.0626
100	2258	958	0.60	0.680	0.28	0.0127	1.01	0.0589
120	2200	945	1.12	0.682	0.23	0.0134	2.02	0.0550
140	2139	928	1.99	0.683	0.20	0.0141	3.90	0.0506
160	2074	909	3.27	0.679	0.17	0.0149	6.44	0.0466

Table 3-2: Heat Pipe Container and Wick Properties for Liquid Capillary Limit Analysis

Heat Pipe Container		Micro-fibrous Metallic Felt Wick and Vapor Core	
$D_{o,HP}$ [cm]	0.635	L_f/D_f	150
$D_{i,HP}$ [cm]	0.432	Cu Thermal Conductivity [W/m-K]	390
L_{tot} [cm]	29.845	$D_{o,w}$ [cm]	0.432
L_e [cm]	5.080	$D_{i,w}$ [cm]	0.368
L_c [cm]	8.128	R_v [cm]	0.184
L_{eff} [cm]	23.241	A_w [cm^2]	0.040
ϕ [rad.]	0	V_w [cm^3]	1.191
Cu Thermal Conductivity [W/m-K]	390	A_v [cm^2]	0.107
		A, Constant [m^2]	6.00E-10
		B, Constant [m^{-2}]	3.30E+7
		$f_s Re_{z,v}$	16

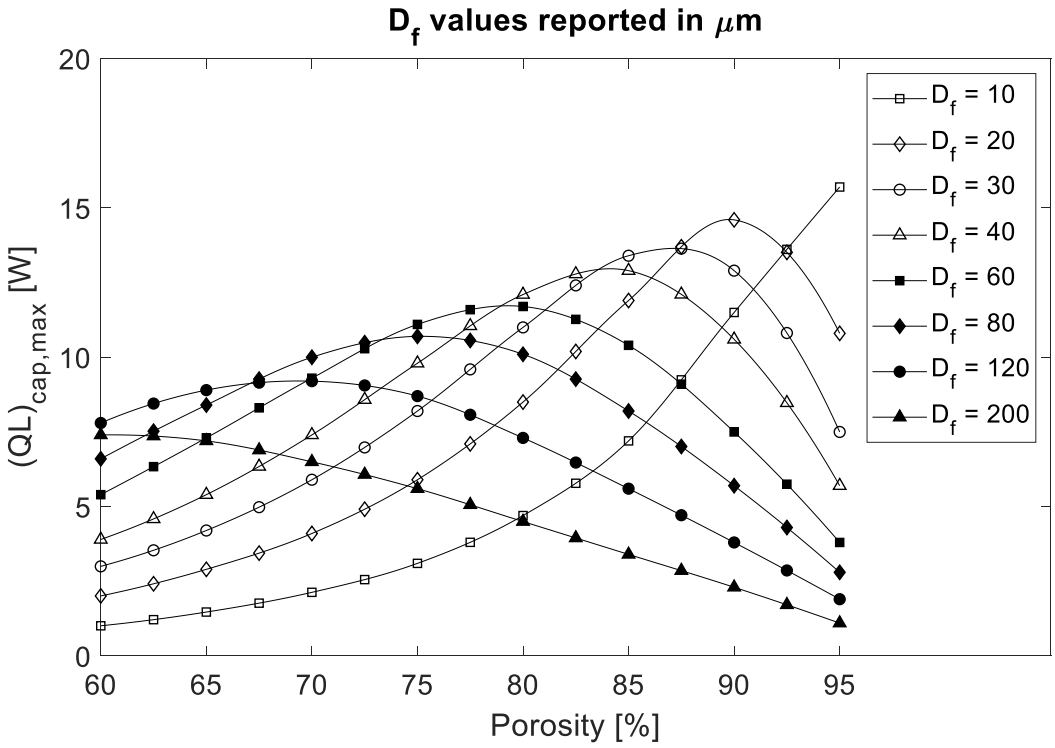

Figure 3-7: Liquid Capillary Limit: T_l = 20°C

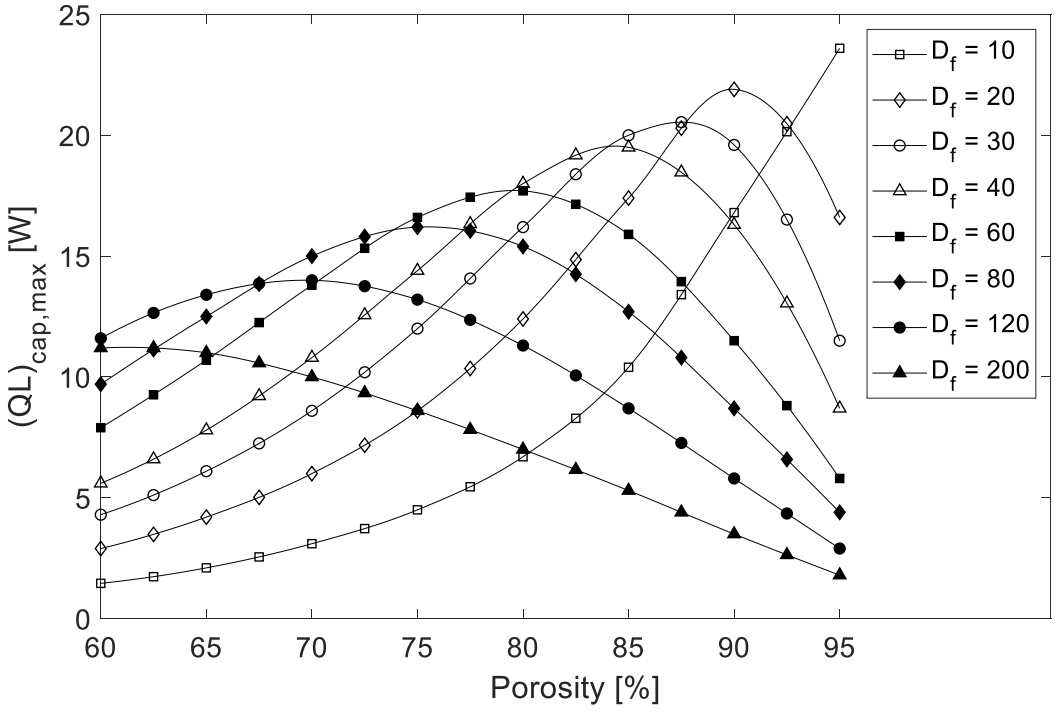

Figure 3-8: Liquid Capillary Limit: T_l = 40°C

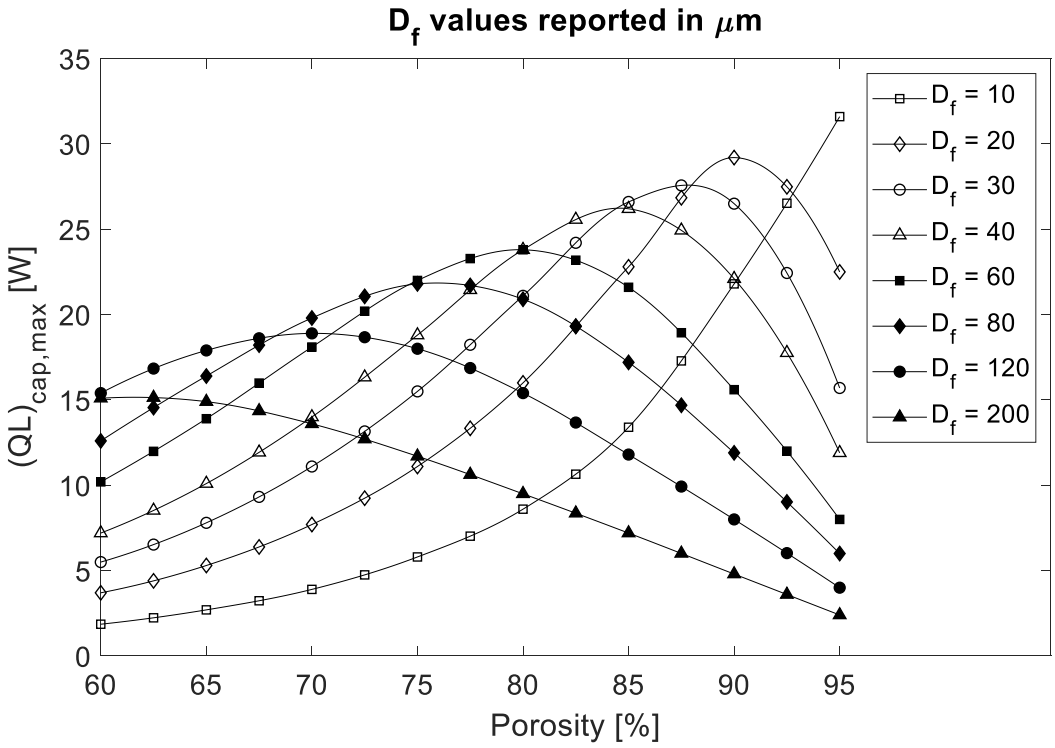

Figure 3-9: Liquid Capillary Limit: T_l = 60°C

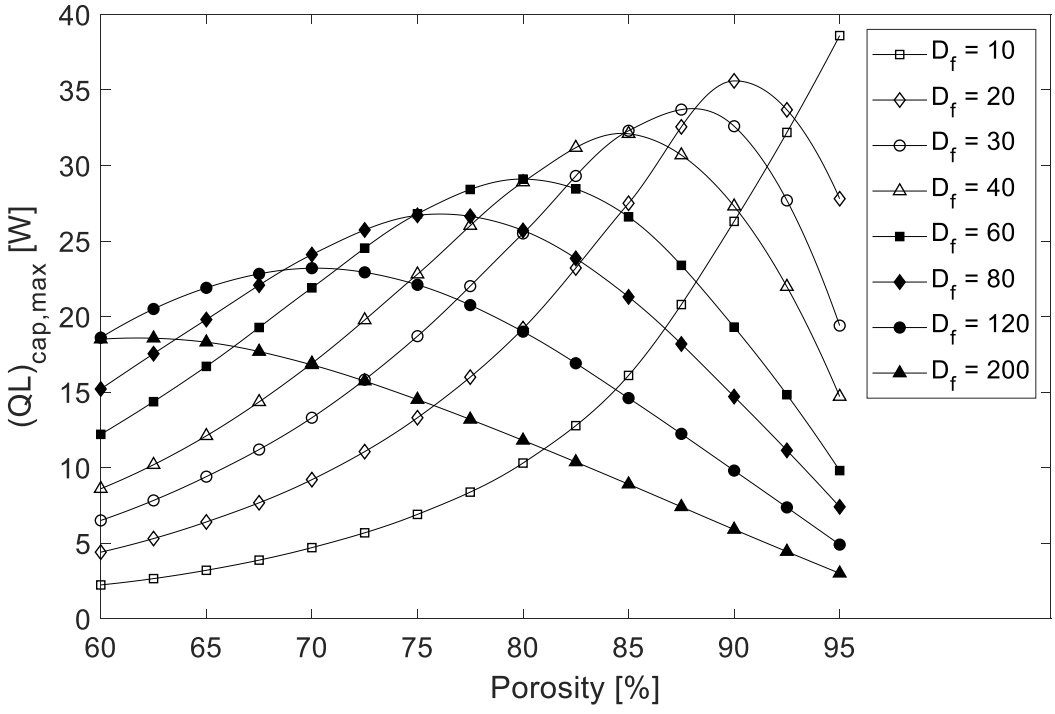

Figure 3-10: Liquid Capillary Limit: T_l = 80°C

It can be seen from the trends in these figures that the liquid capillary limit is a strong function of porosity, wick fiber diameter, and temperature of the working fluid. The liquid capillary limit follows a constant trend, with respect to increasing porosity and fiber diameter, as temperature increases, but varies in magnitude. For example, at each working fluid temperature, the capillary limit increases rapidly with increasing porosity for the smallest diameter fiber (10 μm), but the maximum capillary limit increases with increasing fluid temperature: 15 W at 20°C, 24 W at 40°C , 33 W at 60°C, and 39 W at 80°C. Although the capillary limit increases with porosity for the 10 μm wick fiber, the larger wick fibers achieve a local maximum capillary limit that does not occur at the highest porosity value. It can be seen by examining the plots above that the larger the wick fiber diameter is, the worse it performs at high porosities for a given working fluid temperature. Based on these observed trends, it was concluded that the most ideal wick structure for most operational temperatures in gravity neutral is a combination of a small diameter mesh fiber and a very high wick porosity. These smaller diameter fibers would be more susceptible to deformation and breaking under post-fabrication bending. It was observed in this theoretical analysis that heat pipe performance and capillary limit is a strong function of the wick fiber diameter, porosity, and working fluid temperature. Based on this observation, it was assumed that these effects due to bending are largely influenced by localized changes in the liquid flowing through the wick.

3.4 Effects of Flattening the Evaporator/Condenser

In addition to researching the effects of bending the adiabatic region, the effects of flattening the evaporator and condenser regions was also of interest. In this investigation, the evaporator and condenser regions of a 0.5 in. diameter heat pipe (HP4) were flattened to approximately 50% of their original outer diameter, as seen in Figure 3-11. This corresponds to a flattening ratio of 0.5.

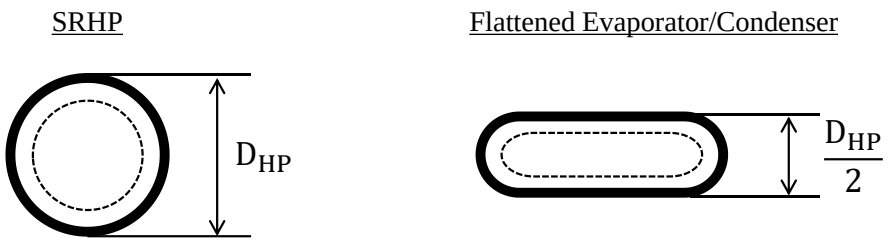

Figure 3-11: Flattening Ratio

In the literature review, the results of K.T Lin's investigation into the effects of flattening Cu/water sintered wick heat pipes were presented. Lin suggested that flattening a heat pipe would result in a degradation of the capillary limit and an increase in the total thermal resistance of the heat pipe [8]. The rationale in support of these results was that at certain flatness ratios, the liquid begins to clog the wick in the condenser region which prevents the liquid from returning to the evaporator region which then results in a gradual dry-out of the heat pipe and an operational failure.

A separate investigation, also dedicated to exploring the influence of flattening on sintered copper wick heat pipes, was conducted by W. Intagun [15]. This study compared a 3D finite-element model of a flattened heat pipe to experimental data. In this investigation, it was discovered that the flattening had a significant effect on the radial resistance and therefore the external wall temperature. Intagun flattened a heat pipe, with an original outer diameter of 6 mm (0.237 in.), and tested it to collect experimental data that was compared to the numerical model. The experimental results showed that when the heat pipe had a flatness ratio of 66% (4 mm final thickness), the temperature difference between the evaporator and condenser region surfaces was approximately 20°C. However, when the heat pipe had a flatness ratio of 50% (3 mm final thickness), the temperature difference decreased to approximately 16°C. When the heat pipe was flattened even further to a flatness ratio of 41.6% (2.5 mm final thickness), the temperature difference increased to be approximately 23°C. These results suggested that flattening affected the operating

temperature difference of the heat pipe and therefore the effective thermal conductivity. It was determined that the decrease in effective thermal conductivity was due to the pressure drop in the vapor core increasing which resulted in a larger axial temperature difference. The conclusion from this investigation was that the increase in the contact surface area between the outer shell and the heat sink due to flattening aided in reducing the radial resistance of the heat pipe and allowed for enhanced heat transfer into and out of the evaporator and condenser region. However, there existed an optimum flatness ratio which offered the ideal surface area and vapor core volume to allow for enhanced heat transfer without inhibiting the vapor flow within the heat pipe.

Since HP4 had a flatness ratio of 50%, it was assumed that the vapor core was still active. Intagun's conclusion that flattening would increase the contact area between the condenser region and the heat sink was applicable under the assumption that the heat sink was applied on a planar surface tangential to the surface of the condenser region shell. Since the heat sink boundary condition for HP4 was applied circumferentially over the entire surface of the condenser region, the contact area did not increase with flattening since the condenser region perimeter was unchanging. Therefore, the benefit of increased contact area leading to decreased radial thermal resistance due to flattening would not have been exploited in the test set-up used for the current experimental investigation. The test set-up used in the current research provided a constant heat flux boundary condition at the evaporator region and a constant temperature boundary condition at the condenser region. This meant that the heat input from the linear power supply was forced in through the evaporator region regardless of the set temperature at the condenser region. Therefore, the axial temperature difference on the outer surface of the heat pipe was controlled and limited by the temperature difference between the surface of the condenser region of the heat pipe and the acting heat sink. During testing the heat sink was held at a constant temperature of 20°C.

4 TESTING

This chapter provides a description of the experimental approach used to investigating the effects of various geometric modifications and configurations on the performance and limits of the heat pipes. An overview of the test matrix, test set-up, and heat pipe preparation and testing procedures is presented.

4.1 Test Matrix

A test matrix consisting of varying heat pipe design parameters was constructed to facilitate the development of an empirical database that would serve to thoroughly represent the effects that bending and flattening have on the thermal conductance and operational limits of Cu/water sintered wick heat pipes. This test matrix, seen in Figure 4-1, was developed based on the six pre-determined major parameters of interest: diameter, flattened end condition, number of bends, bend angle, gravitational angle, and heat input. Each item in Figure 4-1 marked with * or ** was tested at incrementing heat input levels until the capillary limit was reached.

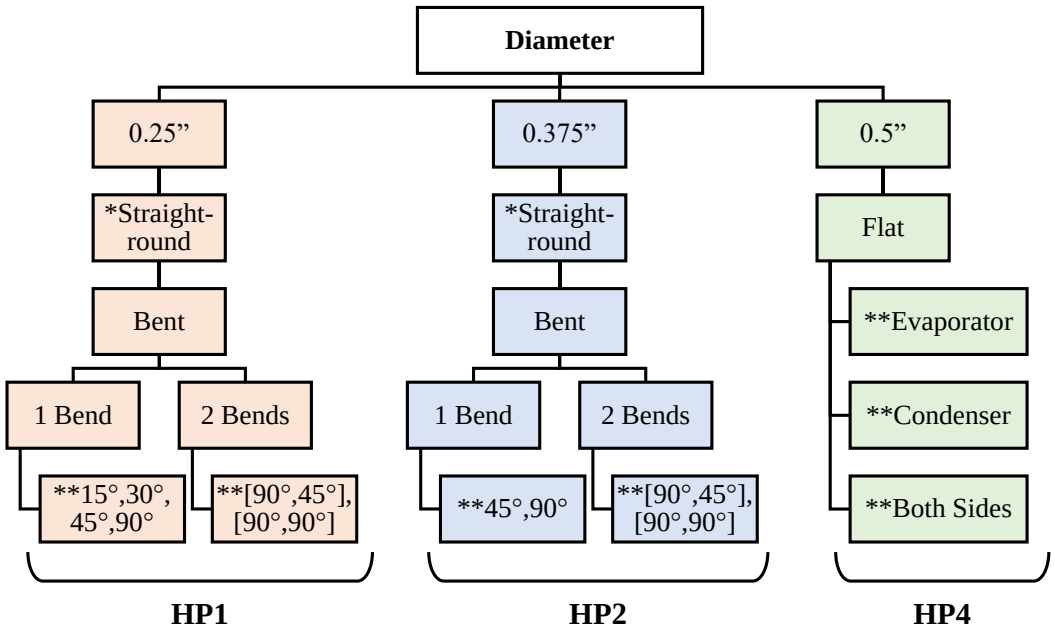

*Tested in GAN, GAS, and GAD
** Tested in GAN only

Figure 4-1: Test Matrix

Each diameter heat pipe, with the available materials, was tested in a straight-round configuration to gather information about unmodified thermal performance. This information also served as a benchmark for the performance values of the geometrically modified heat pipes. By benchmarking the performance of the heat pipes in the straight-round configuration, the effects of bending and flattening were discernable in the test data while additionally removing most of the systematic biases inherent to the test rig. Although any and all systematic biases were assumed to be nominally constant with each test that is run, a thorough parasitic loss model was incorporated to account for these biases and provide more realistic performance data. It should be noted that HP4 was not tested in a straight-round configuration due to lack of available materials. The bending angles that were chosen served to minimize the number of tests needed to comprehensively observe the effects of single bent heat pipes and heat pipes with multiple bends.

4.2 Test Set-up

Each heat pipe was cleansed, filled, instrumented, and tested in-house at AU TherMML Laboratory. Careful and thorough cleaning methods were applied to all test articles to minimize the unknown temperature measurement error due to external oxidation or foreign substance as well as reduce the impedance of axial fluid flow through the wick due to debris and miscellaneous substances. The test set-up consisted of the physical test rig, the test articles, and the DAQ equipment and instrumentation. All of test articles were tested in the same test rig, each with their own set of thermocouples. By testing each heat pipe in the same test system and under the same conditions, any systematic bias on the results was essentially canceled out.

A non-dimensional performance parameter known as copper (Cu) equivalence was used to characterize the effective thermal conductivity of the heat pipes. A detailed description of the meaning of this parameter can be found in Chapter 5. By measuring heat pipe thermal performance in terms of Cu equivalence, the effects that bending and flattening had on the effective thermal conductivity of the heat pipe were isolated from any other forms of systematic bias through test system inefficiencies or measurement error. The copper rods used to establish Cu equivalence were also evaluated for thermal conductivity at incrementing heat input using the same heat pipe test system.

4.2.1 Test Rig Description

The test rig, seen in Figure 4-2, consisted of a heat pipe test article, a heat pipe test stand, foam insulation over the adiabatic region of the test article, ceramic insulation over the evaporator region of the test article, cellulose insulation to seal up gaps between the interface of the heat pipe with the ceramic and foam insulation, a 30V-10A linear power supply with a Nichrome wire heating

element, an IcePoint Cell for thermocouple ground reference, a condenser bulb, a constant temperature water pump routed through the condenser bulb, a Keysight 34980A DAQ unit, three RTDs monitoring external temperature conditions, six T-type thermocouples along the axial direction of the test article, and two T-type thermocouple probes monitoring the condenser bulb flow temperature. Each T-type thermocouple was fabricated in-house at the AU TherMML Laboratory.

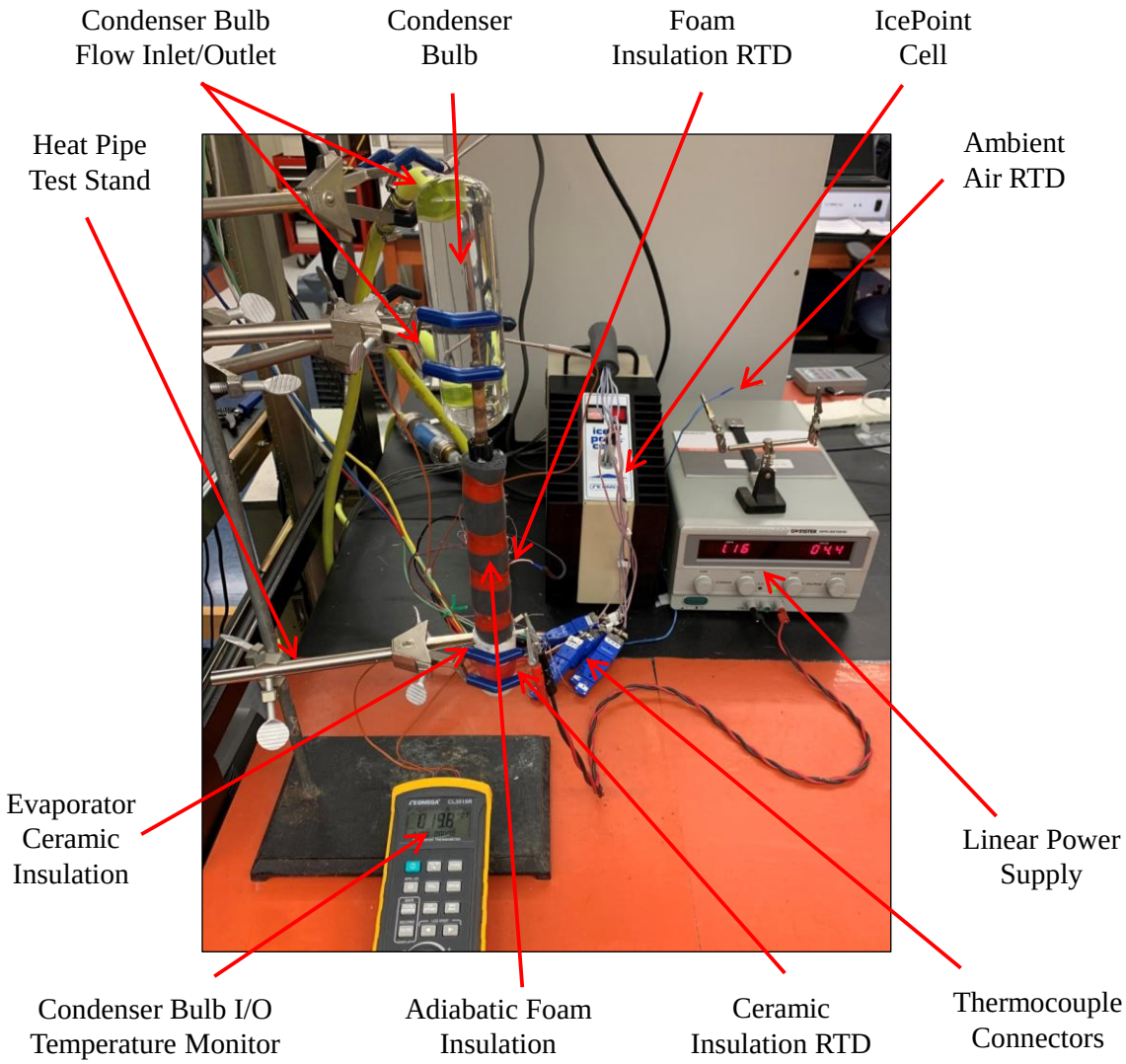

Figure 4-2: Test Set-up

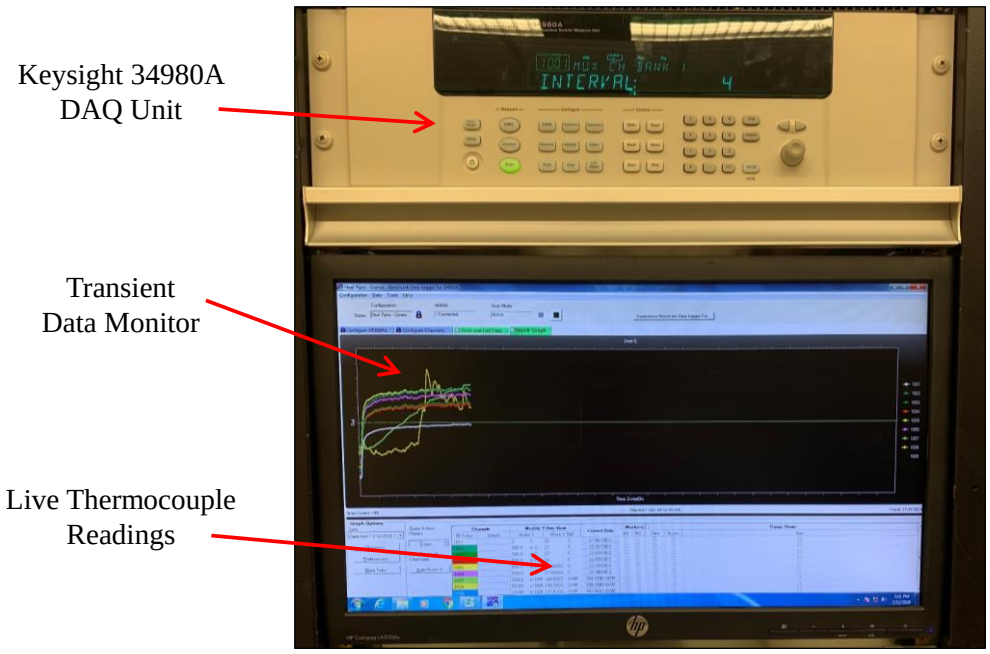

Figure 4-3: DAQ Unit and Data Interface

This test set-up facilitated testing heat pipes of varying sizes at controlled heat input levels, gravitational configurations, and all other parameters of interest. As seen in Figure 4-4, the foam and ceramic insulation materials were each instrumented with a 4-wire RTD to monitor external temperatures used in the parasitic loss model. Thermocouples 2-6 were instrumented along the axial direction of the heat pipe on the surface of the adiabatic region. This allowed the test conductor to monitor the transient response of the adiabatic region of the heat pipe during test operations. Additionally, this set-up provided steady-state discrete temperature data that was used to approximate the axial temperature gradient of the heat pipe for the effective thermal conductivity calculations. Thermocouple 1 was located on the leading edge of the evaporator region and served to monitor the transient behavior of the maximum evaporator temperature. The temperature at this location was monitored in order to visually determine the time at which the heat pipe had reached the capillary limit for each test. This method of determining the capillary limit is explained in detail in Chapter 6.

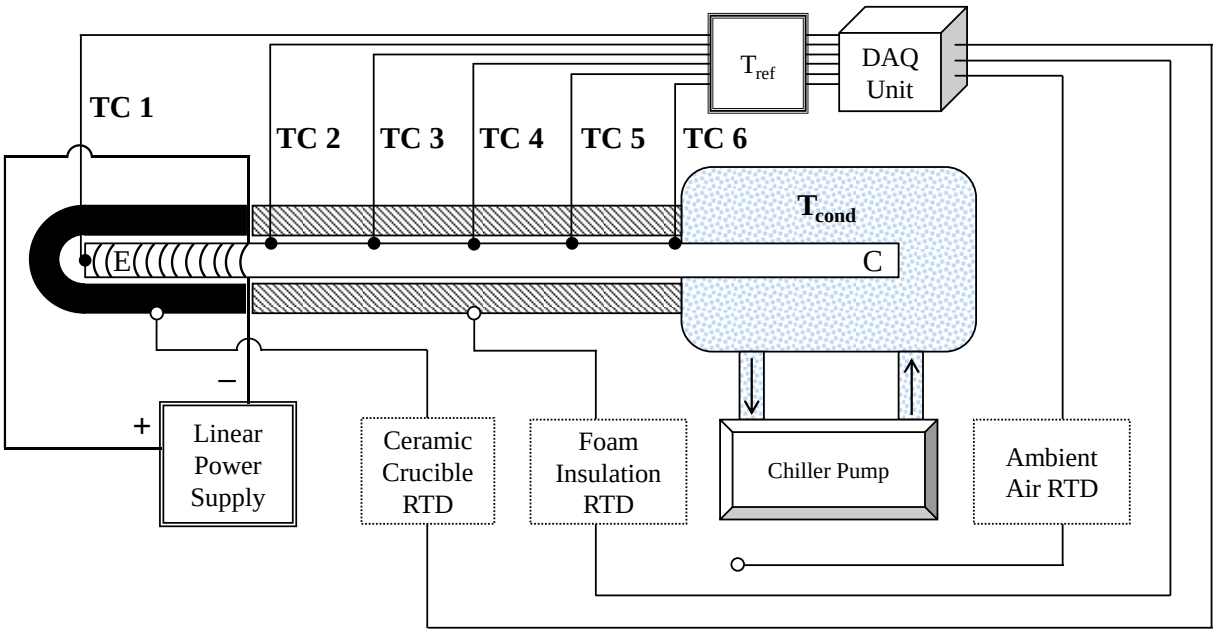

Figure 4-4: Test Article Instrumentation Schematic

4.2.2 DAQ Description

The Keysight 34980A Multifunction Switch DAQ unit was responsible for the automated recording of transient temperature data from thermocouples 1-6 and the three RTDs. The 34980A is an 8-slot mainframe with a 2-wire multiplexer (4-wire optional). The DAQ unit recorded data at a period of 5 s. The Keysight DAQ unit interfaced with 34980A Benchlink Data Logger software for real time data monitoring and logging. Upon completion of each test run, the transient temperature data files were exported through the Benchlink software in comma separated value (csv) files. The manual data recorded by the test conductor was logged using MS Excel 2016. Both the csv files and the MS Excel Worksheet files interfaced with MATLAB R2018a during the data reduction and analysis process, which is further discussed in Chapter 5.

4.3 Preparation and Fill Procedure

The heat pipe fill procedure was a preliminary part of the test procedure that consisted of carefully filling each heat pipe test article with the correct amount of water in order to ensure that they operate correctly. Since the wick thickness, porosity, permeability, and pore size were not definitively known, the charge mass for each heat pipe was experimentally calculated using a null heat pipe that was not used for performance testing in this research. The null heat pipe had a length ($L_{ref,HP}$) of 480 mm (18.9 in.) and a diameter ($D_{ref,HP}$) of 9.525 mm (0.375 in.). The null heat pipe was vacuumed and emptied and the weight was recorded. It was then filled with SF96-50 oil which had a known density of 0.969 g/mL. It was assumed that the oil wet the wick completely and that any excess oil dripped out of the open end of the null heat pipe. This assumption meant that the remaining oil within the wick structure fully populated the porous regions of the wick. After the wick of the null heat pipe was assumed to be fully populated with oil, the heat pipe was weighed again. The difference between the weight of the oil-filled heat pipe and the empty heat pipe was calculated. This weight difference represented the total weight of the oil that fully populated the wick. Once the weight of the oil within the wick was known, the volume (V_{oil}) was then calculated by dividing its mass by its density. This volume represented the porous volume of the sintered felt wick. Since the test articles all had different lengths and diameters than the null heat pipe, equation (4-1) was employed to calculate the porous wick volumes of HP1, HP2, and HP4.

$$V_{porous,wick} = V_{oil}\left(\frac{L_{tot}}{L_{ref,HP}}\right)\left(\frac{D_{HP}}{D_{ref,HP}}\right)^2 \tag{4-1}$$

This equation represents the porous wick volume as a function of the total length and diameter of the heat pipes, where the lengths are linearly proportional and the diameters are squarely proportional. Assuming that the oil fully wet the porous regions of the wick, the charge mass of

the deionized water for each heat pipe was then calculated by multiplying the heat pipe's respective porous wick volume by the density of water, 0.997 g/mL. The fully documented fill procedure can be seen in Appendix A.

4.4 Test Procedure

All heat pipe test articles were tested using the same procedure. This procedure was created to ensure that each heat pipe was tested under constant, repeatable conditions. The test procedure yielded a single data file that represents heat pipe transient and steady-state behavior at incrementing heat input levels. The procedure is capable of being scaled to accommodate a larger test matrix in the future.

4.5 Test Duration and Uniformity

For the sake of future repeatability and scalability, each test was conducted under the same conditions and format. Each test began by applying an initial, small amount of power (between 4 and 10 W depending on the heat pipe) to the evaporator region of the heat pipe. As the entire test system achieved steady-state, the conditions were documented. The power level was then increased and the system was allowed to reach steady-state at the higher heat input level. This process was repeated until the heat pipe's capillary limit was reached. Both the steady-state conditions and the capillary limit were determined by visual inspection of the transient data profiles. During these tests, the DAQ unit recorded transient temperature data of each thermocouple and RTD at a period of 5 s. The input power levels and time markers of the changes in power level were recorded manually for each test. The inlet and outlet temperature of the water flowing through the condenser bulb was also monitored to ensure that the heat sink temperature of 20°C was maintained for each test. This form of testing and data acquisition provided a time

efficient way of collecting a sufficient amount of data which was used to fully characterize the transient and steady-state behavior of the heat pipe under a range of heat input levels. One of the major objectives of this research, as formally stated, was to provide a fundamental database representing heat pipe performance and limits within the pre-determined boundaries of each of the varied parameters: diameter, FEC, bend number, bend angle, gravitational orientation, and heat applied. The test set-up and procedure and the data reduction software tool developed in MATLAB R2018a, were designed to accommodate the expansion of this database by providing the means to include a wider range of independent heat pipe parameters.

5 DATA REDUCTION

This chapter discusses the methods that were used to evaluate heat pipe performance and limits using experimental data. An overview of the data reduction process, analysis program, physical modeling of the test system, performance parameter evaluation, and data uncertainty analysis is presented.

5.1 Performance Evaluation

Heat pipes can be compared and evaluated for a range of performance qualities. One of the most common qualities of interest for heat pipes is effective thermal conductivity. This performance quality represents a heat pipe's capability to transfer a specific amount of thermal energy at a particular temperature difference. Heat pipes can exhibit effective thermal conductivities orders of magnitude greater than copper. The effective thermal conductivity of a heat pipe is calculated by measuring the steady-state temperature gradient between the evaporator and the condenser and evaluating for the k_{eff} value using Fourier's conduction law, as seen in equation (5-1). In this formulation of Fourier's law, Q_{actual} represents the amount of heat applied to the evaporator region of the heat pipe, A_c represents the cross-sectional area of the heat pipe determined by its outer shell diameter, and dT/dx represents the steady-state axial temperature gradient between the evaporator and condenser regions of the heat pipe.

$$k_{eff} = \frac{Q_{actual}}{A_c * \frac{dT}{dx}} \tag{5-1}$$

5.1.1 Copper Equivalence

Although the effective thermal conductivity does provide a metric that can be used to exploit the effects that bending and flattening have on heat pipe performance, a more useful metric can be employed when dealing with experimental data. This metric is known as copper (Cu) equivalence. Cu equivalence is a non-dimensional parameter that directly compares the approximated effective thermal conductivity of a heat pipe to the thermal conductivity of an equivalent copper rod, as seen in equation (5-2). Three Cu 110 rods of diameters 0.25 in., 0.375 in., and 0.5 in., were instrumented and tested in the same manner and process as the heat pipes. By comparing the effective thermal conductivity of heat pipes to the approximated thermal conductivity of similar copper rods, it was assumed that most systematic biases were removed and the true effects of the geometric modifications could be observed through the establishment of a trustworthy data benchmark.

$$\text{Cu Equivalence} = \frac{k_{eff}}{k_{Cu}} \tag{5-2}$$

The thermal conductivity of the copper rods was measured with the same test system that was used to measure the effective thermal conductivity of the heat pipes. Since the copper rods were tested at much lower heat input levels compared to the heat pipes, a linear trendline function was used to approximate the C110 thermal conductivity as a function of heat input. This linear trendline provided the means to extrapolate the corresponding k_{Cu} values used to calculate Cu Equivalence for each heat input level of each heat pipe configuration that was tested. Depending on size, configuration, and orientation, the low-temperature heat pipes investigated in this study exhibit Cu equivalence values ranging from 50-300 times better thermal conductivity than equivalent copper rods. Cu equivalence was used to examine the effects that bending, flattening, and gravitational orientation had on the thermal capabilities of the heat pipes.

5.1.2 Evaporator Temperature

Another commonly used parameter used to characterize steady-state heat pipe performance is evaporator temperature. Since the application of the heat pipes in this research is directed towards electronics thermal management, the evaporator temperature is a relevant parameter because it corresponds directly to the operating temperature of a hypothetical electronic component being cooled by the heat pipe. When analyzing the evaporator temperature of a heat pipe, it is important to note the temperature difference between the evaporator and condenser region as well as the condenser heat sink condition. As discussed in Chapter 3, the condenser heat sink boundary condition has a significant influence on the temperature gradient along the heat pipe, and thus the evaporator temperature and effective thermal conductivity. During each test in the heat pipe testing process, the condenser sink temperature was held at a nominal value of 20°C.

5.1.3 Total Thermal Resistance

The last common parameter used to characterize heat pipe performance is total resistance between the outer surface of the evaporator region and the outer surface of the condenser region, with the major heat path directed through the heat pipe as seen in Figure 1-2. This value is simply the inverse of the conductance of the heat pipe and is calculated as the temperature difference from evaporator to condenser region over the corrected power applied to the evaporator, as seen in equation (5-3).

$$R_{tot} = \frac{T_e - T_c}{Q_{actual}} \tag{5-3}$$

5.2 Raw Data Analysis

In order to thoroughly analyze the heat pipes in this study, discrete temperatures along the heat pipe axis and on the external surfaces of the insulation were measured. The data collection process for each test was automated using a DAQ unit capable of reading transient temperature data from T-type thermocouples and 4-wire RTDs. Each heat pipe was tested at incrementing heat input levels and was allowed to reach steady-state at each of these levels. The resulting data files consisted of the transient temperature data of a heat pipe as it reached steady-state under incrementing heat loads. These files were analyzed in a data reduction program written in MATLAB R2018a called Heat Pipe Data Analyzer (HP-DAN).

5.2.1 Heat Pipe Data Analyzer (HP-DAN)

Since there were several unique heat pipe tests required to develop a useful database, HP-DAN was created to streamline the data reduction process as well as provide a baseline program that could be scaled up to accommodate a much larger test matrix with more variables and parameter ranges for any future research. A single heat pipe test yielded a single data file exported in ".csv" format that contained the transient temperature data of the six thermocouples on surface of the heat pipe, the two RTDs on the surface of the foam and ceramic insulation, and the RTD measuring ambient temperature. The HP-DAN program followed the process seen in Figure 5-1. Each data file was named according to a pre-determined naming structure seen in Figure 5-2.

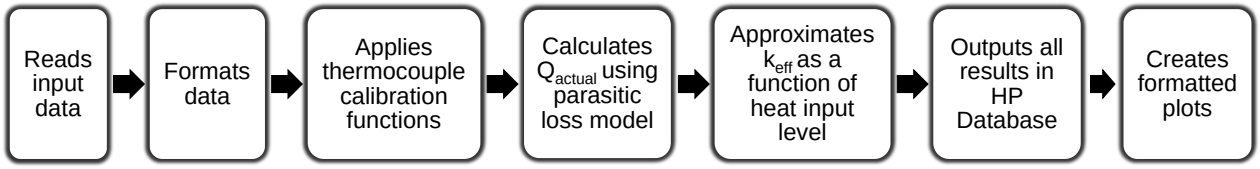

Figure 5-1: HP-DAN Process

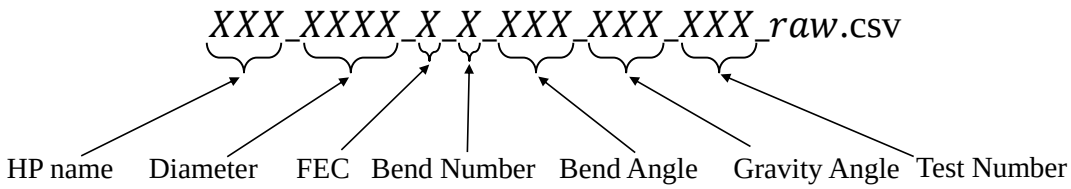

Figure 5-2: Data File Naming Convention

In addition to the raw data files, the HP-DAN program used the manually defined input data to perform its major functions. The data that was manually recorded was the power supplied and the time markers for the power level increases. The power level was determined by examining the voltage and current applied to the Nichrome wire element and calculating electrical power for resistive heating using Ohm's law. The electrical power applied to the Nichrome wire was assumed to be the total heat input into the test system.

The HP-DAN program served to calculate the amount of heat lost to the test system, calibrate the steady-state temperatures for each heat input level of the heat pipe tested, and an approximate the values of effective thermal conductivity for each heat input level. These output parameters were used to calculate additional performance parameters such as total temperature difference between the evaporator and condenser regions, system efficiency as a function of total heat input, copper equivalence, and total heat pipe thermal resistance.

5.2.2 Thermocouple Calibration

Each thermocouple used in the heat pipe testing process was fabricated from 30 gauge T-type thermocouple wire with a standard tolerance of ± 0.5°C. The thermocouple wire was welded using

a thermocouple welder. Since each welded thermocouple bead was inherently unique in shape and size, a linear calibration function was experimentally developed for each individual thermocouple to account for any temperature measurement error attributed to the bead itself. Each thermocouple bead was measured at a nominal low steady-state temperature (20°C) and a nominal high steady-state temperature (110°). The steady-state condition for the low temperature reference was achieved by submerging the thermocouple and the calibrated reference probe in room temperature water. The steady-state condition for the high temperature reference was achieved by isolating the thermocouple and the calibrated reference probe in an insulated oven. The reference probe was a Cole-Parmer 90080-12 Traceable Scientific Thermistor Thermometer that was calibrated to ± 0.01°C. This thermometer was used as the true reference point measurement for all thermocouple calibrations.

5.2.3 Parasitic Loss Model

The parasitic loss model, incorporated into the data reduction process, modeled the heat lost from the heat pipe outer insulation to the surrounding lab environment. The model incorporated mixed convection and radiation from the ceramic and foam insulation and produced a Q_{actual} value that represented the actual amount of heat that was applied to the heat pipe. The Q_{actual} value was equal to the total amount of heat applied by the linear power supply minus the heat lost due to convection and radiation to the ambient environment, as seen in equation (5-4).

$$Q_{actual} = Q_{in} - Q_{conv,cer} - Q_{conv,foam} - Q_{rad,cer} - Q_{rad,foam} \quad (5\text{-}4)$$

This loss model operated under the following assumptions:

a. Constant properties of the surrounding insulation

b. Mixed convection on the outer insulation surface

c. Ambient air velocity of 0.1 m/s

d. Insulation emissivity of 0.9

e. Measured dimensions accurate to 0.001 in.

The equations and input parameters used in the parasitic loss model calculations can be seen in Appendix B. The model calculated composite convective and radiative heat losses between both the ceramic and foam insulation regions, as depicted in Figure 5-3. The detailed dimensions of each heat pipe and the outer insulation can be seen in Table 5-1.

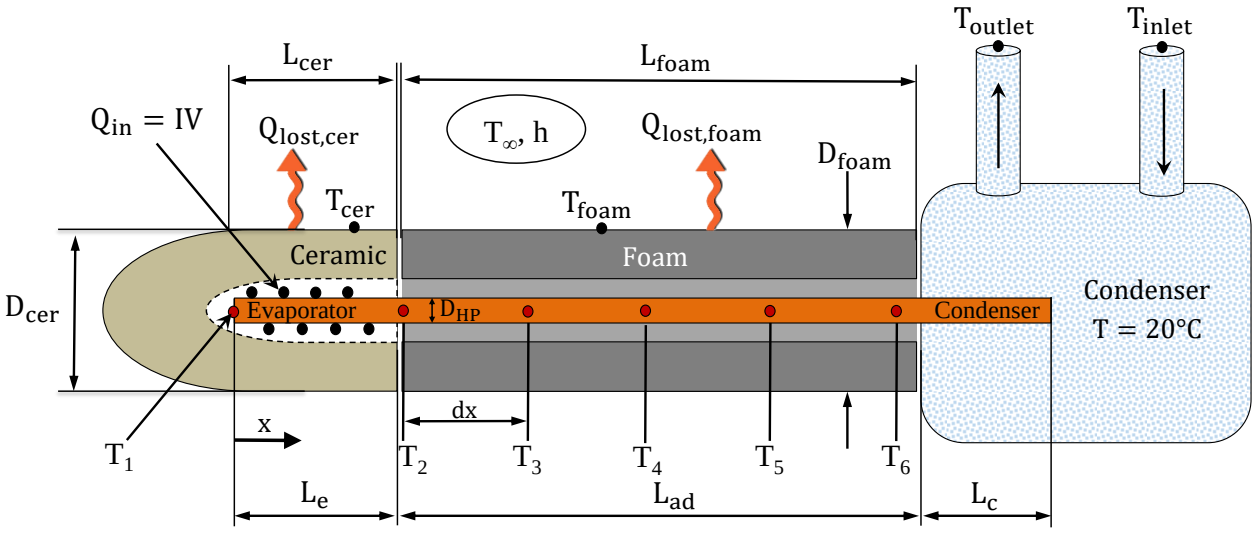

Figure 5-3: Parasitic Loss Model

Table 5-1: Heat Pipe and Insulation Dimensions

	Heat Pipe						Foam Insulation		Ceramic Crucible	
Name	L_{tot}	L_e	L_{ad}	L_c	dx	D_{HP}	L_{foam}	D_{foam}	L_{cer}	D_{cer}
	in	in.	in.	in.	in.	in.	in.	in.	in.	in.
HP1	11.2	2	6.2	3	1.5	0.25	7	1.255	2.375	1.38
HP2	11.75	2	6.5	3.25	1.5	0.375	5.5	1.255	2.375	1.38
HP4	9.25	2	4.05	3.2	0.85	0.5	2.625	1.255	2.375	1.38

5.2.4 Effective Thermal Conductivity

Once the thermocouples had been calibrated and the Q_{actual} values were obtained, the HP-DAN program began calculating the effective thermal conductivity of the heat pipe by approximating the axial temperature gradient using a linear temperature difference seen in equation (5-5), where Δx represents the distance between T_2 and T_5.

$$\left(\frac{dT}{dx}\right) \cong \frac{T_2 - T_5}{\Delta x} \tag{5-5}$$

With the approximate linear temperature gradient known, the effective thermal conductivity was then approximated using equation (5-6) where A_c is the cross sectional area of the heat pipe with respect to the outer diameter.

$$k_{eff} = \frac{Q_{actual}}{A_c \frac{dT}{dx}} \tag{5-6}$$

The effective thermal conductivity, k_{eff}, represents a heat pipe's capability of transferring heat at a particular temperature difference. The relevant temperature difference used in this approximation is the difference between the T2 and T5. For each heat pipe test, this temperature difference was assumed to be the best representation of the measureable temperature difference between the

evaporator region and condenser region, where $T_2 = T_e$ and $T_5 = T_c$. This temperature difference governed the effective thermal conductivity, and therefore the Cu equivalence, of the heat pipe.

5.3 Data Uncertainty Analysis

The major performance parameters that were used to characterize the effects of bending and flattening were Cu equivalence, evaporator temperature, and total resistance relative to the heat input. The expanded formulations for each of these performance parameters can be seen in equations (5-7), (5-8), and (5-9), with the exception of evaporator temperature which was a measured value for each test, with an uncertainty of ± 0.5°C.

$$\text{Cu Equivalence} = \frac{k_{eff}}{k_{Cu}} \tag{5-7}$$

$$k_{eff} = \frac{Q_{actual}}{A_c \frac{dT}{dx}} = \frac{Q_{actual}}{\frac{\pi}{4}(D_{HP})^2 \frac{T_e - T_c}{dx}} \tag{5-8}$$

$$R_{tot} = \frac{T_e - T_c}{Q_{actual}} \tag{5-9}$$

The heat input level was corrected with the parasitic loss model to represent the actual amount of heat entering the evaporator region of the heat pipe as seen in equations (5-10) and (5-11).

$$Q_{actual} = Q_{in} - Q_{conv,cer} - Q_{conv,foam} - Q_{rad,cer} - Q_{rad,foam} \tag{5-10}$$

$$Q_{actual} = Q_{in} - h_{mixed} A_{cer}(T_{cer} - T_{amb}) - h_{mixed} A_{foam}(T_{foam} - T_{amb}) - \varepsilon\sigma A_{cer}\left({T_{cer}}^4 - {T_{amb}}^4\right) - \varepsilon\sigma A_{foam}\left({T_{foam}}^4 - {T_{amb}}^4\right) \tag{5-11}$$

A data uncertainty analysis was performed to account for errors in the measurements of heat input, dimensions, and temperature as well as the parasitic loss model assumptions. The uncertainty analysis calculations for the heat input calculation can be seen in Appendix C. The maximum total

percent uncertainty in the corrected heat input calculations was ± 8%. This value was calculated under the assumption that the calculated mixed convection heat transfer coefficient had an uncertainty of 25% and the assumed value for emissivity had an uncertainty of 15%. Since Cu equivalence is a comparative parameter benchmarked by the thermal conductivity of Cu 110, any major biases or uncertainties in the data due to the test system or measurement units were eliminated when this parameter was used. However, as a conservative estimate, the Cu equivalence parameter was given an uncertainty of ± 1% based on the temperature data scatter. The total resistance uncertainty was calculated as ± 71.2% based on the assumption that the thermocouple readings contained an uncertainty of 0.5°C. In actuality, the calibration of these thermocouples diminished that uncertainty to approximately 0.1°C. However, as a conservative estimate, based on the difficult nature of cataloging the thermocouples used for each test, the manufacturer's uncertainty of 0.5°C was used for the total resistance uncertainty analysis. If the thermocouple uncertainty were to be changed to 0.1°C in the total resistance uncertainty analysis, the uncertainty of the total resistance would decrease to ± 10%.

6 RESULTS AND DISCUSSION

This chapter presents the resulting performance data for all of the heat pipes that were tested. The data is presented in a manner that allows performance trends to be exploited and analyzed in order to postulate an understanding of the effects that the geometric modifications and configurations have on the performance and operational limits of the heat pipes.

6.1 Heat Pipe Operating Parameters

Three heat pipes were tested for their performance under various geometric modifications. HP1 and HP2 were both tested in a straight-round configuration and several different bent adiabatic region configurations. HP4 was tested with a single side (evaporator region) flattened, single side (condenser region) flattened, and in a double-flat configuration where both the evaporator and condenser regions were flattened. Table 6-1 displays the dimensional and physical properties and parameters of each heat pipe that was tested. The fill ratio parameter corresponded to the ratio of the fluid charge volume to the calculated pore volume. It can be seen that HP4 had three different charge masses corresponding to its three unique flattened end configurations. This was due to the fact that the flattening process required opening the heat pipe end cap, flattening the end, re-sealing, and refilling the heat pipe. Alternatively, the bending process used on HP1 and HP2 did not require opening the heat pipe, so the charge mass remained exact for every bent configuration of both of these heat pipes. When HP4 was refilled for each of the flattened end configurations, it was filled to the correct charge mass per the approximated pore volume as best as the heat pipe fill system would allow.

Table 6-1: Heat Pipe Dimensions and Properties

Heat Pipe	Characteristics	Diameter	Length	Calculated Pore Volume	Charge Mass	Fill Ratio
		in.	in.	mL	g	
HP1	SRHP and Bent	0.25	11.2	1.12	1.22	1.09
HP2	SRHP and Bent	0.375	11.75	2.65	2.67	1.01
HP4	Flattened Evap.	0.5	9.25	3.71	3.74	1.01
HP4	Flattened Cond.	0.5	9.25	3.71	3.69	0.99
HP4	Both Ends Flat	0.5	9.25	3.71	3.92	1.06

6.2 Determining the Capillary Limit

The capillary limit was determined by inspecting the TC 1 and TC 2 steady-state values at each heat input level. The general trend for incrementing heat input was that the surface temperature of the heat pipe increased uniformly with increasing heat, but the temperature difference would stay relatively constant. This is the rationale behind a heat pipe's inherent behavior of increasing in effective thermal conductivity as heat input is increased. At some point, however, the heat input reaches the capillary limit of the heat pipe, at which point the wick structure is incapable of returning the working fluid from the condenser to the evaporator causing the axial temperature gradient to increase significantly. This phenomenon results in a sudden decrease in effective thermal conductivity and is indicated by a spike in the evaporator temperature. For these tests, the capillary limit was monitored visually using TC 1 trends. The capillary limit was reached whenever TC 1 began to show a sudden and sharp increase of temperature with respect to all other temperature readings. This would indicate the wick drying out in the evaporator. Figure 6-1 depicts the steady-state temperature profiles of HP1 SRHP in GAN at incrementing heat input levels. It can be seen that at Q_{actual} equal to 16 W, TC 1 sustained a sudden increase from approximately 36°C to approximately 58°C.

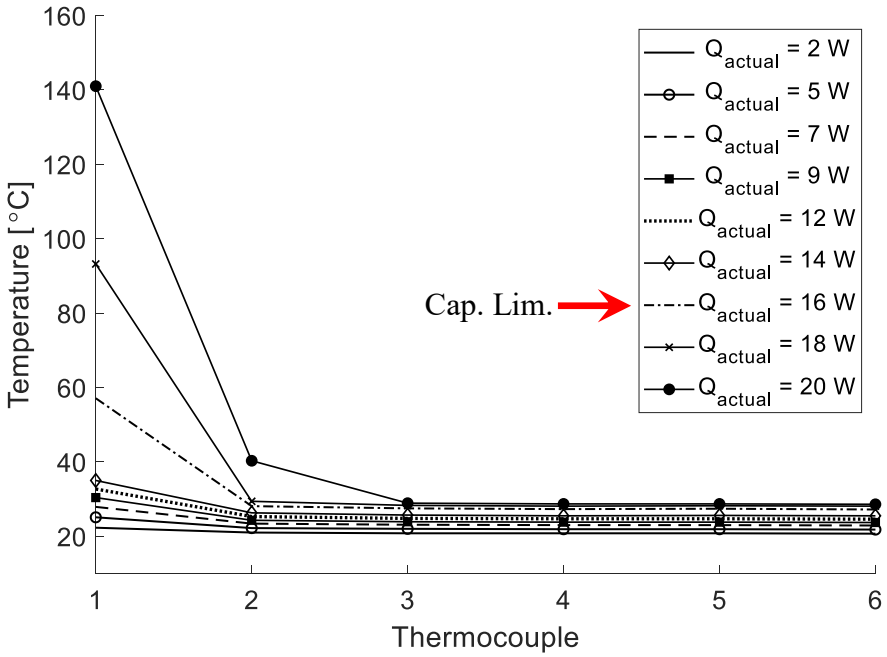

Figure 6-1: Steady-state Temperature Profiles of HP1 SRHP – GAN (Capillary Limit Criteria Example)

As the heat was increased further to 18 W and then 20 W, TC 1 began to increase even more and TC 2 also began to sustain a noticeable increase in temperature. The corresponding approximated effective thermal conductivity for HP1 SRHP in GAN can be seen in Figure 6-2.

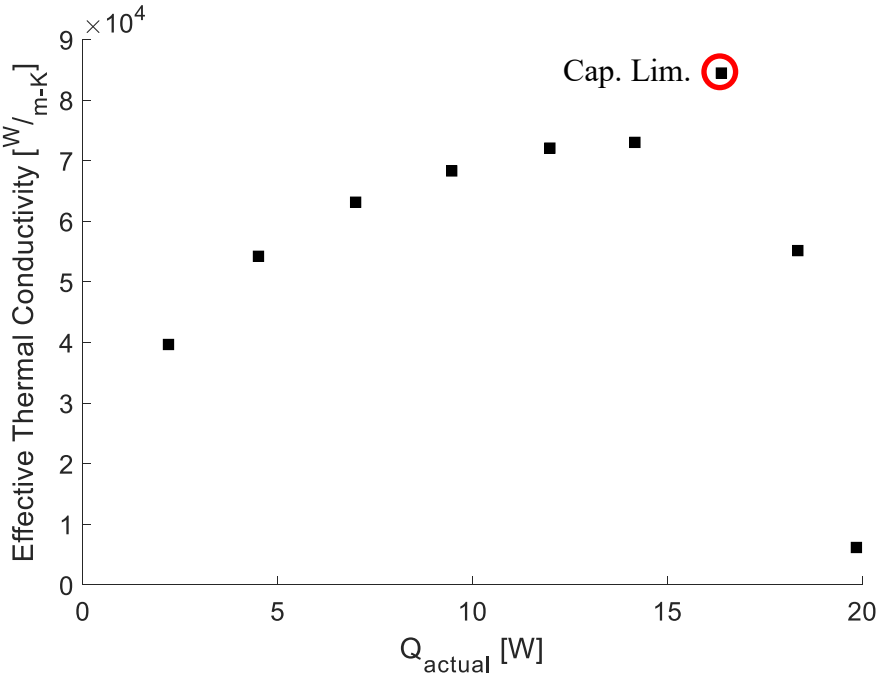

Figure 6-2: Effective Thermal Conductivity of HP1 SRHP – GAN (Capillary Limit Criteria Example)

These effective thermal conductivity values are approximate based on the linear temperature difference between TC 2 and TC 5. It can be seen that the effective thermal conductivity increases gradually until it hits a peak at approximately 16 W. At this point, the effective thermal conductivity has reached its maximum value for this particular heat pipe. This value is a function of many parameters such as charge mass, wick properties, and condenser region boundary condition. After this point is reached, any additional heat added to the heat pipe will significantly degrade the effective thermal conductivity, as seen in Figure 6-2.

6.3 Comprehensive Testing Results

The comprehensive results for every testing configuration of HP1, HP2, and HP4 at the observed capillary limits can be seen in Table 6-2. This table provides the maximum copper equivalence, the maximum effective thermal conductivity, the evaporator temperature, and the total temperature difference between the evaporator and condenser regions for each test in the test matrix. Images of HP1, HP2 and HP4 can be seen in each of the tested configurations in Figure 6-3 through Figure 6-17.

Table 6-2: Results Data at Capillary Limits

Heat Pipe	Geometric Modification	Cap. Limit	Max. Cu eq.	Max. k_{eff}	Evap. Temp.	Temp. Diff.
		W	--	W/m-K	°C	°C
HP1	SRHP-GAN	16.4	281	84464	28.1	0.7
	SRHP-GAS	38.4	247	69222	38.3	2
	SRHP-GAD	5.6	94	29058	26.4	0.7
	1 Bend - 15°	18.9	153	45591	31.3	1.5
	1 Bend - 30°	23.2	259	76060	36.7	1.1
	1 Bend - 45°	23.6	223	65501	35.2	1.3
	1 Bend - 90°	21.3	96	28421	38	2.7
	2 Bends - 90°,45°	25.5	87	25528	48.6	3.6
	2 Bends - 90°,90°	26.4	126	36685	52.1	2.6
HP2	SRHP-GAN	74.7	178	79923	78.8	1.5
	SRHP-GAS	141.6	99	55400	88.2	4.1
	SRHP-GAD	13.7	63	21977	69.1	1
	1 Bend - 45°	57.8	169	71294	76.8	1.3
	1 Bend - 90°	74.9	446	200243	78	0.6
	2 Bends - 90°,45°	73.7	155	69506	78.4	1.7
	2 Bends - 90°,90°	79.5	107	49078	79.3	2.6
HP4	Flattened Evap.	163	45	14372	55.2	5.8
	Flattened Cond.	170.7	121	37948	63.9	2.3
	Both Ends Flat	155	20	6393	57.4	12.4

Figure 6-3: HP1 SRHP Image

Figure 6-4: HP1 [1-15°] Image

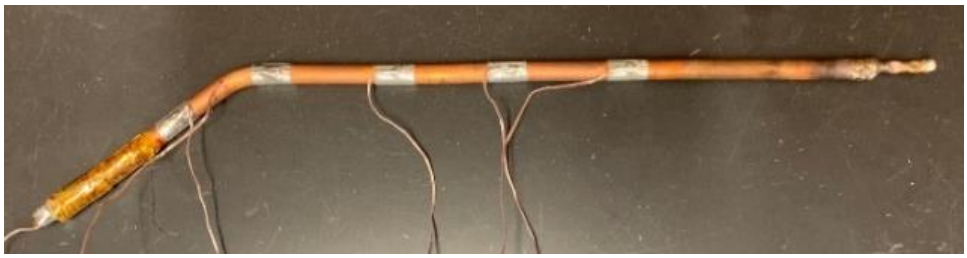

Figure 6-5: HP1 [1-30°] Image

Figure 6-6: HP1 [1-45°] Image

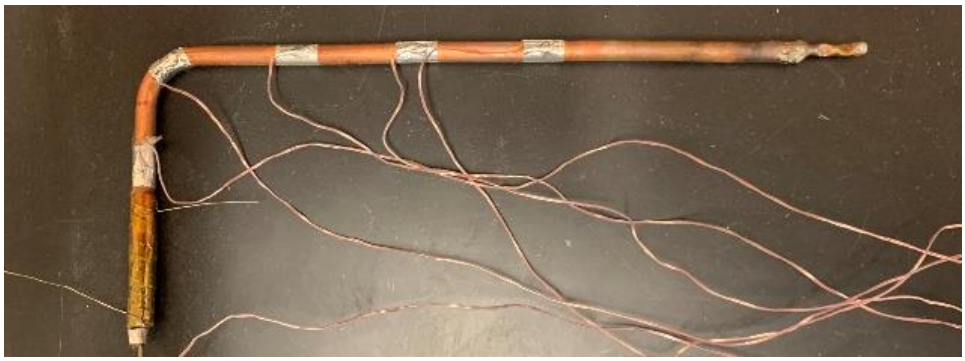

Figure 6-7: HP1 [1-90°] Image

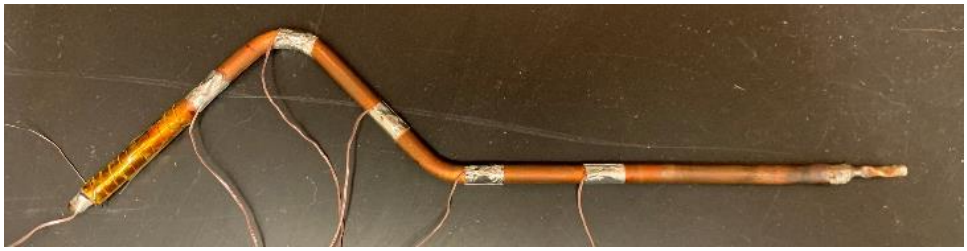

Figure 6-8: HP1 [2-90°, 45°] Image

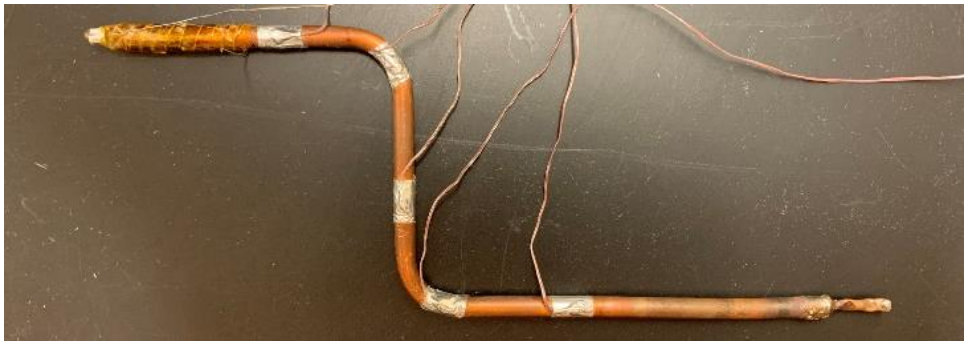

Figure 6-9: HP1 [2-90°, 90°] Image

Figure 6-10: HP2 SRHP Image

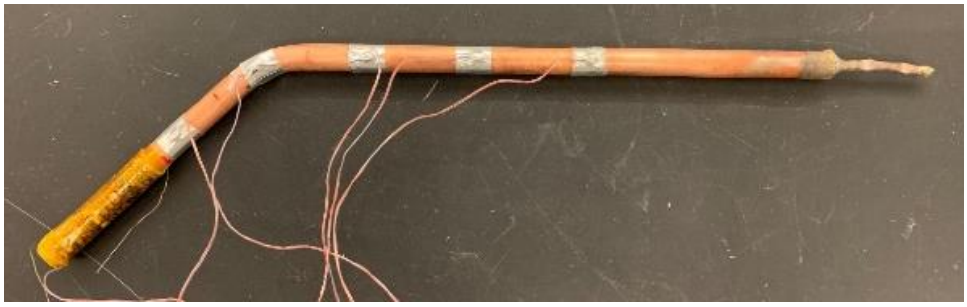

Figure 6-11: HP2 [1-45°] Image

Figure 6-12: HP2 [1-90°] Image

Figure 6-13: HP2 [2-90°, 45°] Image

Figure 6-14: HP2 [2-90°, 90°] Image

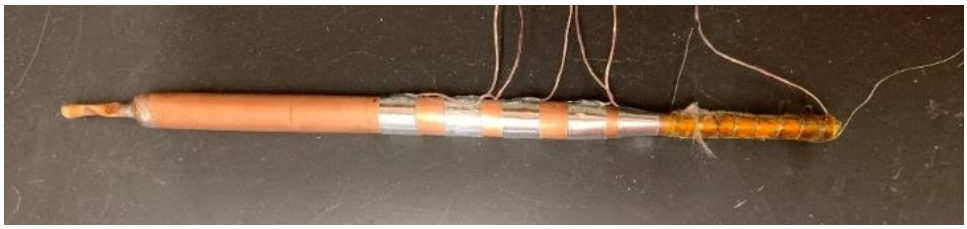

Figure 6-15: HP4 –Flattened Evaporator Image

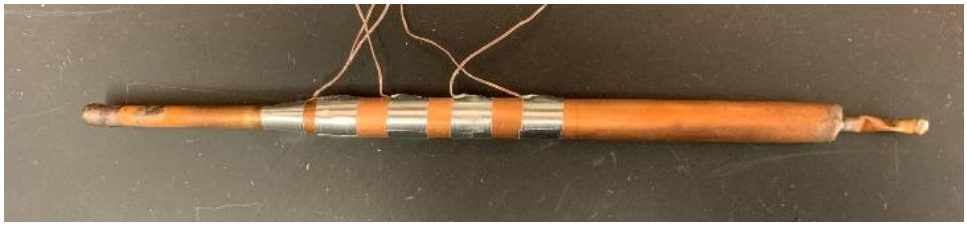

Figure 6-16: HP4 –Flattened Condenser Image

Figure 6-17: HP4 –Both Ends Flat Image

Due to the time length of each test and the need to acquire information on so many different heat pipe configurations, each configuration was only tested once. The experimental results provided in this research offer insight into the behavior of the three heat pipes that were tested. The performance trends that were observed provide useful information about the behavior of these heat pipes, but the confidence level of the empirical characterization would be increased tremendously if the tests were repeated. That being said, the information provided in this research still serves as a good foundation for characterizing the effects of bending and flattening on the performance and limits of sintered felt wick heat pipes.

6.3.1 Effects of Gravitational Orientation on SRHP Performance

The HP1 and HP2 SRHPs were both tested in gravity neutral (GAN), gravity assist (GAS), and gravity adverse (GAD). The effect of the gravitational force on the performance of the heat pipes was significant. Figure 6-18 through Figure 6-35 show the Cu equivalence, evaporator temperature, and total resistance as a function of heat input for both HP1 and HP2 in each of the gravitational orientations. Based on this data, the following observations were made:

***Capillary limits on Cu equivalence plots are marked with a red circle around the data point*

(I) *Intuitive observation*
(NI) *Non-intuitive observation*
(NO) *Neutral observation*

Comparing HP1 SRHP to HP2 SRHP

1. **(I)** The capillary limit for HP2 SRHP was much greater than the capillary limit for HP1 SRHP in all gravitational configurations. This was presumably due to the fact that larger heat pipes inherently have a higher charge mass and therefore require more heat to reach capillary dry-out than smaller heat pipes.
2. **(NO)** The copper equivalence for HP1 SRHP was greater than the copper equivalence of HP2 SRHP in each gravitational configuration. The Cu equivalence is controlled by the approximated effective thermal conductivity of the heat pipe and the amount of heat applied to the evaporator region. The effective thermal conductivity is a function of several parameters such as the heat pipe materials, working fluid properties, and wick properties.
3. **(I)** The GAD configuration significantly decreased the copper equivalence for both HP1 and HP2 SRHPs. This was an unsurprising result. Due to the fact that the water must flow against gravity during its return from the condenser region to the evaporator region, both the capillary limit and Cu equivalence were decreased significantly.

HP1 SRHP behavior in GAN, GAS, and GAD

1. **(I)** The Cu equivalence of HP1 SRHP was the greatest in GAN, lesser in GAS, and least in GAD. This is well known behavior and is supported in the literature review.
2. **(I)** The capillary limit of HP1 SRHP was greatest in GAS, lesser in GAN, and least in GAD. This is well known behavior and is supported in the literature review.
3. **(I)** The evaporator temperature of HP1 SRHP remained relatively constant for GAN and GAD and slightly higher in GAS when the heat pipe was operating within its limits. It ranged from 20-30°C for both GAN and GAD, and from 20-45°C in GAS. A presumable

justification for the higher achievable evaporator temperature in the GAS configuration is the heat pipes ability to reach a much higher capillary limit when the working fluid is assisted by gravitational forces. Since gravity was aiding in returning the working fluid to the evaporator region, the heat pipe continued to operate at much higher levels compared to the GAN and GAD orientations. This means that although it was still operational, the higher heat input level increased the evaporator temperature above the limits in the GAN and GAD configurations.

HP2 SRHP behavior in GAN, GAS, and GAD

1. **(I)** The Cu equivalence of HP2 SRHP was the greatest in GAN, lesser in GAS, and least in GAD. This is well known behavior and is supported in the literature review.
2. **(I)** The capillary limit of HP2 SRHP was greatest in GAS, lesser in GAN, and least in GAD. This is well known behavior and is supported in the literature review.
3. **(I)** The evaporator temperature of HP2 SRHP remained relatively constant for all gravitational orientations when the heat pipe was operating within its limits. The same effect of GAS orientation resulting in a higher evaporator temperature at the capillary limit is rationalized by the same explanation of the identical phenomenon occurring in HP1 data. The higher achievable evaporator temperature in the GAS configuration reflects the heat pipe's ability to reach a much higher capillary limit when the working fluid is assisted by gravitational forces, and thus transfer more heat prior to dry-out failure.

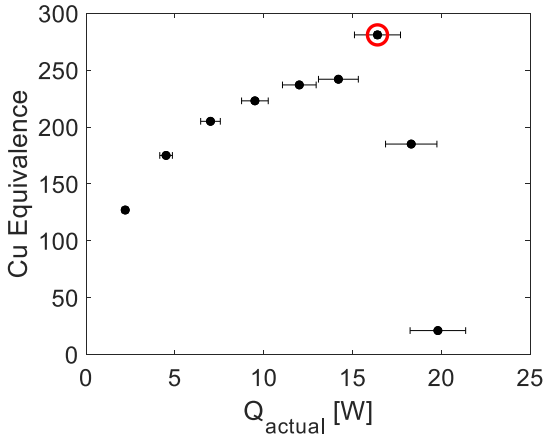

Figure 6-18: HP1-GAN Cu Equivalence

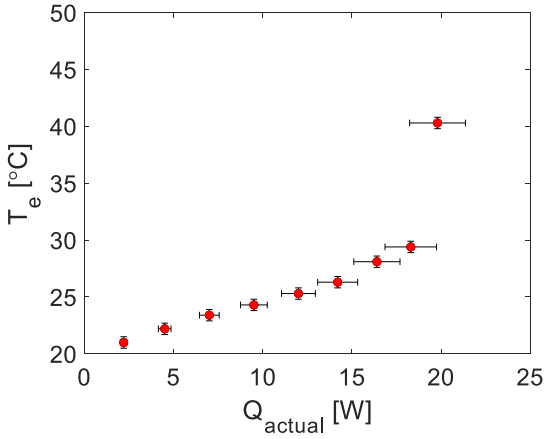

Figure 6-19: HP1-GAN Evaporator Temperature

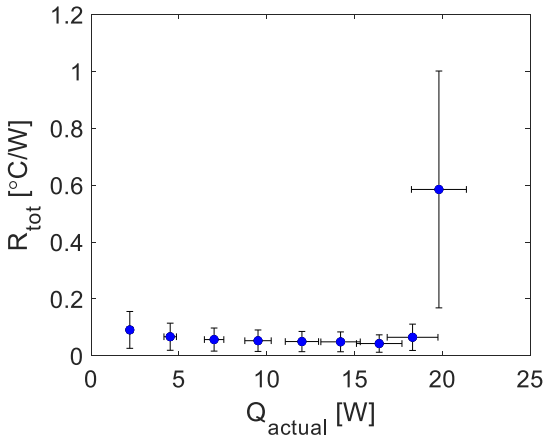

Figure 6-20: HP1-GAN Total Resistance

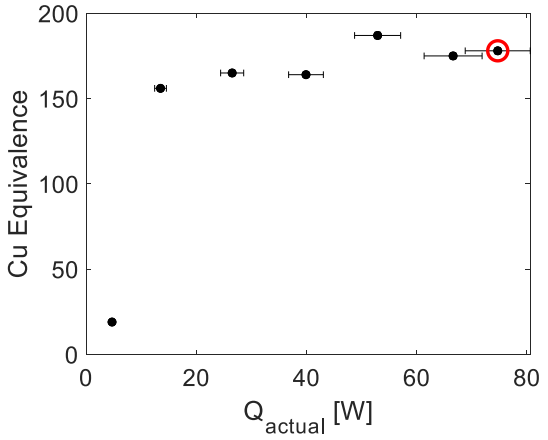

Figure 6-21: HP2 GAN Cu Equivalence

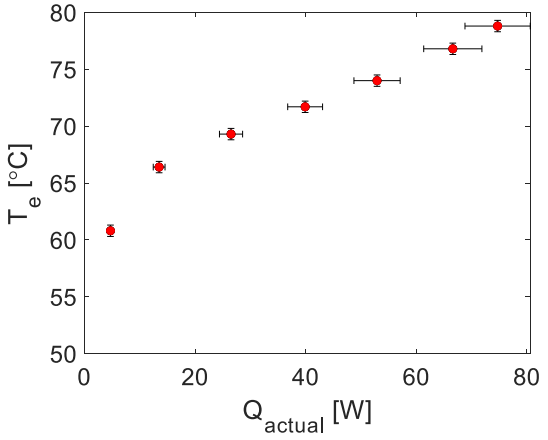

Figure 6-22: HP2-GAN Evaporator Temperature

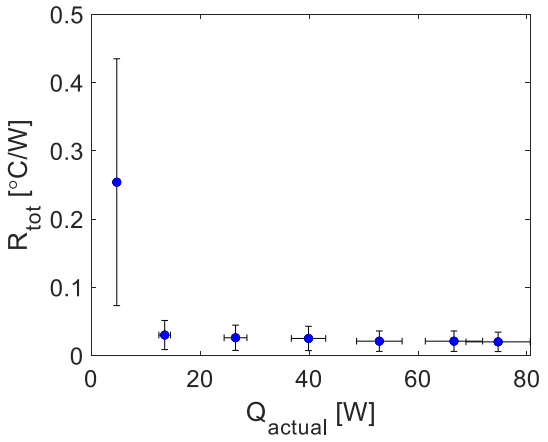

Figure 6-23: HP2-GAN Total Resistance

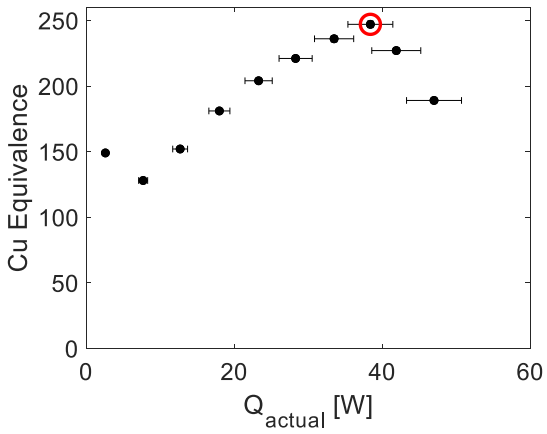

Figure 6-24: HP1-GAS Cu Equivalence

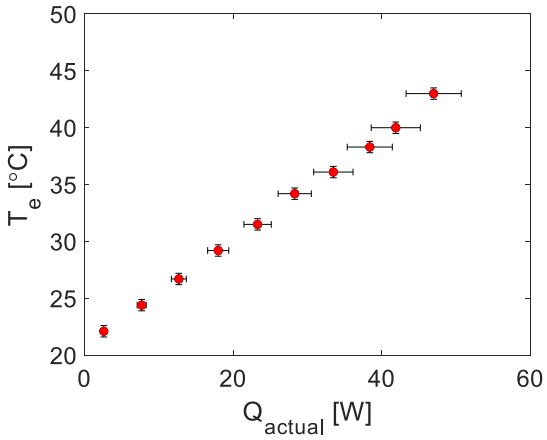

Figure 6-25: HP1-GAS Evaporator Temperature

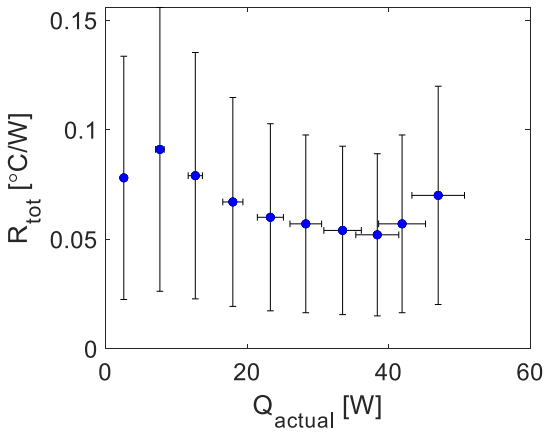

Figure 6-26: HP1-GAS Total Resistance

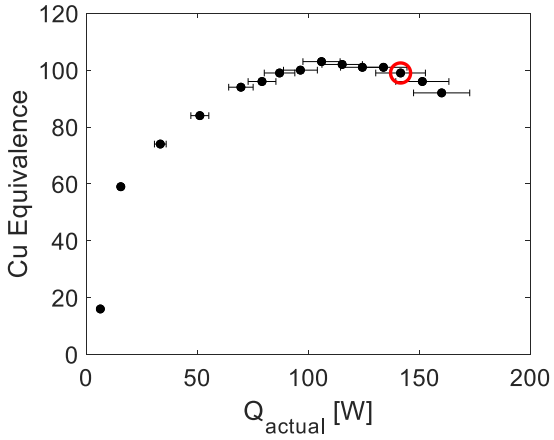

Figure 6-27: HP2-GAS Cu Equivalence

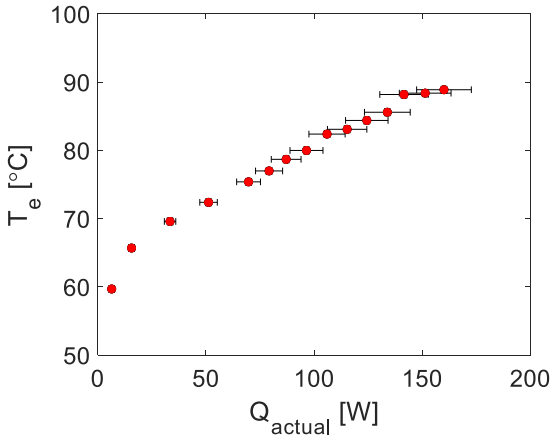

Figure 6-28: HP2-GAS Evaporator Temperature

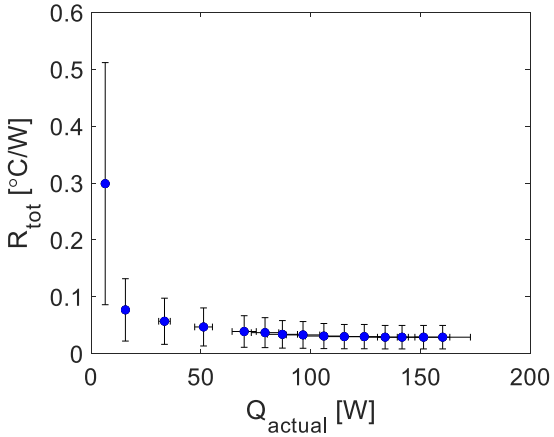

Figure 6-29: HP2-GAS Total Resistance

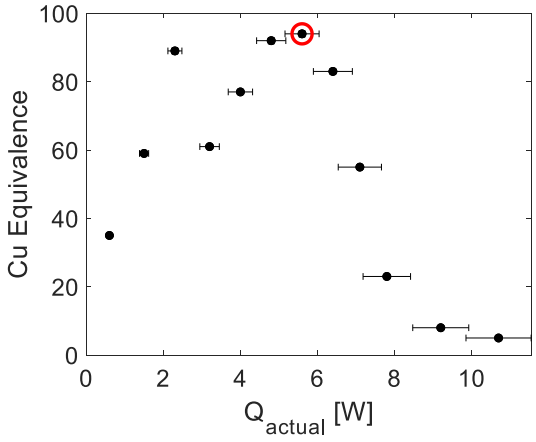

Figure 6-30: HP1-GAD Cu Equivalence

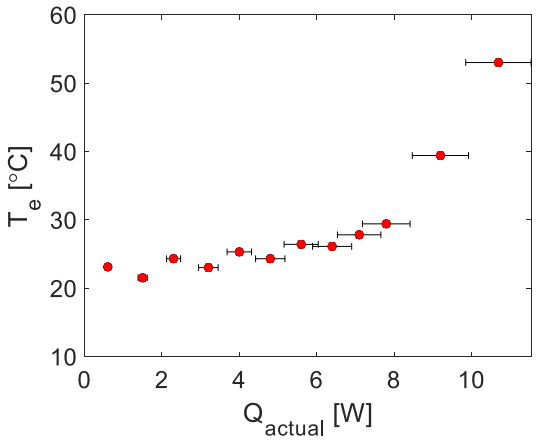

Figure 6-31: HP1-GAD Evaporator Temperature

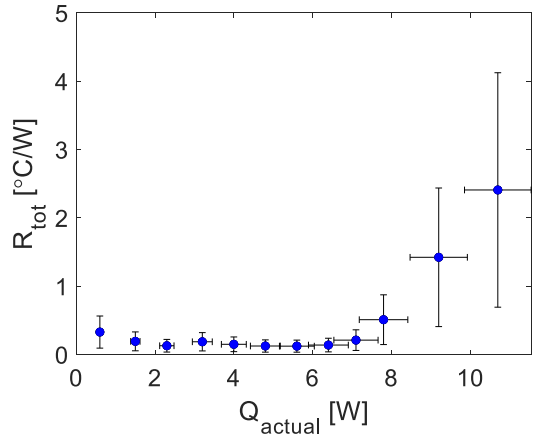

Figure 6-32: HP1-GAD Total Resistance

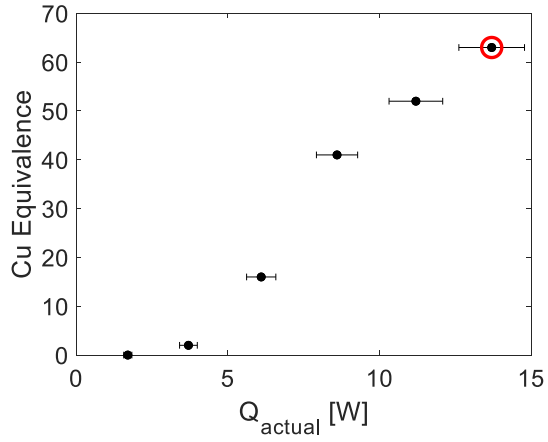

Figure 6-33: HP2-GAD Cu Equivalence

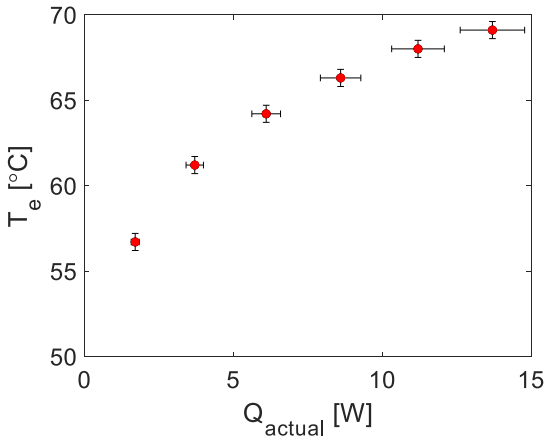

Figure 6-34: HP2-GAD Evaporator Temperature

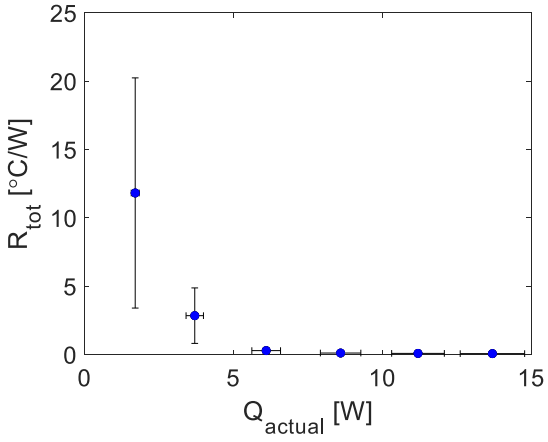

Figure 6-35: HP2-GAD Total Resistance

6.3.2 Effects of Bending on Performance

Both HP1 and HP2 were tested in straight-round and bent configurations. HP1 was bent with 1 bend at 15°, 30°, 45°, and 90° and with 2 bends with the first bend at 90° and the second bend at 45° and 90°. HP2 was bent with 1 bend at 45° and 90° and with 2 bends with the first bend at 90° and the second bend at 45° and 90°. HP1 was initially bent at 15° and then 30° in order to ensure that the vapor core would not seal off and to ensure that the wick would stay intact under bending, as either of those circumstances would result in a non-functional heat pipe. Each bent heat pipe was tested in GAN only. The behavior of the heat pipes under bent conditions was compared to their respective performances in the straight-round configurations. Based on the data seen in Figure 6-36 through Figure 6-65, the following observations were made:

***Capillary limits on Cu equivalence plots are marked with a red circle around the data point*

HP1 – Bent

1. **(NI)** It was observed that the capillary limit increased from 16.4 W (SRHP) to approximately 23 W in the single-bent configurations, and 25 W in the double-bent configurations. This is non-intuitive based on the analysis performed in Chapter 3 which suggested that bending may cause degradation of the capillary limit. However, in the literature review, J. Chen also noticed an increase in capillary limit directly correlated to an increase in bending angle [9].

2. **(I)** The data suggests that the capillary limit was enhanced when HP1 was bent, but the increase from 23 W in the single-bent configurations to 25 W in the double-bent configurations does not definitively support the idea of additional benefits from multiple bends. The capillary limit determination criteria along with the discretely tested values of heat input could have easily lead to an over or underestimation of the capillary limit by a

few Watts. Additionally, the ± 8% error of Q_{actual} determined in the uncertainty analysis suggests that the capillary limit of the single-bent and double-bent heat pipe configurations were the essentially the same at approximately 24 W.

3. **(NI)** It was also observed that the Cu equivalence changed sporadically as a function of the bending angle. The SRHP GAN configuration exhibited a maximum Cu equivalence of 281. When HP1 was bent with 1 bend at 15°, the Cu equivalence decreased to 153. However, when the heat pipe was bent further to 30° and then 45°, the Cu equivalence shot back up to 259 and 223, respectively. When the heat pipe was bent to 90° the Cu equivalence degraded to 96 and when a second bend was introduced the Cu equivalence floated around between 85 and 125.

4. **(I)** The evaporator temperature followed the same linear trend with power for each bent configuration, but spanned various ranges depending on the configuration. The HP1 [2-90°, 90°] configuration had the highest evaporator temperatures ranging from 37°C at low power (3.4 W) to 54°C at high power (28.1 W).

HP2 – Bent

1. **(NI)** The most noticeable observation in the bent HP2 test data was the incredibly high Cu equivalence of HP2 [1-90°]. This configuration reached a maximum Cu equivalence of 446 (k_{eff} of 200,243 W/m-K) and outperformed every heat pipe in every configuration tested by a factor of 2 or 3. There is no known reason as to why this configuration exhibited such a high Cu equivalence, but this behavior is in agreement with other results found in literature. As discussed in Chapter 3, J. Chen investigated the effects of bending FPHPs with bending angles of 0°, 30°, 60°, and 90°. Chen observed that the effective thermal conductivity of the heat pipes increased gradually with increasing bend angle, but stayed

between 1800 and 3200 W/m-K for bending angles 0°, 30°, and 60° [9]. However, when the heat pipe was bent to 90°, the effective thermal conductivity shot up to approximately 6400 W/m-K [9]. Although the heat pipes used in this investigation are slightly different from the FPHPs used in Chen's research, the resulting trends are similar.

The rationale behind this noticeable increase in conductance at 90° is not easily determined. One possible explanation is that bending the heat pipe significantly alters the wick structure at the location of the bend. This may impact the pore structure both internally and at the surface interface of the vapor core. On the inner radius of the bend, the wick structure is compressed and on the outer radius, it is stretched apart. One of the theories discussed in Chapter 3 was that a heat pipe's conductance was significantly influenced by the liquid and vapor pressure drops. If the wick pore structure is significantly deformed at the at the surface in contact with the vapor core, then the resulting influence on the radius of the menisci at this surface changes the pressure drop between the liquid and vapor. This could have an effect on the measured temperatures of the evaporator and condenser locations at the opposite ends of the adiabatic section. Recall, the heat pipe's conductance was derived using measurements from thermocouples mounted on the outer shell of the heat pipe container. For these measurements the thermocouples were mounted on the neutral axis of the bend (normal to the bend plane). Furthermore, it is not known if the observations made in this work would have been different if the thermocouples were mounted within the bend plane, and how the difference would have been influenced by if they were located along the inner or outer bend circumference. Without further testing with the thermocouples located along the inner and outer bend plane as well as the neutral axis, it cannot be determined if the heat pipe conductance improved at 90° or if the observed increase in

conductance was idiosyncratic of how the measurements were taken and used in the data reduction to derive the thermal conductance.

2. **(NI)** All of the bent configurations except for HP2 [1-90°] exhibited a decrease in Cu equivalence compared to the SRHP GAN Cu equivalence.

3. **(NO)** The capillary limit was relatively unchanging for most of the bent configurations. The limit was reached at approximately 75 W for HP2 SRHP GAN and all bent configurations with the exception of [1-45°]. The [1-45°] capillary limit outlier does not fall within the ± 8% uncertainty of Q_{actual} when comparing it to the 75 W capillary achieved by the other configurations, but it could be a result of the visual capillary limit criteria.

4. **(I)** The evaporator temperature of HP2 did not vary significantly among the different bent configurations and followed the same linear trend with heat input for all tests.

5. **(I)** HP2 exhibited a decrease in Cu equivalence in all double-bent configurations, following the same trend as HP1.

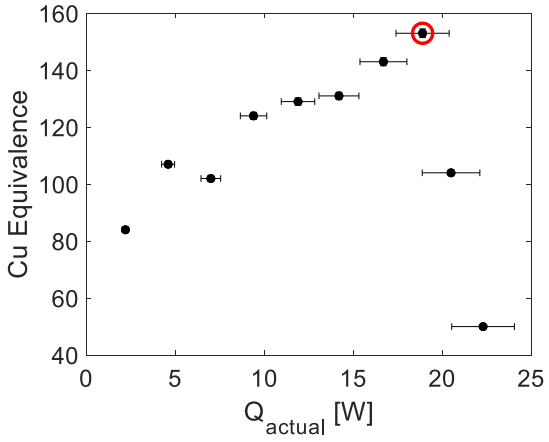

Figure 6-36: HP1 [1-15°] Cu Equivalence

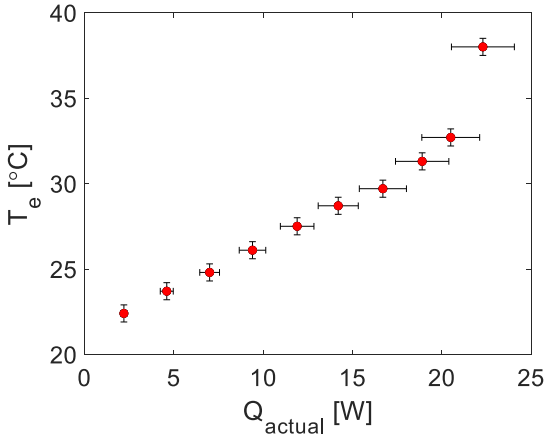

Figure 6-37: HP1 [1-15°] Evaporator Temperature

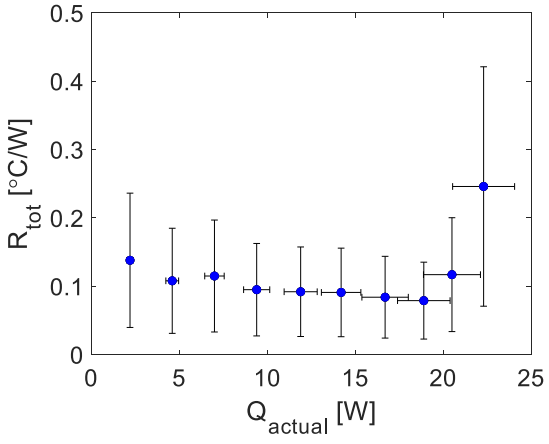

Figure 6-38: HP1 [1-15°] Total Resistance

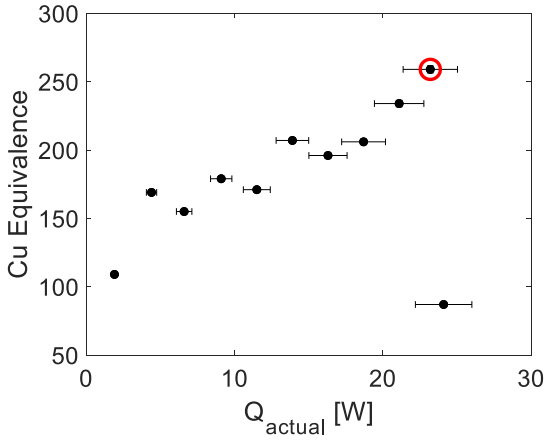

Figure 6-39: HP1 [1-30°] Cu Equivalence

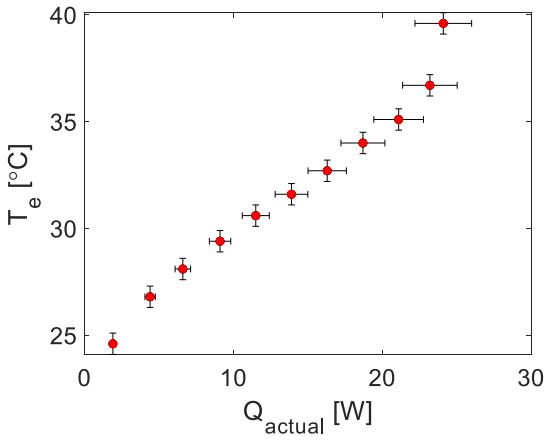

Figure 6-40: HP1 [1-30°] Evaporator Temperature

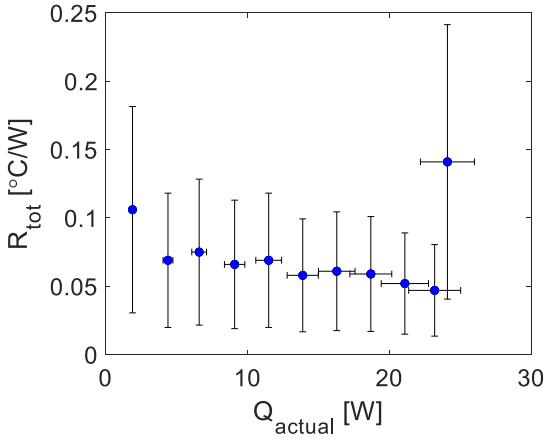

Figure 6-41: HP1 [1-30°] Total Resistance

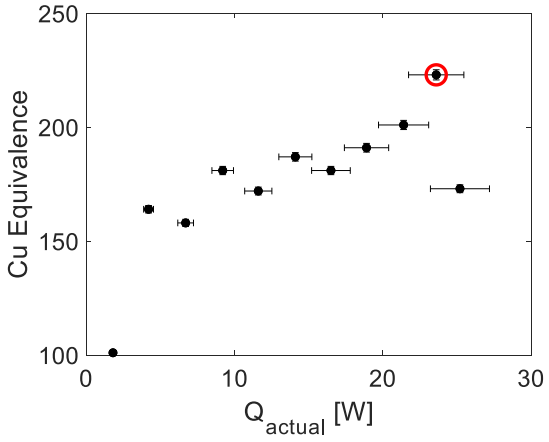

Figure 6-42: HP1 [1-45°] Cu Equivalence

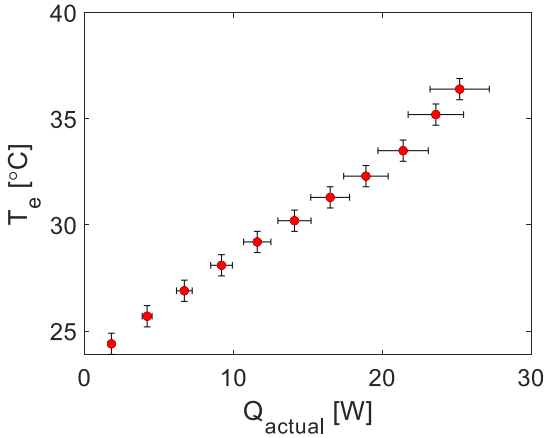

Figure 6-43: HP1 [1-45°] Evaporator Temperature

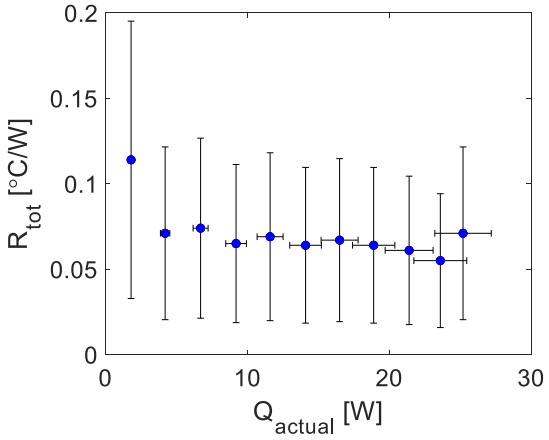

Figure 6-44: HP1 [1-45°] Total Resistance

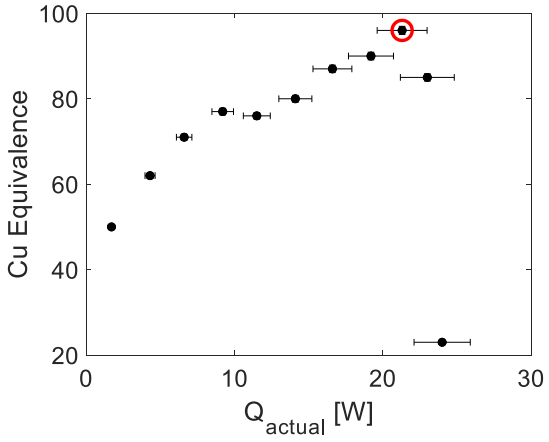

Figure 6-45: HP1 [1-90°] Cu Equivalence

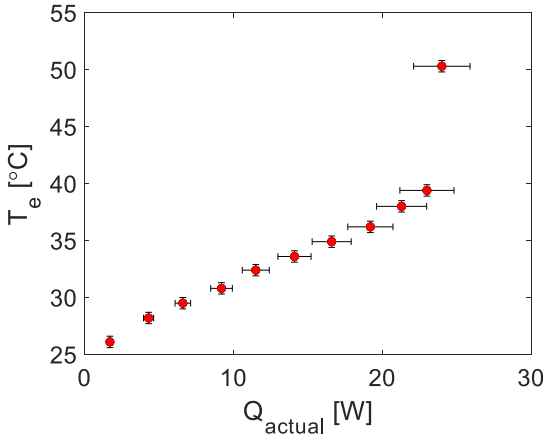

Figure 6-46: HP1 [1-90°] Evaporator Temperature

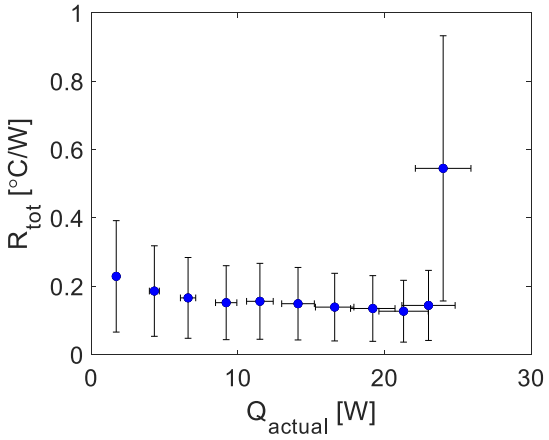

Figure 6-47: HP1 [1-90°] Total Resistance

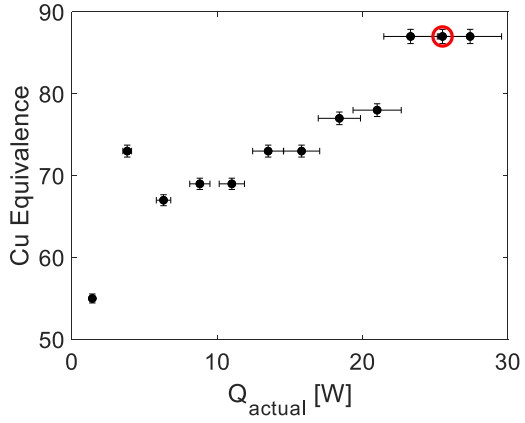

Figure 6-48: HP1 [2-90°, 45°] Cu Equivalence

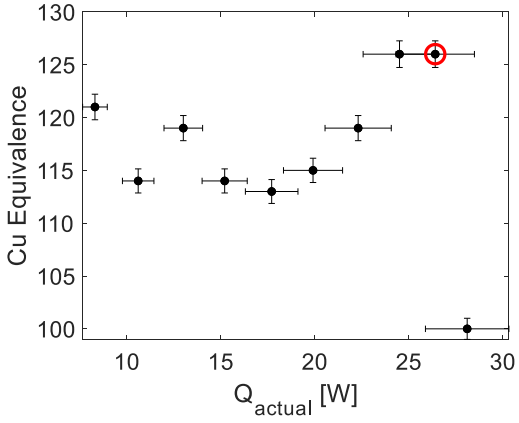

Figure 6-51: HP1 [2-90°, 90°] Cu Equivalence

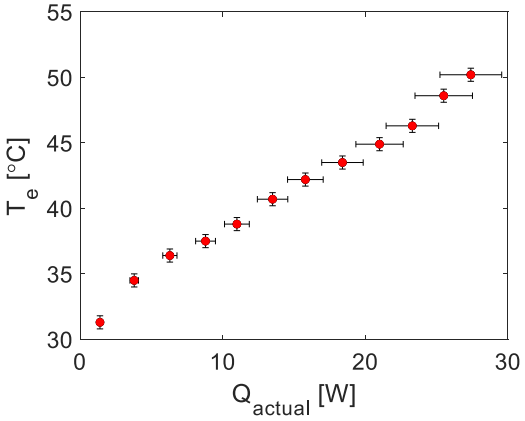

Figure 6-49: HP1 [2-90°, 45°] Evaporator Temperature

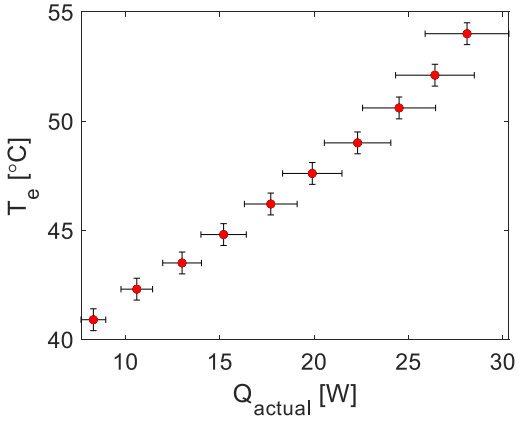

Figure 6-52: HP1 [2-90°, 90°] Evaporator Temperature

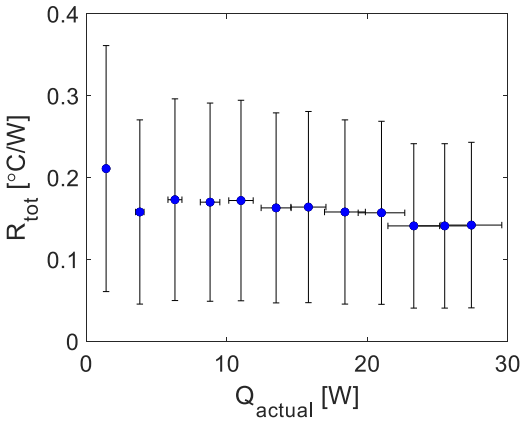

Figure 6-50: HP1 [2-90°, 45°] Total Resistance

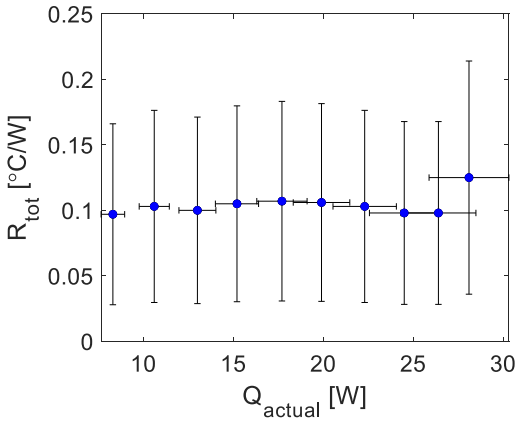

Figure 6-53: HP1 [2-90°, 90°] Total Resistance

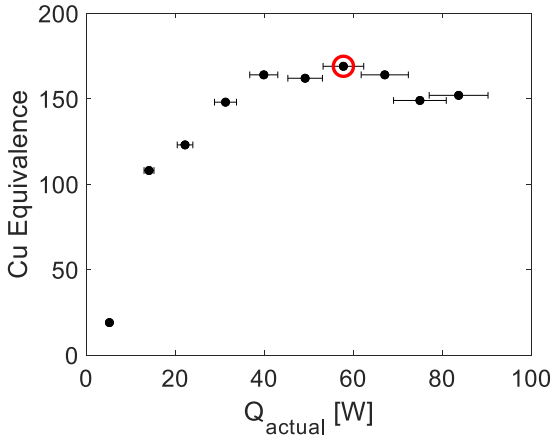

Figure 6-54: HP2 [1-45°] Cu Equivalence

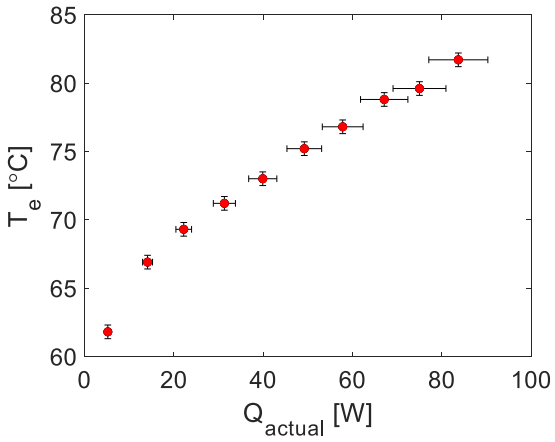

Figure 6-55: HP2 [1-45°] Evaporator Temperature

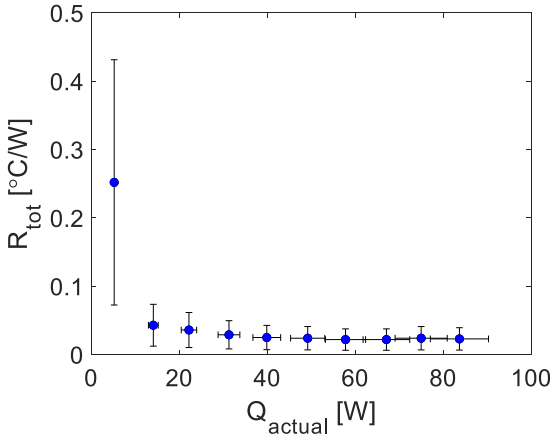

Figure 6-56: HP2 [1-45°] Total Resistance

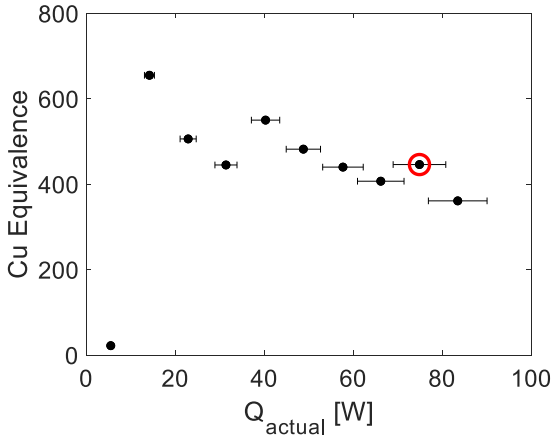

Figure 6-57: HP2 [1-90°] Cu Equivalence

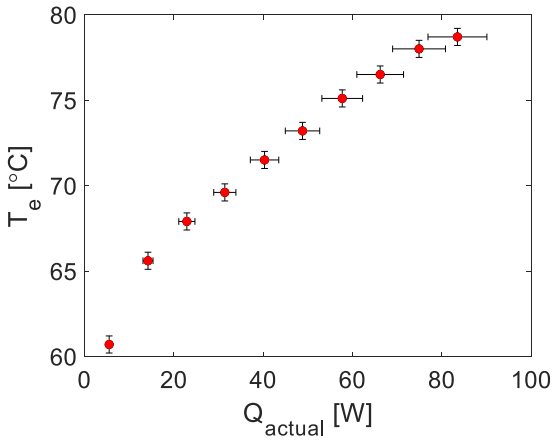

Figure 6-58: HP2 [1-90°] Evaporator Temperature

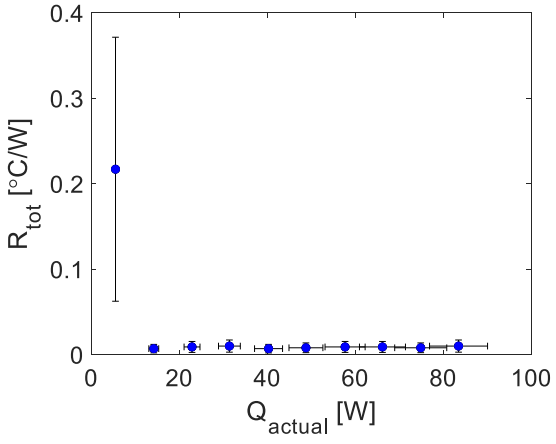

Figure 6-59: HP2 [1-90°] Total Resistance

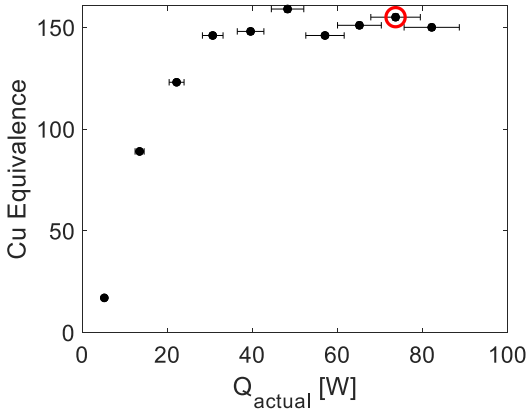

Figure 6-60: HP2 [2-90°, 45°] Cu Equivalence

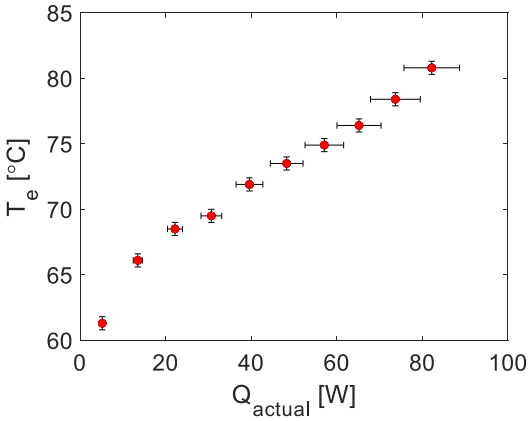

Figure 6-61: HP2 [2-90°, 45°] Evaporator Temperature

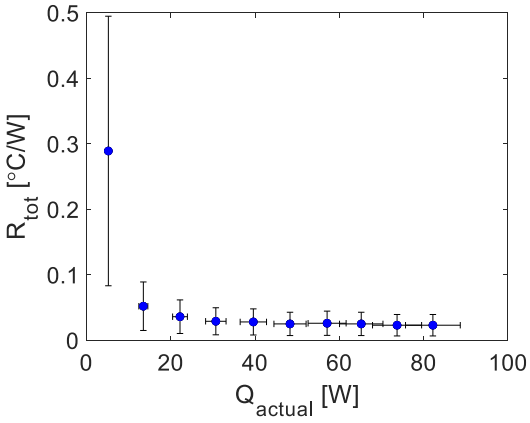

Figure 6-62: HP2 [2-90°, 45°] Total Resistance

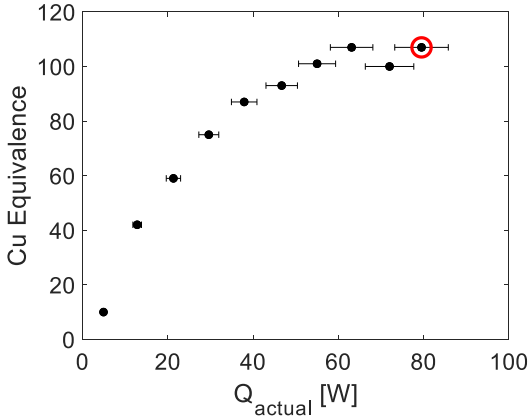

Figure 6-63: HP2 [2-90°, 90°] Cu Equivalence

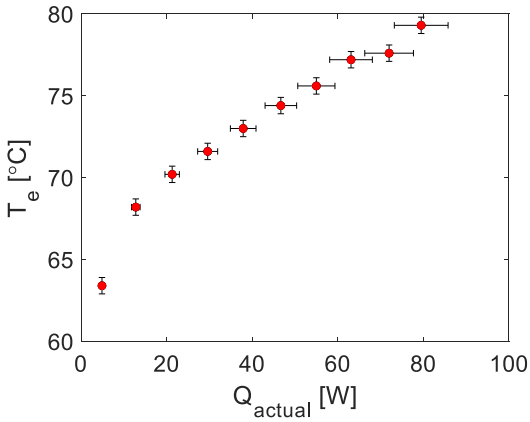

Figure 6-64: HP2 [2-90°, 90°] Evaporator Temperature

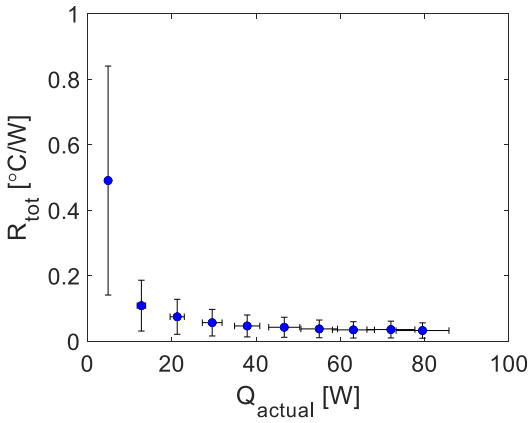

Figure 6-65: HP2 [2-90°, 90°] Total Resistance

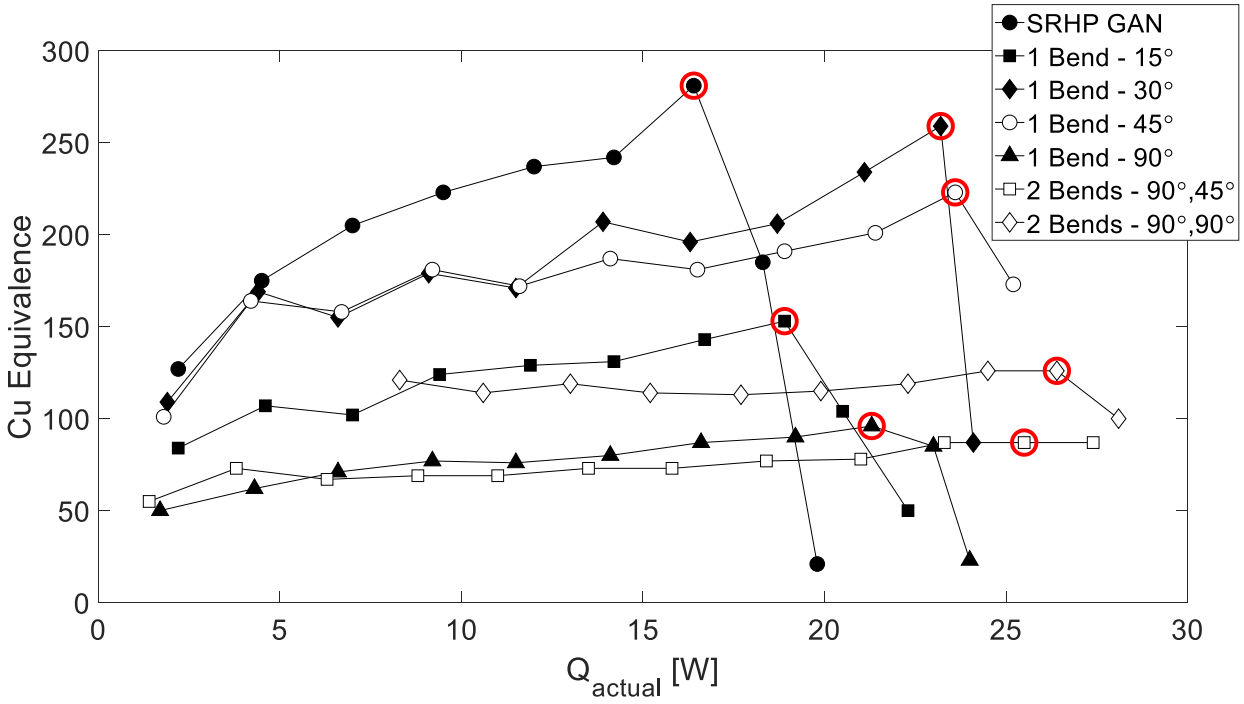

Figure 6-66: Cu Equivalence HP1 (All Bending Angles)

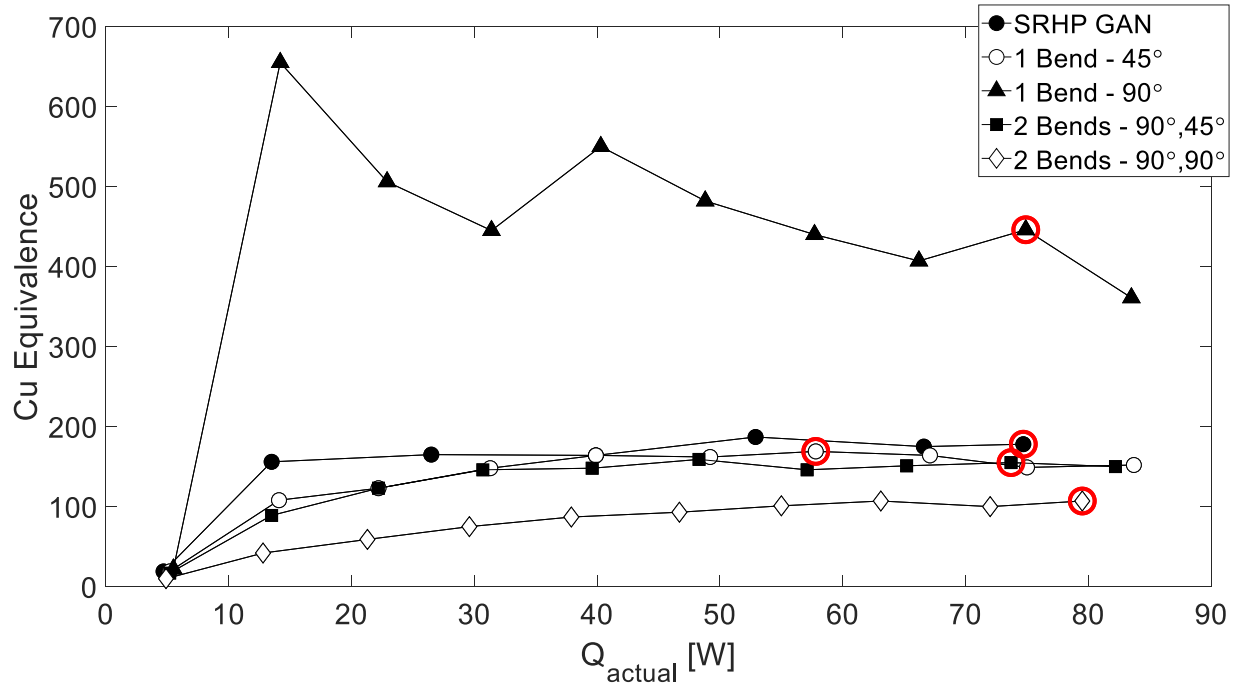

Figure 6-67: Cu Equivalence HP2 (All Bending Angles)

6.3.3 Comparing the Effects of Bending to Similar Research

A similar study in which a Cu/water sintered felt wick heat pipe was tested under various bent configurations was performed by a former researcher in the AU TherMML Laboratory. The results from his research were compared to the experimental results in the current study to examine the differences in the measured and predicted heat pipe performance parameters. In the previous research, a 0.25 in. diameter heat pipe, designated as HP02, was tested under bent configurations. HP02 was tested in a test system that also employed a water cooled condenser bulb, but the evaporator region was heated with a solid block heater rather than Nichrome wire. The thermocouples for HP02 were located at the inner edge of the evaporator and condenser regions. The former research did not include insulation around the heat pipe. HP1, HP2, and HP4 were likely to have similar wick properties as the heat pipes used in the previous work done by Odhekar and Harris [16], but their properties were not definitively known. The assumed wick properties that were employed in the previous research can be seen in Table 6-3.

Table 6-3: D.D. Odhekar's Heat Pipe Specifications [16]

Property	HP02
Container Outer Diameter	6.35 mm (0.25 in.)
Working Length	276.2 mm (10.87 in.)
Evaporator Length	38.1 mm (1.5 in.)
Condenser Length	38.1 mm (1.5 in.)
Adiabatic Length	200 mm (7.87 in.)
Sintered Metal Felt Wick Thickness	0.3175 mm (0.0125 in.)
Porosity	87%
Length of Metal Felt Strands	10 mm (0.39 in.)
Diameter of Metal Strands	3.5E-2 mm (0.0014 in.)
Working Fluid Charge Mass	1.3 g (1.3 mL)
Permeability	442.76 μm^2 (6.94E-8 in^2)

In Odhekar's research, HP02 was tested in the same bent configurations as HP1 in the current research with 1 bend at 15°, 30°, 45°, and 90°. The parameters of the heat pipes used in both the current and former research efforts can be seen in Table 6-4.

Table 6-4: Parameters of Heat Pipes Compared to Former Research

Parameter	**Current Research**	**Odhekar** [11]
Diameter	6.35 mm (0.25 in.)	6.35 mm (0.25 in.)
Evaporator Length	50.80 mm (2 in.)	38.10 mm (1.5 in.)
Condenser Length	76.20 mm (3 in.)	38.10 mm (1.5 in.)
Adiabatic Length	157.48 mm (6.2 in.)	200 mm (7.87 in.)
Effective Length	220.98 mm (8.7 in.)	238 mm (9.37 in.)
Charge Mass	1.22 mL (1.22 g)	1.26 mL (1.26 g)

There were some differences in the physical parameters of the heat pipes compared, such as differing lengths for each of the three major regions and slightly different charge masses, but the testing and performance characterization methods were similar enough to justify direct comparison. The experimental capillary limit and evaporator temperature from each of the research efforts were compared, as seen in Table 6-5.

Table 6-5: Reported Values Evaporator Temperature and Corresponding Capillary Limit for Bent Heat Pipe Tests in Current and Former Research

Heat Pipe Configuration	**Current Research**			**Odhekar** [11]	
	Reported T_e [°C]	Reported Cap. Lim. [W] (Q_{in})	Reported Corrected Cap. Lim. [W] (Q_{actual})	Reported T_e [°C]	Reported Cap. Lim. [W] (Q_{in})
SRHP-GAN	28.1	21.1	16.4	27.2	23.5
1 Bend - 15° GAN	31.3	24.0	18.9	31.1	25.7
1 Bend - 30° GAN	36.7	30.1	23.2	35.8	28.2
1 Bend - 45° GAN	35.2	30.3	23.6	34.3	27.4
1 Bend - 90° GAN	38.0	27.1	21.3	39.4	30.0

It can be seen that the reported capillary limits and evaporator temperatures are very similar between the two investigations. The subtle differences can be attributed to a variety of factors such as different charge masses, differences in the test system, differences in the DAQ system, etc. The corrected reported capillary limit, seen in Table 6-5, represents the reported Q_{actual} values at the observed capillary limits. The research done by Odhekar neglected to include a parasitic loss model and thus reported the total power input (Q_{in}) as the capillary limit of the pipe at the failure point. A graphical representation of capillary limit and evaporator temperature comparisons between the two investigations can be seen in Figure 6-68 and Figure 6-69.

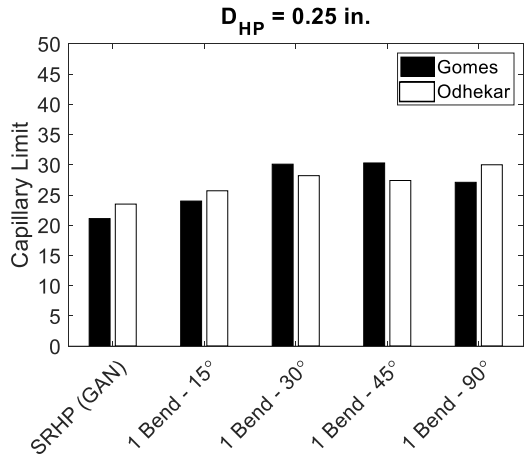

Figure 6-68: Capillary Limit Comparison

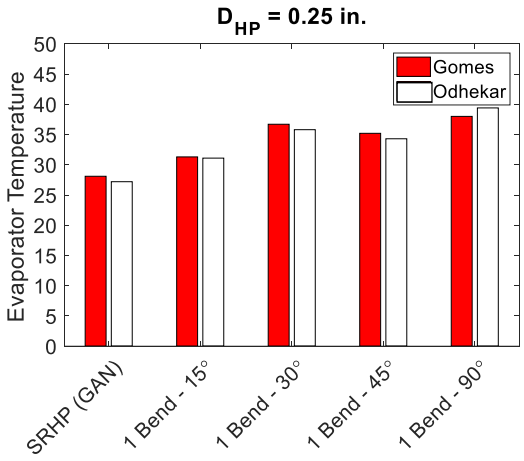

Figure 6-69: Evaporator Temperature Comparison

The capillary limits for HP1 were all within 10.5% of the limits that Odhekar reported for HP02, and the measured evaporator temperatures only differed by 3.5% between the two heat pipes. This comparison served to validate the accuracy of the experimental approach used in this research. When comparing the evaporator temperatures of two heat pipes, it is important to consider the condenser boundary condition. The condenser temperature directly influences the heat pipe's thermal behavior and therefore the evaporator temperature. If the condenser temperatures were different between the two experimental efforts, a more appropriate comparative performance

parameter would have been the temperature difference between the evaporator and condenser region. By comparing the temperature difference, any change of the temperature scale or unit system influencing the comparative analysis would be eliminated. Since, however, HP1 and Odhekar's HP02 were both tested with a constant 20°C condenser region boundary condition, the evaporator temperatures were able to be compared directly. Odhekar also concluded that during his calculations of energy loss in the bended section of the heat pipe, it was found that it was very low and practically incapable of affecting the capillary limit [16]. He suggested that the effect of pressure loss due to bending was found to be negligible and three to four orders of magnitude smaller than the capillary pumping pressure showing that any increase in the temperature drop due to bending is due to the obstruction in the flow of liquid returning to the evaporator from the condenser [16].

6.3.4 Comparing the Experimental Results to the Vapor Core Theoretical Analysis

The vapor core analysis performed in Chapter 3 was used to compare the experimental total resistance values to theoretical results in order to develop a better understanding of the effects of bending on heat pipe performance. Experimental data in Figure 6-20 showed that HP1 SRHP exhibited a total resistance of 0.053 °C/W at a heat input of 10 W and an operating temperature of 25°C. When it was bent with 1 bend at 45° (Figure 6-44), the total resistance value increased by approximately 22.6%. Based on the theoretical analysis of heat transport losses due to increased vapor pressure drop in bent heat pipes, the total resistance should have increased by only 13.4%. When the same analysis was compared to experimental resistance values for a heat input of 15 W and an operating temperature of 25°C, the theoretical analysis predicted an 18.3% increase in total resistance, but the experimental data showed that there was a 30.6% increase. It was determined that the theoretical analysis slightly under predicts the percent increase, or penalty, of the total

resistance. The rationale behind this under prediction was that the analysis did not account for all influential factors of vapor core phenomenon. The analysis assumed an incompressible liquid flow in the vapor core, when in reality, the working fluid should be treated as a saturated vapor. It was determined that vapor core phenomenon is likely a contributing factor to the effects of bending on the thermal performance of heat pipes, but that there are likely other significant factors that impart a greater influence the performance.

6.3.5 Effects of Flattening on Performance

HP4 was tested in three different flattened end configurations: flattened evaporator, flattened condenser, and both ends flat (double-flat). The 0.5 in. diameter heat pipe was flattened to an outer thickness of approximately 0.25 in. for each flattened end configuration. The condenser region length was approximately 3.2 in. and the evaporator region length was approximately 2 in. for each test. Due to a lack of available materials, HP4 was not tested in a straight-round configuration, however, the effects of flattening on the performance and operational limits were still observed and compared. Since HP4 was a larger diameter heat pipe, the amount of heat required to reach the capillary limit was significantly higher than that of the smaller diameter heat pipes. That being said, the linear power supply and Nichrome wire were the limiting factors on testing HP4 to its capillary limit. During many of the tests, the Nichrome wire reached temperatures exceeding its structural integrity which resulted in the termination of the test and a false reporting of the capillary limit for HP4. In actuality, the capillary limit for this 0.5 in. diameter heat pipe was likely higher than reported, but for the purposes of this investigation, the limited data set was considered sufficient to compare the effects of flattening on overall performance of the heat pipe.

Recapping on the test system boundary conditions mentioned in Chapter 4, the test set-up used to collect data on these heat pipes administered a constant heat flux boundary condition on the surface of the evaporator region and a constant temperature boundary condition on the surface of the condenser region. These conditions allowed the thermal performance of the heat pipe to be analyzed easily and the effects of the geometric modifications to be exploited. However, with heat being forced into the condenser through the resistive heat of the Nichrome wire, the thermal performance of the heat pipe was limited by the amount of heat leaving the condenser region. Therefore, geometric modifications to the evaporator and condenser regions were likely to have significant effects on the overall thermal performance of the heat pipes. HP4 was tested in three distinct flattened configurations in GAN and the following observations were made based on the data seen in Figure 6-70 through Figure 6-78:

***Capillary limits on Cu equivalence plots are marked with a red circle around the data point*

HP4 – Flattened

1. **(NO)** The most noticeable observation was that the flattened condenser configuration significantly outperformed both the flattened evaporator configuration and the double-flat configuration with respect to Cu equivalence. The research done by W. Intagun, discussed in Chapter 4, reported experimental results supporting the fact that flattening heat pipes can decrease their total thermal resistance in some cases, resulting in an increase in effective thermal conductivity [15].
2. **(NI)** In contrast to the typical trend of Cu equivalence corresponding inversely to evaporator temperature, the flattened condenser configuration had a much higher evaporator temperature than either of the other two configurations while also exhibiting a

higher Cu equivalence. Each configuration did, however, follow the same evaporator temperature trend with respect to heat input.

3. ****(NO)** The Cu equivalence of HP4 was the greatest in the flattened condenser configuration, lesser in the flattened evaporator configuration, and least in double-flat configuration.

4. **(I)** The capillary limit of HP4 remained relatively constant for each flattened end configuration. Again, the reported capillary limits for HP4 do not necessarily represent the actual operational limit of the heat pipe since the test system was the limiting factor on increasing the heat load. The capillary limits for HP4 were likely higher than the ones that were reported in this research.

5. **(NI)** There was a sharp increase in the Cu equivalence of HP4 for each flattened end configuration at approximately 130 W.

**It is important to note that the double-flat heat pipe experienced damage to the wick structure in the evaporator region during the post-fabrication flattening process. During the flattening process, the wick structure cracked and exhibited brittle qualities. This was presumably due to the excessive heat treatment of the wick which was performed to build up the oxide layer which would aid in the working fluid wetting the wick. Although the wick was damaged, it was apparent from the test results that the double-flat HP4 still operated as a heat pipe. The double-flat results are still useful in examining the effects of flattening on Cu equivalence and capillary limit. However, additional tests should be performed to determine if the degradation in Cu equivalence was idiosyncratic to the damage in the wick or if it was inherent to the double-flat configuration.

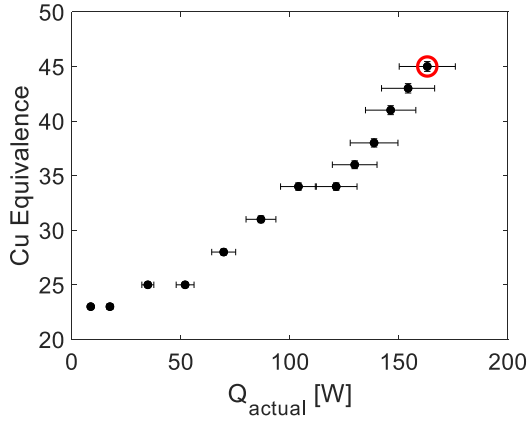

Figure 6-70: HP4 – Flattened Evaporator Cu Equivalence

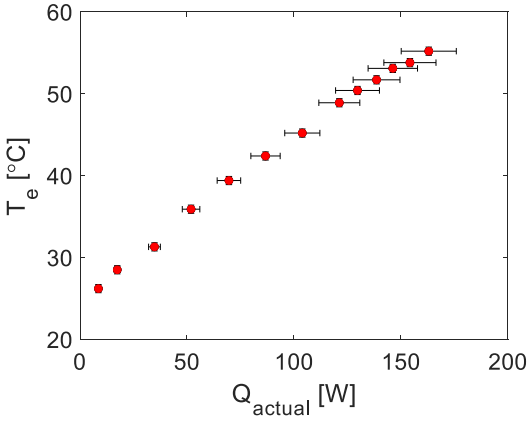

Figure 6-71: HP4 – Flattened Evaporator Evaporator Temperature

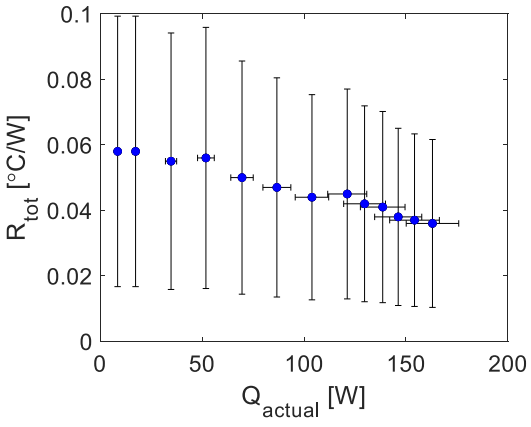

Figure 6-72: HP4 – Flattened Evaporator Total Resistance

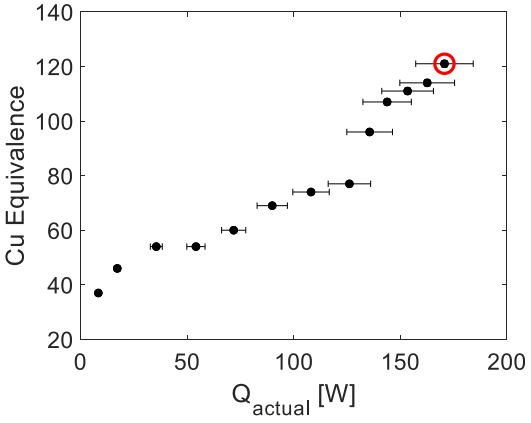

Figure 6-73: HP4 – Flattened Condenser Cu Equivalence

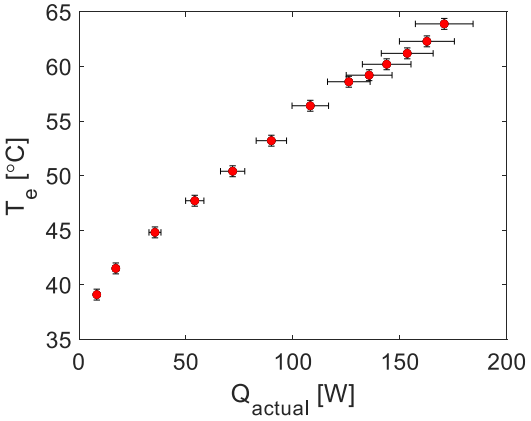

Figure 6-74: HP4 – Flattened Condenser Evaporator Temperature

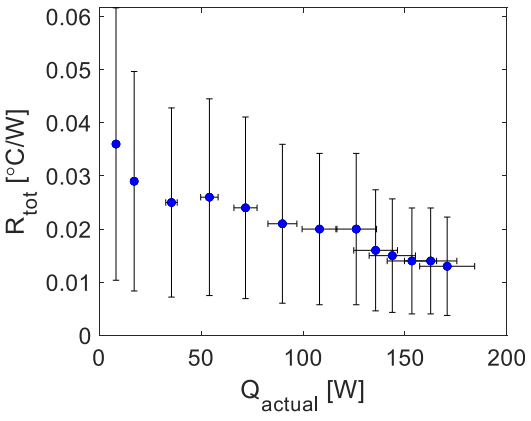

Figure 6-75: HP4 – Flattened Condenser Total Resistance

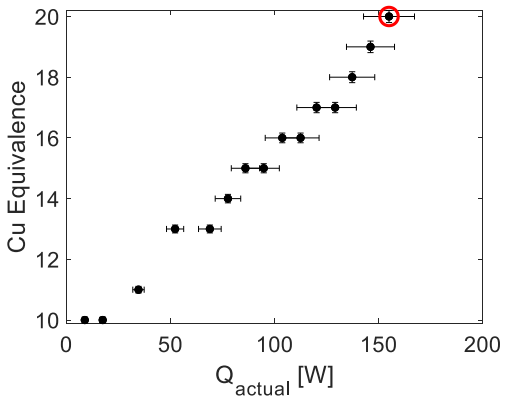

Figure 6-76: HP4 – Double-Flat Cu Equivalence**

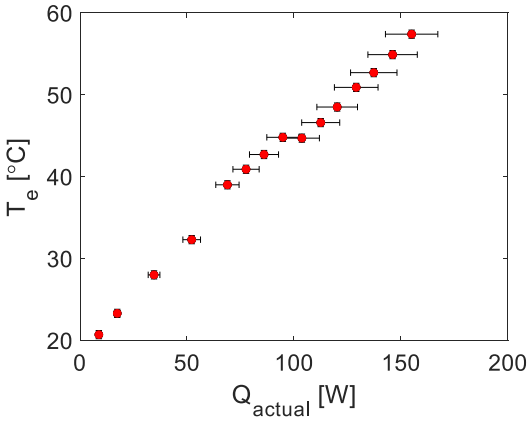

Figure 6-77: HP4 – Double-Flat Evaporator Temperature**

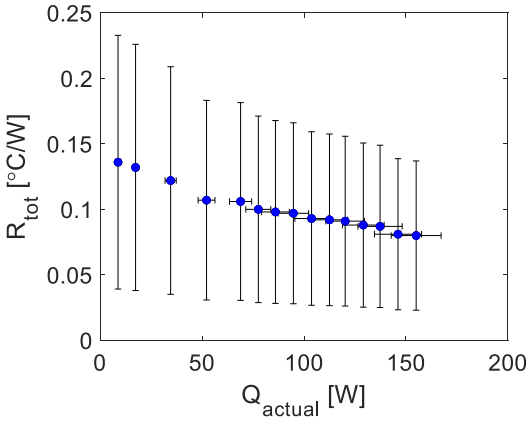

Figure 6-78: HP4 – Double-Flat Total Resistance**

***The evaporator region wick was broken during the flattening process for the double-flat HP4 test. This may have affected the heat pipe's Cu equivalence by degrading it below the single-flat flattened evaporator configuration.*

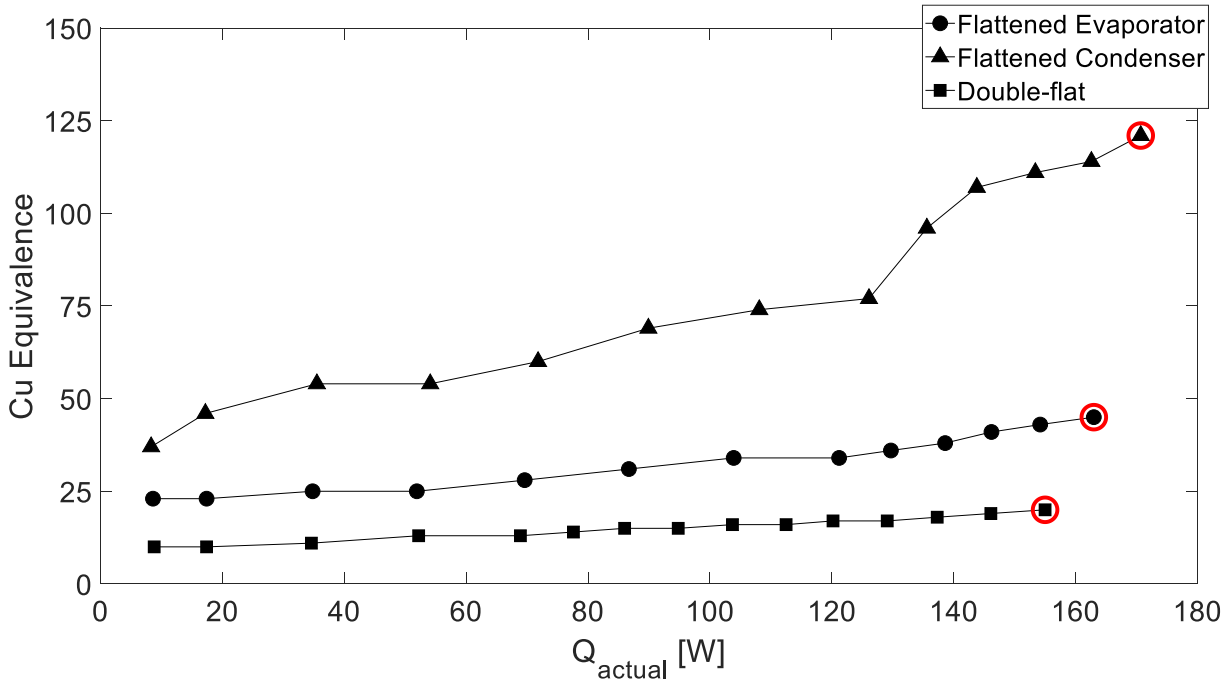

Figure 6-79: Cu Equivalence HP4 (All Flattened End Conditions)

6.3.7 Performance at Capillary Limit for All Heat Pipes

The capillary limits and corresponding maximum Cu equivalence's for each heat pipe configuration are compared in Figure 6-80. This information represents both the operational limits and the corresponding maximum thermal performance of each heat pipe. It can be seen in Figure 6-80 that some heat pipes were favorable for high Cu equivalence while some offered usefulness in the form of a very high capillary limit. The limits of operation and application are dictated primarily by these two performance parameters. The following observations were made from comparing the performance limits of each of the heat pipes that were tested:

Capillary Limit and Maximum Cu Equivalence for All Heat Pipes

1. **(I)** Capillary limit increased with increasing diameter and was also drastically influenced by the gravitational orientation.

2. **(I)** HP1 exhibited a relatively low range of capillary limits (20 - 27 W), but experienced high Cu equivalence values ranging from 150 to 300 times the thermal conductivity of copper. The Cu equivalence values of HP1 even surpassed the performance of HP2 in many cases.

3. **(NO)** HP2 [1-90°] seemed to be the most versatile heat pipe with respect to a relatively high capillary limit and Cu equivalence compared to the rest of the heat pipes that were tested.

4. **(I)** HP4 exhibited high capillary limits exceeding 150 W, but operated at the low Cu equivalence range of the HP1 and HP2 GAD configuration performances, which were within the range of 50 to 100 times better than copper.

5. **(I)** The GAD configuration degraded both the capillary limit and Cu equivalence of HP1 and HP2.

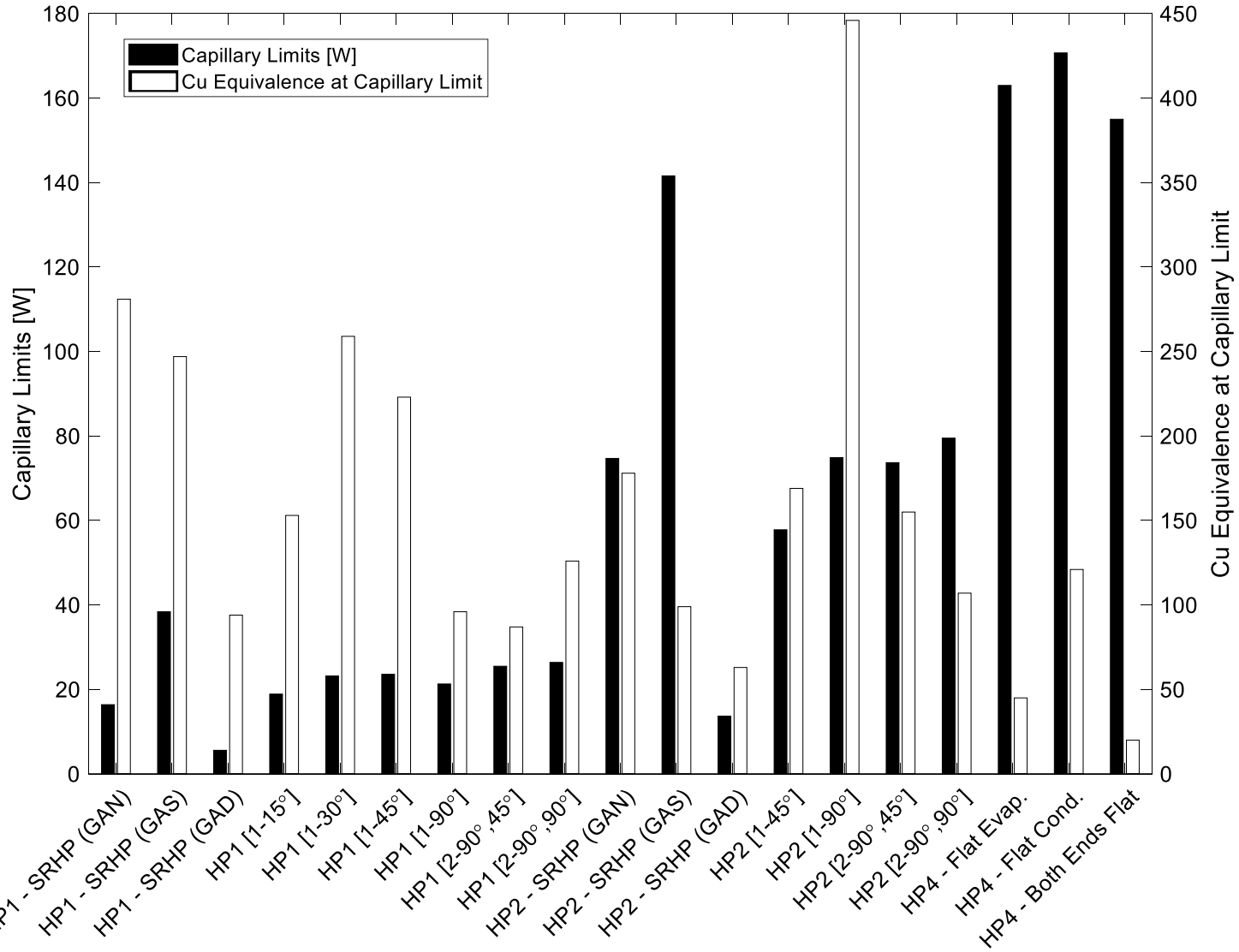

Figure 6-80: Capillary Limits and Corresponding Cu Equivalence

6.4 Explanation of Unknown Parameters

Although the data trends are useful in examining the effects of bending and flattening on effective thermal conductivity, evaporator temperature, and capillary limit, there are several unknown parameters about the heat pipes that inhibit developing definitive conclusions about the behavioral trend differences. HP1, HP2, and HP4 were manufactured well before this research began and the major unknown parameters revolved around the properties of the wick structure. The unknown parameters of the heat pipes were wick porosity, wick permeability, sintered fiber diameter, and sintered fiber length. Another possible source of error in the characterization of these heat pipes was the method used to fill them with the working fluid. Each heat pipe was filled through a valve on the end cap of the condenser region. This valve was snipped off prior to testing and left a small un-wicked volume of the heat pipe where a small percentage of the working fluid might have been trapped. If a this small percentage of the calculated charge mass were to be trapped in the un-wicked region during operation, then the wick structure may not have been completely filled with the working fluid which may have affected the performance and limits of the heat pipes. In some configurations, specifically GAD, this un-wicked volume may have caused a degradation in performance and limits. To circumvent possible dry-out of the heat pipe due to trapped fluid in the un-wicked volume, each heat pipe was slightly overfilled. Each of these unknown parameters contribute to what may be idiosyncratic behavior of the heat pipes. It may be true that the tests could be repeated with similar results, but in order to be certain, the heat pipes must be manufactured and tested under known wick properties and operational parameters.

6.5 Usefulness and Application of Data

The data collected for these heat pipes serves as a foundation for developing a comprehensive database representing the performance and limits of various bent, flattened, and straight-round heat pipes. This database encompasses the range of design variables explored in this investigation, but is also capable of being expanded to include a wider range of design variables such as additional bending angles or different gravitational orientations for the geometrically modified configurations. The data that was collected, analyzed, and formatted in this study serves as a baseline characterization of the effects that bending and flattening have on capillary limit, effective thermal conductivity (Cu equivalence), evaporator temperature, and several other performance parameters for Cu/water heat pipes in a gravity neutral configuration. If this comprehensive database were to be further developed to prove repeatability, companies in the aerospace and defense industry could reference this information when implementing heat pipes into a systems level thermal analysis. A database containing repeatable results could be used to predict the heat pipe's performance and limits under the geometric modifications. This information could aid in the design and optimization of heat pipe integrated thermal management systems to minimize weight, power, or spatial requirements of the electronics system.

A performance/limit plot comparing the operable ranges of power along with the corresponding evaporator temperatures for each heat pipe in this study can be seen in Figure 6-81. This plot is useful in determining which heat pipe offers the best solution when imposing operating power and evaporator temperature requirements. Typically, these requirements are determined based on the operating conditions of the electronic component that interacts with the heat pipe. From the information of the performance vs. limits for the heat pipes in this study, the following observations were made:

Evaporator Temperature and Corresponding Heat Input for Operational Range of All Heat Pipes

1. **(I)** HP1 maintained relatively low evaporator temperatures within the operational heat input range from nearly room temperature at low powers (~2 W) to 30°C – 50°C when approaching the capillary limit.
2. **(I)** HP2 operated at a much higher evaporator temperature range compared to HP1 and HP4. Albeit, HP2 offered excellent Cu equivalence within its operational range, the steady-state evaporator temperature with respect to the power input was relatively high, ranging from around 55°C – 80°C.
3. **(I)** Bending did not have a significant effect on evaporator temperature or capillary limit for HP2.
4. **(I)** HP4 had the largest operational heat input range and therefore the largest steady-state evaporator temperature range. The 0.5 in. diameter heat pipe operated at temperatures near 20°C at low powers (~8 W). As it approached its capillary limit between 155 and 170 W, the evaporator temperature ranged between 55°C and 65°C.

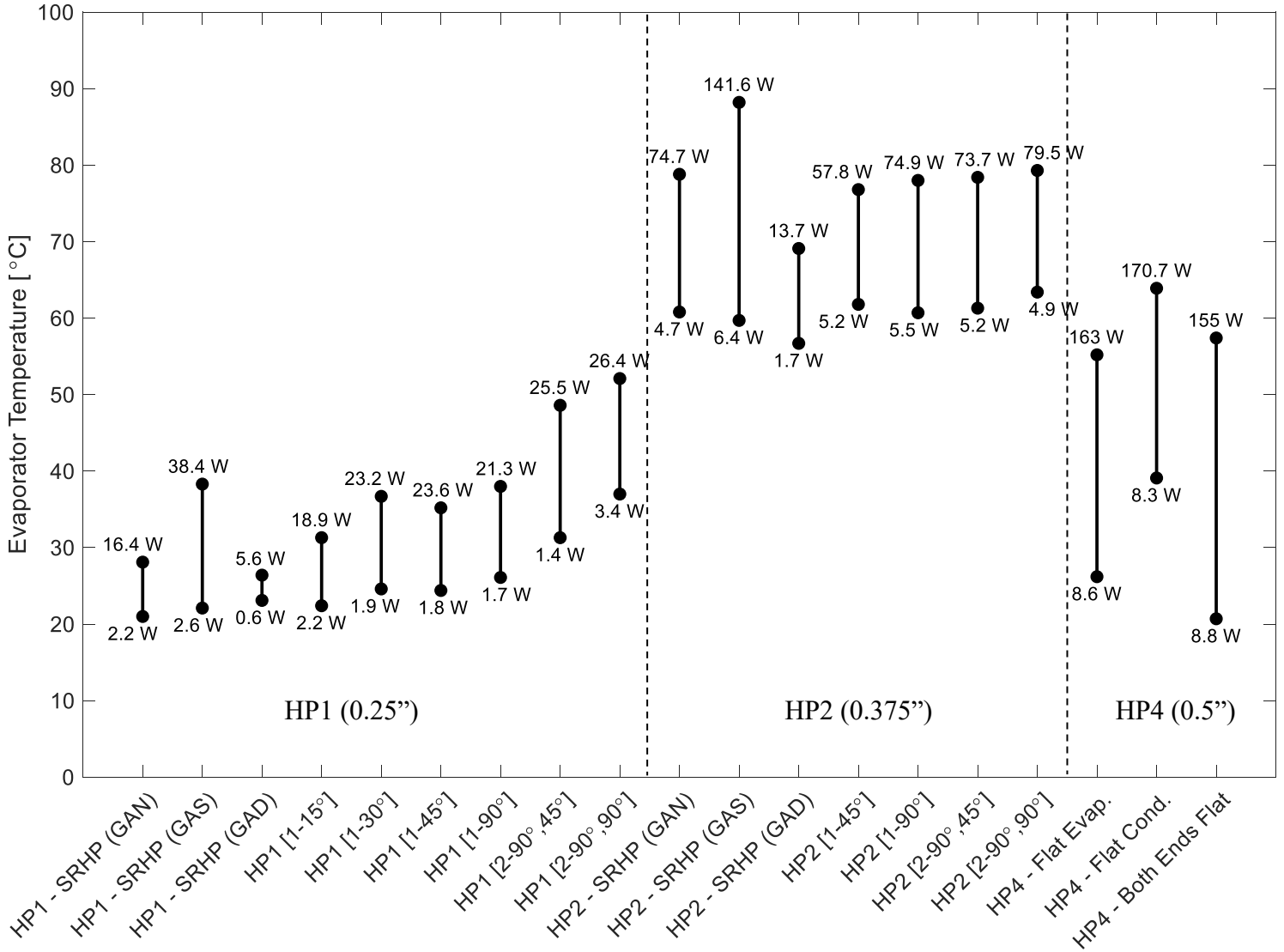

Figure 6-81: Evaporator Temperature and Corresponding Heat Input for Operational Range of All Heat Pipes

7 CONCLUSION

This chapter discusses the major applications and benefits of the results of this investigation. In addition to a thorough description of the usefulness of the data, the boundaries and limitations of the results are elaborated upon as well as the next steps required to further develop a trustworthy basis for the analysis of the performance and limits of geometrically modified heat pipes.

7.1 Data Application

The main deliverables from this study were the experimental heat pipe performance database, the observed trends of the effects of bending and flattening on performance and operational limits, the MATLAB data reduction and formatting tool (HP-DAN), and the formatted data plots that display heat pipe performance within their operational limits. The heat pipe database contains steady-state temperature data for each heat pipe at discrete heat input levels within each of their operational ranges. The following parameters were recorded at steady-state for each heat pipe at each incrementing heat input:

- Total power input (Q_{in})
- Corrected heat input (Q_{actual})
- Heat efficiency of the system (Q_{actual} / Q_{in})
- Temperature at evaporator/adiabatic region interface (T_e)

- Temperature at adiabatic/condenser region interface (T_c)
- Total temperature difference along adiabatic region (ΔT)
- Total thermal resistance of the heat pipe (R_{tot})
- Approximate effective thermal conductivity (k_{eff})
- Approximate Cu equivalence

This information was used to exploit the trends of the heat pipe's behavior during normal operations. The observed trends discussed in this investigation characterized the effects that bending, flattening, and gravitational orientation had on the heat pipe's effective thermal conductivity and operational limits as well as the other tertiary performance parameters stored in the database. The software tool used to analyze this data performed several functions including applying calibration functions to the thermocouple to minimize fabrication bias on measurement, applying a parasitic loss model to account for waste heat that was not transferred by the heat pipe, approximating performance parameters that were not directly measured, and formatting results in a manner that allowed for easy observation of general performance trends. The formatted plots provide the service of exploiting the performance trends of the discrete data that was collected and approximated. This discrete data could also be mathematically interpolated to generate continuous performance functions which could be used to estimate heat pipe performance parameters outside of the discretely measured data.

The overall benefit and product of this investigation is information of heat pipe performance under geometric modifications. This information provides a foundation for the development of repeatable performance data that can be used to aid in thermal management of electronic systems in the defense and aerospace industry.

7.2 Limits on Results

The results gathered from this experimental investigation serve to provide a baseline for developing empirical and repeatable characterization of the effects of bending and flattening on the thermal performance of Cu/water sintered felt wick heat pipes. The database that was developed throughout this study contains information that reflects these performance effects at the pre-determined configurations. This database is limited in the sense that there are several configurations that were not explicitly tested and are therefore not able to be definitively characterized. There are means of predicting the information outside of the current database, such as mathematically interpolating the results to provide continuous performance functions. However, without the repeatability of the test data in the database, these methods would incur large amounts of uncertainty and would not be reliable for a dedicated design tool. This database provides the information required to further investigate some of the heat pipe design variables and their effects on performance. A continuation of testing could result in the development of a reliable database that could be incorporated into a dedicated heat pipe design and analysis tool.

7.3 Future Work

The future work for this research will likely involve manufacturing several identical heat pipes similar to HP1, HP2, and HP4, and testing them under various design parameters such as gravitational orientation, number of bends, bending angle, flatness ratio, charge ratio, and many others. Many of these parameters may be combined in future work. For example, the bent and flattened heat pipes may be tested in various gravitational orientations or with various working fluid charge ratios. The research efforts will transition seamlessly to characterizing the thermal performance and operational limits of heat pipes manufactured in-house. The in-house manufactured heat pipes will have known wick properties and operational parameters, and will

undergo performance and operational limit testing as a continuation of the research sponsored by L3Harris Technologies.

REFERENCES

[1] A. Bar-Cohen, K. Matin, N. Jankowski, and D. Sharar, "Two-Phase Thermal Ground Planes: Technology Development and Parametric Results," *J. Electron. Packag. Trans. ASME*, vol. 137, no. 1, pp. 1–9, 2015.

[2] K. P. Bloschock and A. Bar-Cohen, "Advanced thermal management technologies for defense electronics," *Def. Transform. Net-Centric Syst. 2012*, vol. 8405, no. May 2012, p. 84050I, 2012.

[3] G. M. Grover and R. H. Chrisman, "United States Patent - Heat Pipe," no. 19, p. 11, 1987.

[4] A. Fagrhi, *Heat Pipe Science and Technology*, 2nd ed. University of Connecticut: Global Digital Press, 2016.

[5] C. C. Silverstein, *Design and Technology of Heat Pipes for Cooling and Heat Exchange*. Washington D.C.: Taylor & Frances, 1992.

[6] H. G. Hameed, "Numerical and Experimental Study of Flow and Heat Transfer Enhancement in a Cylindrical Heat Pipe Using Nanofluid," no. January, 2015.

[7] N. Sangpab, N. Kimura, P. Terdtoon, P. Sakulchangsatjatai, N. Kammuang-lue, and M. Murakami, "Combined effect of bending and flattening on heat transfer performance of cryogenic sintered-wick heat pipe," *Appl. Therm. Eng.*, vol. 148, no. March 2018, pp. 878–885, 2019.

[8] K. T. Lin and S. C. Wong, "Performance degradation of flattened heat pipes," *Appl. Therm. Eng.*, vol. 50, no. 1, pp. 46–54, 2013.

[9] J. S. Chen and J. H. Chou, "The length and bending angle effects on the cooling performance of flat plate heat pipes," *Int. J. Heat Mass Transf.*, vol. 90, pp. 848–856, 2015.

[10] H. Z. Tao, H. Zhang, J. Zhuang, and W. Jerry Bowman, "Experimental study of heat transfer performance in a flattened AGHP," *Appl. Therm. Eng.*, vol. 28, no. 14–15, pp. 1699–1710, 2008.

[11] D. D. Odhekar, “Experimental Investigation of Bendable Heat Pipes,” *Auburn Univ.*, 2005.

[12] C. K. Loh, E. Harris, and D. J. Chou, “Comparative study of heat pipes performances in different orientations,” *Annu. IEEE Semicond. Therm. Meas. Manag. Symp.*, pp. 191–195, 2005.

[13] A. Fagrhi, *Heat Pipe Science and Technology*, 1st ed. Washington D.C.: Taylor & Frances, 1995.

[14] C. M. White, “Stream-Line Flow Through Curved Pipes,” *Proc. R. Soc.*, vol. A123, pp. 645–663, 1929.

[15] W. Intagun, P. Terdtoon, and P. Sakulchangsatjatai, “Flattening effect on heat transfer characteristics of a sintered-wick heat pipe,” *Am. J. Appl. Sci.*, vol. 10, no. 7, pp. 760–766, 2013.

[16] D. D. Odhekar and D. K. Harris, “Experimental investigation of bendable heat pipes using sintered copper felt wick,” *Thermomechanical Phenom. Electron. Syst. -Proceedings Intersoc. Conf.*, vol. 2006, pp. 570–577, 2006.

[17] F. P. Incropera, D. P. Dewitt, T. L. Bergman, and A. S. Lavine, *Fundamentals of Heat and Mass Transfer*, 7th ed. Hoboken: John Wiley & Sons, Inc., 2011.

APPENDIX A. HEAT PIPE PREPARATION AND FILL PROCEDURE

1. Attach heat pipe Schrader valve fitting to vacuum fitting
2. Open the 3-way valve to the (1) position and vacuum heat pipe down to ~100 mtorr
3. Once vacuumed, turn the 3-way valve back to the closed configuration and remove heat pipe from vacuum apparatus
4. Weigh empty heat pipe (with all instrumentation) on scale and record weight
5. Fill the heat pipe with the pre-determined charge mass of deionized water plus an additional milliliter so that the heat pipe is slightly overfilled

   **Fill heat pipe with water from reservoir by carefully turning the 3-way valve to the (2) position

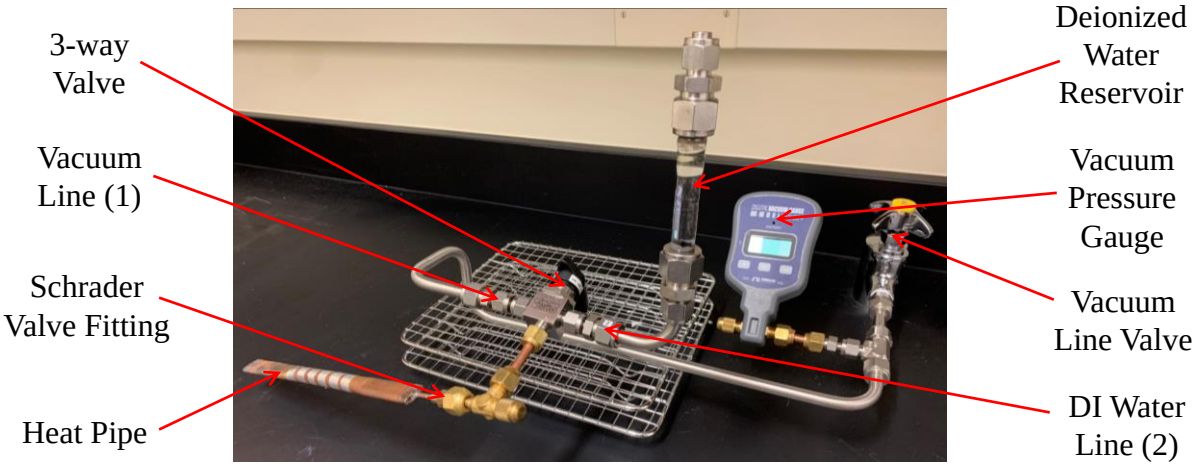

Figure A-1: Heat Pipe Fill System

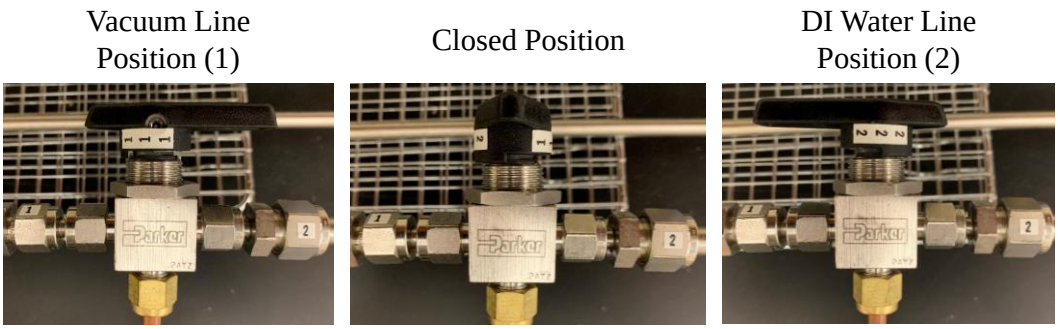

Figure A-2: 3-way Valve Positions

6. Weigh the filled heat pipe (with all instrumentation) and record weight
7. Arrange overfilled heat pipe vertically with Schrader valve up, connect linear power supply leads to Nichrome wire, and connect thermocouples to DAQ unit

   * * Condenser bulb and insulation not included in the following steps
8. Begin recording transient temperature data before turning on the power supply
9. Apply approximately 30 W of power to the evaporator region of the heat pipe
10. When all thermocouples read > 100°C, carefully tap on Schrader valve with a small metal object (such as an Allen wrench). High-pressured vapor will escape from Schrader valve
11. Turn off the power supply, disconnect the leads and thermocouples, and use thermal glove to remove heat pipe from vertical stand
12. Weight heat pipe (with all instrumentation) and record weight
13. Repeat steps 7-12 until heat pipe weight indicates a charge mass that corresponds to the desired pre-determined charge ratio
14. Once heat pipe is filled to desired charge ratio, snip off Schrader valve and seal the end

APPENDIX B. PARASITIC LOSS MODEL

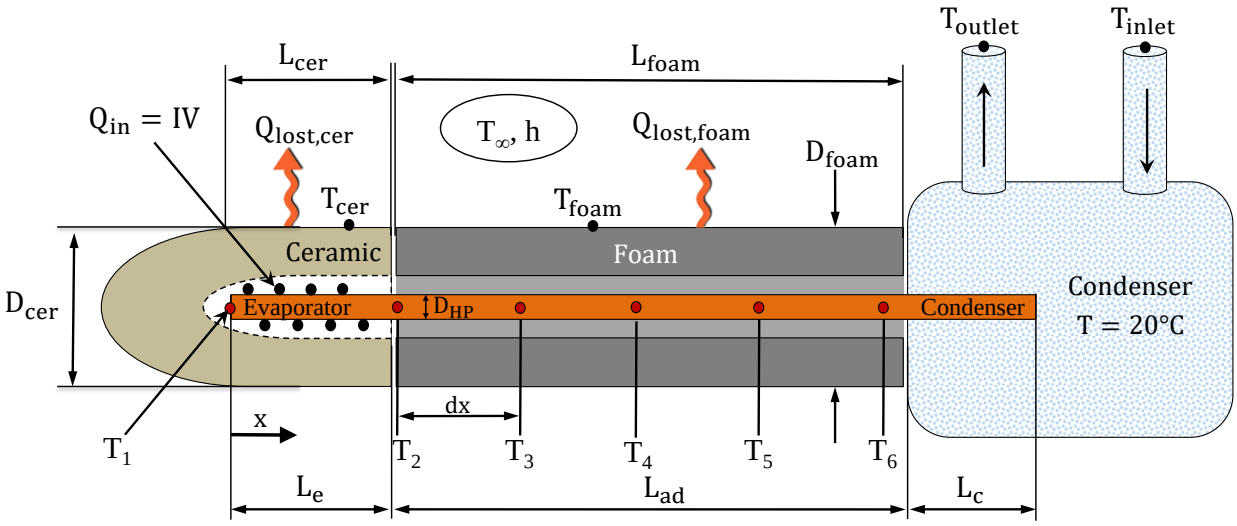

Figure B-1: Parasitic Loss Model Schematic

Table B-1: Parasitic Loss Model Reference Dimensions

	Heat Pipe						Foam Insulation		Ceramic Crucible	
Name	L_{tot} in	L_e in.	L_{ad} in.	L_c in.	dx in.	D_{HP} in.	L_{foam} in.	D_{foam} in.	L_{cer} in.	D_{cer} in.
HP1	11.2	2	6.2	3	1.5	0.25	7	1.255	2.375	1.38
HP2	11.75	2	6.5	3.25	1.5	0.375	5.5	1.255	2.375	1.38
HP4	9.25	2	4.05	3.2	0.85	0.5	2.625	1.255	2.375	1.38

Energy Balance

- Mixed convection and radiation heat loss from foam and ceramic insulation:

$$Q_{actual} = Q_{in} - Q_{conv,cer} - Q_{conv,foam} - Q_{rad,cer} - Q_{rad,foam}$$

$$Q_{actual} = Q_{in} - h_{mixed}A_{cer}(T_{cer} - T_{amb}) - h_{mixed}A_{foam}(T_{foam} - T_{amb}) - \varepsilon\sigma A_{cer}\left({T_{cer}}^4 - {T_{amb}}^4\right) - \varepsilon\sigma A_{foam}\left({T_{foam}}^4 - {T_{amb}}^4\right)$$

Surface Areas

- Foam insulation surface area: $A_{foam} = \pi D_{foam} L_{foam}$

- Ceramic crucible surface area: $A_{cer} = \pi D_{cer} L_{cer} + \frac{\pi}{2}{D_{cer}}^2$

Radiation Losses

- Foam insulation radiation heat loss: $Q_{rad,foam} = \varepsilon\sigma A_{foam}\left({T_{foam}}^4 - {T_{amb}}^4\right)$

- Ceramic crucible radiation heat loss: $Q_{rad,cer} = \varepsilon\sigma A_{cer}\left({T_{cer}}^4 - {T_{amb}}^4\right)$

- Stefan-Boltzmann constant: $\sigma = 5.67E-8\frac{W}{m^2K^4}$

Mixed Convection Losses

- Foam insulation mixed convection heat loss: $Q_{conv,foam} = h_{mixed}A_{foam}(T_{foam} - T_{amb})$

- Ceramic crucible mixed convection heat loss: $Q_{conv,cer} = h_{mixed}A_{cer}(T_{cer} - T_{amb})$

Mixed Heat Transfer Coefficient

The mixed convection heat transfer coefficient was calculated individually for both the foam insulation and the ceramic crucible. The following equations are used for both analyses. The * superscript represents interchangeability between foam insulation and ceramic crucible parameters for respective heat transfer coefficient calculations.

- Film temperature: $T_{film}{}^{*} = \frac{T^{*}+T_{inf}}{2}$ $\beta^{*} = \frac{1}{T_{film}{}^{*}}$

- Rayleigh Number [17]: $Ra^{*} = \frac{g\beta^{*}(T^{*}-T_{amb})D^{*3}}{\nu_{air}\,\alpha_{air}}$

- Free convection Nusselt Number [17]: $Nu_{free}{}^{*} = 0.48Ra^{*0.25}$

- Reynold's Number: $Re^{*} = \frac{U_{inf}D^{*}}{\nu_{air}}$

- Forced convection Nusselt Number [17]:

$$Nu_{forced}{}^{*} = 0.3 + \frac{0.62Re^{*0.5}Pr_{air}{}^{\frac{1}{3}}}{\left[1+\left(\frac{0.4}{Pr_{air}}\right)^{\frac{2}{3}}\right]^{\frac{1}{4}}}\left[1+\left(\frac{Re^{*}}{282{,}000}\right)^{\frac{5}{8}}\right]^{\frac{4}{5}}$$

- Mixed convection Nusselt Number [17]: $Nu_{mixed}{}^{*} = \left(Nu_{free}{}^{*3} + Nu_{forced}{}^{*3}\right)^{\frac{1}{3}}$

- Mixed convection heat transfer coefficient: $h_{mixed}{}^{*} = \frac{k_{air}Nu_{mixed}{}^{*}}{D^{*}}$

APPENDIX C. UNCERTAINTY ANALYSIS

- Parasitic loss model energy balance:

$$Q_{actual} = Q_{in} - Q_{conv,cer} - Q_{conv,foam} - Q_{rad,cer} - Q_{rad,foam}$$

$$\frac{UQ_{actual}}{Q_{actual}} = \sqrt{\left(\frac{UQ_{conv,cer}}{Q_{conv,cer}}\right)^2 + \left(\frac{UQ_{conv,foam}}{Q_{conv,foam}}\right)^2 + \left(\frac{UQ_{rad,cer}}{Q_{rad,cer}}\right)^2 + \left(\frac{UQ_{rad,foam}}{Q_{rad,foam}}\right)^2}$$

- Heat lost due to convection from the ceramic crucible

$$Q_{conv,cer} = h_{mixed} A_{cer} (T_{cer} - T_{amb})$$

$$\frac{UQ_{conv,cer}}{Q_{conv,cer}} = \sqrt{\left(\frac{\partial Q_{conv,cer}}{\partial h_{mixed}} Uh_{mixed}\right)^2 + \left(\frac{\partial Q_{conv,cer}}{\partial A_{cer}} UA_{cer}\right)^2 + \left(\frac{\partial Q_{conv,cer}}{\partial T_{cer}} UT_{cer}\right)^2 + \left(\frac{\partial Q_{conv,cer}}{\partial T_{amb}} UT_{amb}\right)^2}$$

- Heat lost due to convection from the foam insulation

$$Q_{conv,foam} = h_{mixed} A_{foam} (T_{foam} - T_{amb})$$

$$\frac{UQ_{conv,foam}}{Q_{conv,foam}} = \sqrt{\left(\frac{\partial Q_{conv,foam}}{\partial h_{mixed}} Uh_{mixed}\right)^2 + \left(\frac{\partial Q_{conv,foam}}{\partial A_{foam}} UA_{foam}\right)^2 + \left(\frac{\partial Q_{conv,foam}}{\partial T_{foam}} UT_{foam}\right)^2 + \left(\frac{\partial Q_{conv,cer}}{\partial T_{amb}} UT_{amb}\right)^2}$$

- Heat lost due to radiation from the ceramic crucible

$$Q_{rad,cer} = \varepsilon \sigma A_{cer} \left({T_{cer}}^4 - {T_{amb}}^4\right)$$

$$\frac{UQ_{rad,cer}}{Q_{rad,cer}} = \sqrt{\left(\frac{\partial Q_{rad,cer}}{\partial \varepsilon} U\varepsilon\right)^2 + \left(\frac{\partial Q_{rad,cer}}{\partial A_{cer}} UA_{cer}\right)^2 + \left(\frac{\partial Q_{rad,cer}}{\partial T_{cer}} UT_{cer}\right)^2 + \left(\frac{\partial Q_{rad,cer}}{\partial T_{amb}} UT_{amb}\right)^2}$$

- Heat lost due to radiation from the foam insulation

$$Q_{rad,foam} = \varepsilon \sigma A_{foam} \left({T_{foam}}^4 - {T_{amb}}^4\right)$$

$$\frac{UQ_{rad,foam}}{Q_{rad,foam}} = \sqrt{\left(\frac{\partial Q_{rad,foam}}{\partial \varepsilon} U\varepsilon\right)^2 + \left(\frac{\partial Q_{rad,foam}}{\partial A_{foam}} UA_{foam}\right)^2 + \left(\frac{\partial Q_{rad,foam}}{\partial T_{foam}} UT_{foam}\right)^2 + \left(\frac{\partial Q_{rad,foam}}{\partial T_{amb}} UT_{amb}\right)^2}$$

- Ceramic crucible surface area

$$A_{cer} = \pi D_{cer} L_{cer} + \frac{\pi}{2} {D_c}^2$$

$$\frac{UA_{cer}}{A_{cer}} = \sqrt{\left(\frac{\partial A_{cer}}{\partial D_{cer}} UD_{cer}\right)^2 + \left(\frac{\partial A_{cer}}{\partial L_{cer}} UL_{cer}\right)^2}$$

- Foam insulation surface area

$$A_{foam} = \pi D_{foam} L_{foam}$$

$$\frac{UA_{foam}}{A_{foam}} = \sqrt{\left(\frac{\partial A_{foam}}{\partial D_{foam}} UD_{foam}\right)^2 + \left(\frac{\partial A_{foam}}{\partial L_{foam}} UL_{foam}\right)^2}$$

- Total thermal resistance

$$R_{tot} = \frac{T_e - T_c}{Q_{actual}}$$

$$\frac{UR_{tot}}{R_{tot}} = \sqrt{\left(\frac{\partial R_{tot}}{\partial T_e} UT_e\right)^2 + \left(\frac{\partial R_{tot}}{\partial T_c} UT_c\right)^2 + \left(\frac{\partial R_{tot}}{\partial Q_{in}} UQ_{actual}\right)^2}$$